Geochemistry, Geophysics, Geosystems®

AGU ADVANCING EARTH AND SPACE SCIENCE

RESEARCH ARTICLE
10.1029/2023GC010876

Key Points:

- There are significant differences in average composition, *T*, and *P* of the experimental database for each element in different phases
- Number of experimental determinations, even within a group of elements that behave systematically (e.g., REE) may vary by a factor of five
- Data coverage differences impact the predictive power of the regressions on which we rely trace element partitioning models

Supporting Information:

Supporting Information may be found in the online version of this article.

Correspondence to:

G. K. Ustunisik,
Gokce.Ustunisik@sdsmt.edu

Citation:

Cung, E. W., Ustunisik, G. K., Wolf, A. S., & Nielsen, R. L. (2023). The influence of database characteristics on the internal consistency of predictive models of trace element partitioning for clinopyroxene, garnet, and amphibole. *Geochemistry, Geophysics, Geosystems*, *24*, e2023GC010876. https://doi.org/10.1029/2023GC010876

Received 20 JAN 2023
Accepted 14 APR 2023

Author Contributions:

Conceptualization: Gokce K. Ustunisik, Roger L. Nielsen
Data curation: Erica W. Cung
Formal analysis: Erica W. Cung, Gokce K. Ustunisik, Aaron S. Wolf, Roger L. Nielsen
Funding acquisition: Gokce K. Ustunisik
Investigation: Erica W. Cung, Gokce K. Ustunisik, Roger L. Nielsen

The Influence of Database Characteristics on the Internal Consistency of Predictive Models of Trace Element Partitioning for Clinopyroxene, Garnet, and Amphibole

Erica W. Cung[1], Gokce K. Ustunisik[1,2], Aaron S. Wolf[3], and Roger L. Nielsen[1,4]

[1]Department of Geology and Geological Engineering, South Dakota School of Mines and Technology, Rapid City, SD, USA, [2]Department of Earth and Planetary Sciences, American Museum of Natural History, New York, NY, USA, [3]Department of Earth and Environmental Sciences, University of Michigan, Ann Arbor, MI, USA, [4]College of Earth, Ocean, and Atmospheric Sciences, Oregon State University, Corvallis, OR, USA

Abstract Understanding the processes that produce the major and trace element signature of igneous materials requires quantitative models of the behavior of trace elements under the full range of natural conditions. Such predictive models are based on the results of laboratory experiments used to calibrate expressions via regression analysis. The predictive accuracy of those expressions depends on the number of experiments where a specific element was measured and the analytical precision/accuracy of the measurements, together with models that accommodate the known dependencies. A factor that has rarely been considered in such models is the "coverage" with respect to the range of composition, pressure, and temperature in the experimental data. The goal of this research is to evaluate how partition coefficients (D_i) for clinopyroxene, amphibole, and garnet correlate with a variety of intensive and compositional variables for minerals with different substitution mechanisms. Our results show that the number of experimental determinations, even within a group of elements that behave systematically (e.g., REE), may vary by as much as a factor of five. Further, there are significant differences in the average composition, temperature, and pressure of the experimental database for each element. In addition, the combination of database differences and analytical precision for each element result in systematic differences in the magnitude of the controlling parameters. All of these factors impact the predictive power of the regressions on which we rely and can produce a bias in the predicted behavior that may be correlated with analytical error or average composition of the experiments.

1. Introduction

Much of our knowledge regarding the differentiation of the terrestrial planets is based on quantitative models that describe the behavior of trace elements under changing magmatic conditions. Such predictive models simulate how various differentiation processes (e.g., melting, crystallization, mixing, and diffusion) influence the trace element composition of natural materials. The results can then be used to understand the expected impact of different processes and create a framework with which to compare the trace element signature of naturally evolving magmatic systems.

Modeling how magmatic processes are reflected in the geochemical signature of igneous systems requires that we know how trace elements are exchanged among coexisting phases, including melt, crystal, vapor, and fluid. This behavior is often expressed in terms of a simple mathematical expression—the partition coefficient ($^{\text{mineral-melt}}D_i$), which is equal to the ratio of the trace element abundance in the coexisting phases of interest, typically the concentration in the mineral to that in the melt from which the mineral formed (Beattie et al., 1993; Irving, 1978; Onuma et al., 1968). Trace elements partition into minerals by substituting for major elements (e.g., Si, Al, Mg, and Ca in specific crystallographic sites; Goldschmidt, 1937) with the specific substitution mechanism depending on the chemical similarity between the trace element (e.g., valence, ion radius) and the site occupied by the major element in the crystal structure.

Interpretation of the trace element signature of any system is complicated by the fact that trace element partitioning behavior is dependent on a number of parameters, including pressure (P), temperature (T), and composition. Therefore, the accuracy of predictive models is limited by the existence of a means for obtaining accurate values of partition coefficients for the system of interest. Equally important, these parameters are not independent of one another. Our understanding of the details of how partition coefficients are dependent on P, T, and composition,

Methodology: Erica W. Cung, Gokce K. Ustunisik, Aaron S. Wolf, Roger L. Nielsen
Project Administration: Gokce K. Ustunisik
Software: Aaron S. Wolf
Supervision: Gokce K. Ustunisik, Roger L. Nielsen
Visualization: Erica W. Cung, Gokce K. Ustunisik, Aaron S. Wolf, Roger L. Nielsen
Writing – original draft: Erica W. Cung, Gokce K. Ustunisik, Roger L. Nielsen
Writing – review & editing: Erica W. Cung, Gokce K. Ustunisik, Aaron S. Wolf, Roger L. Nielsen

and the degree of the interdependence of the controlling parameters is largely based on the results of laboratory experiments and limited by the degree to which they obtain equilibrium and may be analyzed precisely (Nielsen et al., 2017; Weiser et al., 2023). The results of experiments conducted at different *P*, *T*, and compositions can be used as the basis for the calculation of a numerical expression that describes how a trace element behaves over some definable range of conditions (e.g., Bédard, 2014; Mollo et al., 2018; Nielsen, 1988; Sun & Liang, 2012, 2013; Sun et al., 2017; Wood & Blundy, 2001; Yao et al., 2012). A complete treatment of trace element behavior requires that such expressions, calibrated to experimental data, exist for every element of interest in every phase present in the system of interest.

The accuracy and predictive power of these expressions depend on a number of factors, both analytical and theoretical. For example, using formation reactions (e.g., REEMgAlSiO$_6$; Nielsen, 1990) for the trace element components to calculate the partitioning behavior is rooted in the basic thermodynamics of mineral-melt phase equilibria, mass balance, substitution mechanisms, and site occupancy (Blundy & Wood, 2003; Ghiorso & Sack, 1995; Goldschmidt, 1937; Nielsen, 1988; Wood & Fraser, 1976). Such expressions include terms that approximate the activity of the phase components but require assumptions for correlations between composition and activity.

As new experimental data are generated, our ability to quantify trace element partitioning behavior should continuously improve. The increase in the number of experiments and enhanced analytical precision will, theoretically, allow us to develop quantitative models for trace element behavior appropriate for a wider range of natural conditions. However, that is only true if the additional data set adequately covers the range of possible natural magmatic compositions and that we understand how specific trace elements substitute into specific minerals based on regressions that include the parameters listed above and are calibrated to experimental data (e.g., Nielsen & Beard, 2000; Bédard, 2006; Blundy & Wood, 2003; Nielsen, 1988) and evaluated in terms of their ability to reproduce the calibration data set.

Many studies adopt the empirical regression modeling approach for trace element partitioning (e.g., Bédard, 2007; Nielsen et al., 2017) using the existing experimental database to calibrate predictive models. These investigations typically propose a variety of substitution mechanisms, regression types (linear, multiple) as well as a more or less formal treatment of analytical and experimental error. However, none have quantitatively evaluated the impact of differences in data coverage on the predictive power of these models. When different trace elements are analyzed in different numbers of experiments of varying composition, pressure, and temperature, we can reasonably expect that the resulting model accuracy and consistency will be compromised in ways that may not be obvious (e.g., irregularities between predicted rare earth element partition coefficients as a function of atomic number). The development of more accurate predictive models depends on our ability to identify how the differences between the data sets for individual elements influence the predictive power of potential models. Therefore, rather than developing new models for partitioning behavior, our focus is on the evaluation of the magnitude of the impact of calibration on different experimental data sets. An important aspect of this work is its role in ongoing efforts to develop a comprehensive and accessible trace element partitioning database (traceDs database—https://www.earthchem.org/communities/experimental-petrology/, Nielsen et al., 2015), which is part of the EarthChem/IEDA2 initiative to provide access to the results of both experimental and analytical information on natural earth materials (Profeta et al., 2023). The objective of this research is to use and expand the traceDs experimental data set to better understand the data characteristics for the minerals garnet, amphibole, and clinopyroxene. The data sets for each mineral were examined to identify the dependencies (e.g., how does $^{\text{mineral-melt}}D_i$ vary as a function of temperature, pressure, composition, substitution mechanism). The identity and magnitude of the differences between the partitioning behavior of each trace element in each phase can be quantified by comparing the regression parameters calculated from the data as a function of the number of experiments the compositional range of the data available for each element in those phases and the range of measured and predicted partition coefficients.

2. Compositional and Thermodynamic Controls on Trace Element Partitioning

This investigation focuses primarily on the partitioning behavior of the rare earth elements (REE) and the high field strength elements (HFSE) between clinopyroxene, amphibole, garnet, and melt. There are three reasons why REE and HFSE are selected for this study. First, REE have the same charge, +3 over much of the range of natural conditions (exceptions for Eu, Ce), but systematically decreasing ionic radii from La to Lu. Second, for HFSE, the ionic radius stays largely the same, but the ionic charge varies from +4 to +5. Third, these elements range

from mildly incompatible to compatible among these three phases. Therefore, these phases have a significant, if not controlling, influence on the evolution of the trace element signature of igneous systems (Green, 1994; Irving, 1978). Further, the behavior of these two groups of elements is systematic within the group, but their behavior differs from one phase to another (Nielsen, 1990).

To understand how different REE or HFSE substitute into a crystal structure and how that influences compositional dependence, we must first look into the characteristics of the lattice sites into which they substitute. In most cases, the general mechanism by which different trace elements substitute is known. What is less understood are the differences between how the substitution mechanism influences compositional, *T* and *P* dependences as well as behavioral differences for different minerals (Mollo et al., 2020). Before we can evaluate how partition coefficients vary by temperature, pressure, and composition, it is important that we review the structural context that dictates the substitution mechanism, which in turn controls how partitioning behavior is correlated to (or caused by) a given substitution pair.

Clinopyroxene is a single chain monoclinic inosilicate with the general formula of XYZ_2O_6. The Si_2O_6 chains are bonded to a layer of octahedrally coordinated cation bands, which also extend parallel to the c-axis. The octahedral sites consist of M1 (Y site) and M2 (X site) octahedra sandwiched between two chains of tetrahedral sites. The Y (M1) site is occupied by smaller cations Mn^{+2}, Fe^{+2}, Mg^{+2}, Al^{+3}, Cr^{+3}, or Ti^{+4}, where the X (M2) site properties depend on the symmetry of the crystal lattice. In monoclinic pyroxenes, the X (M2) site is a large distorted octahedral site occupied by the larger cations including Na^+, Ca^{+2} which are in eightfold coordination. The Z site is tetrahedrally coordinated and generally filled with Si^{+4} or Al^{+3}. The M1 cation strip is bonded to oxygen atoms of two oppositely oriented tetrahedral chains. Together, these form a tetrahedral-octahedral-tetrahedral (t-o-t) strip. Most trace elements with a charge of +1, +3, +4, or +5 substitute into M sites in pyroxene by paired substitution, most often with Al in either the *Y* (M1) site (paired with +1 ions in the X (M2) site) or with Al in the tetrahedral site for +3, +4, or +5 ions.

Amphibole is an inosilicate with doubled Si_4O_{11} chains running parallel to c-axis, with the general formula of $W_{0\text{-}1}X_2Y_5Z_8O_{22}(OH,F)_2$ (Leake et al., 1997). These chains are bonded to octahedral strips consisting of three regular octahedral sites (M1, M2, M3) and one larger 6- to 8-fold X (M4) site. In addition, there is an even larger 10- to 12-fold A (W) site that is either vacant or partially filled with Na^+ or K^+. The Z site is the tetrahedral site typically occupied by Si^{+4} or Al^{+3}. The relatively large X (M4) site accommodates Na^+, Ca^{+2}, Mn^{+2}, Fe^{+2}, Fe^{+3}, or Mg^{+2}. Four important substitutions that may occur in amphiboles are Al with Si; (Mg, Fe^{+2}) with (Al, Fe^{+3}); Na^+ with Ca^{+2}; and Na (K) into the A site (Beard et al., 2019; Hilyard et al., 2000). Nearly complete substitution takes place between Na^+ with Ca^{+2} and among Mg^{+2}, Fe^{+2}, and Mn^{+2}. There is limited substitution between Fe^{+3} and Al^{+3} and between Ti^{+4} and other Y site cations. Al^{+3} can partially substitute for Si^{+4} in the tetrahedral Z site. As a result of the complexity in its formula, amphiboles can be split into four groups that are dependent on the cation occupying the X site. These four subgroups are as follows: (a) iron-magnesium-manganese amphibole, (b) calcic amphibole, (c) sodic-calcic amphibole, and (d) sodic amphibole. The progression from tremolite-hornblende-tschermakite requires the substitution in the M4 and T sites of MgSi with AlAl. Edenite and pargasite can be derived from tremolite and hornblende by adding Na in the A site along with the substitution of Al^{+3} for Si^{+4} (Hilyard et al., 2000; Leake et al., 1997).

Garnet is a nesosilicate made up of alternating ZO_4 isolated tetrahedra and YO_6 octahedra bonded at the corners with the general formula of $X_3Y_2Z_3O_{12}$. The X site is usually occupied by divalent cations (Ca, Mg, Fe, Mn^{+2}) and the Y site by trivalent cations (Al, Fe, Cr^{+3}) in an octahedral and tetrahedral framework, respectively, with $(SiO_4)^{-4}$ occupying the tetrahedra site. An important difference in the substitution mechanism between garnet versus clinopyroxene and amphibole is the presence of octahedrally coordinated Si at high pressure (Hazen et al., 1994). The high-pressure garnet component (majorite) accommodates Si in the site normally occupied by Al, Fe, or Cr by a paired substitution with Mg ($Mg_3(MgSi)Si_3O_{12}$).

As noted above, expressions used for predicting partition behavior are based on experiments conducted under controlled conditions. Experimental determinations, as opposed to measurements based on phenocrysts/matrix, have the advantage that we control temperature, pressure, time, and composition. There are a number of different approaches that have been used to develop predictive models for trace element partitioning (Blundy & Wood, 2003). These methods involve regression analysis based on experimental data done within a framework of lattice strain, substitution mechanism together with thermodynamic constraints (Mollo et al., 2020; Wood & Fraser, 1977).

The development of quantitative models of trace element behavior requires that we decide which parameters have the greatest impact in our regressions. We can begin by considering the formation reaction for the trace element component in the mineral. Ideally, we could develop expressions that include an equilibrium constant based on that formation reaction. However, such an analysis depends on our understanding of the activity of the mineral and melt components, the impact of the substitution mechanism and lattice strain caused by the substitution (Blundy & Wood, 2003; Nielsen, 1988; Wood & Blundy, 1997; Wood & Fraser, 1976). For example, one may consider the formation reaction for a possible Sm component in clinopyroxene (cpx) (Nielsen, 1990):

$$SmO_{1.5}\,(NM) + AlO_{1.5}\,(NM) + SiO_2\,(NF) + FMO\,(NM) = SmFMAlSiO_6\,(cpx)$$

where NF and NM refer to network former and network modifier components, respectively, and FMO is FeO and MgO normalized to the sum of the NM. For the purposes of this investigation, NM and NF are as defined by Nielsen (1985), where Si, KAl, and NaAl complexes form networks with shared oxygens, and Mg, Fe, Ca, Ti, and Al above the sum of alkalis modify those networks by bonding with oxygen. This model assumes that the activity of components is proportional to the sum of cations with similar behavior. This reaction assumes that Sm occupies the M2 site in clinopyroxene, paired with Al in the T site for charge balance. The activity of the melt components was assumed to be related to the mole fraction of network formers (NF) and network modifiers (NM) in the melt (Nielsen, 1988). For trace element components, the values for the activity coefficient, enthalpy, and entropy are not experimentally determined. However, the equilibrium constant for the formation of samarium clinopyroxene can be approximated by the application of any one of a number of empirical models of activity (Nielsen, 1985) or lattice strain (Wood & Blundy, 2001) designed to accommodate aspects inherent in non-ideal mixing (cases where the activity coefficient is not unity).

Such models are only applicable for the range of composition for which they are calibrated. Extrapolation outside of the calibration data set can cause departure from the actual composition activity relations (e.g., will not accurately simulate the activity coefficients). Further, any such analysis can be complicated by differences in the configuration of the data set in terms of composition, experimental conditions and analytical error used to calibrate the models (number, range of P, T, composition of experiments). Since this investigation focuses on the nature of the impact of differences in calibration data on regression constants, we will apply the simplest description of partitioning behavior, the partition coefficient ($^{\text{mineral-melt}}D_{\text{i}}$), defined as follows:

$$D\text{i} = \frac{C_i^{\text{mineral}}}{C_i^{\text{melt}}}$$

where C is concentration. We will use this approximation to develop and evaluate a set of predictive models for trace element behavior by including terms that are based on observed dependencies of the partition coefficient on temperature, pressure, and a number of compositional parameters. The choice of compositional terms is based on the formation reaction of components involving specific trace elements in specific minerals. This approach can be first simplified into its most basic form that describes only a single dependence, for example, the temperature-dependence of the partition coefficient $^{\text{cpx-melt}}D_{\text{i}}$. To a first order (in temperature), the mineral-melt partition coefficient ($^{\text{mineral-melt}}D_{\text{i}}$) can be expressed in terms of reciprocal temperature (1/T) in this equation:

$$\ln^{\text{mineral}-\text{melt}} D_{\text{i}} = \frac{a}{T} + +\text{b}$$

where a is a proxy for enthalpy (H) and b is a proxy for entropy (S) as per the basic expression for the equilibrium constant for the trace element component formation reaction at constant pressure.

$$\text{RTlnK} = \Delta\text{H}^0 - \text{T}\Delta\text{S}^0$$

Since we understand that charge balance is required for many formation reactions (Wood & Blundy, 2001), and we are using concentration rather than activity to describe partitioning behavior, we expect that ln D_{i} will be dependent on the concentration (as well as a number of other parameters) of the charge balancing component—Al in the case of most REE and HFSE (Mollo et al., 2020).

Our approach will be to examine the impact of specific characteristics of the calibration data set on the regression parameters that constitute the core of predictive models. In effect, we asked "How sensitive are regression

parameters to differences in the data set characteristics, including analytical and experimental uncertainty, the number of experiments and the range of composition represented by these experiments?" We will examine the patterns within the regression parameters describing known dependencies within groups of trace elements (e.g., REE) and what those patterns can tell us about the magnitude of difference sources of uncertainty as well as possible pathways to improving the predictive power of models for trace element behavior. The specific patterns can be interpreted using the trends observed within the regression parameters for each element in each phase as well as the correlation of calculated and experimental values. For example, based on the systematic changes in ionic radius within the REE, the regression parameters describing temperature dependence should either be constant or change systematically. If the regression parameters that define the dependencies vary irregularly between elements with similar ionic radius and charge, then any predictive model based on those parameters will result in modeled behavior that is irregular (e.g., not a smooth pattern of predicted partition coefficients across the REE).

There are a number of data characteristics that may result in deviation from predicted patterns. The specific differences in experimental data include the number of experimental determinations for each element in each mineral, analytical uncertainty based on count rate, analytical uncertainty related to analytical volume, experimental error (disequilibrium, errors in method) and the average phase composition for the data available for each element in each phase (e.g., average SiO_2 of the liquids in all experiments where Sr was determined for clinopyroxene and co-existing melt; Nielsen et al., 2020). Finally, the efficacy of the model used to describe the dependencies (melt component activity model, elastic strain, assumed substitution mechanism, etc.) can produce bias in the predictive models (Nielsen et al., 2017). Each of these sources of uncertainty will impact the predictive characteristics of the regression constants and the patterns of calculated/experimental values exhibited using the calibration data.

Analytical error related to counting statistics will result in symmetrically distributed error about the average value, not in irregularity of the patterns within a group of elements where there is expectation of systematic behavior (e.g., REE, HFSE, LILE). In contrast, analytical error related to the presence of multiple phases in the analytical volume (e.g., caused by inclusions of more than one phase—typically glass in this context) represents an unmodeled source of variation. Analysis of different points by electron microprobe (EMP) versus laser ablation inductively coupled plasma mass spectrometry (laser ICP-MS) or secondary ion mass spectrometry (SIMS) will cause the trend of calculated versus experimental values for incompatible elements to exhibit a slope less than 1:1 because the experimental values are elevated by the inclusion of glass. Further, both types of uncertainty would result in more scatter for elements with lower average partition coefficients (assuming that concentration is related to analytical accuracy/precision; Nielsen et al., 2017).

Compositional dependencies are accommodated in trace element models by the application of constraints ranging from melt component activity models to elastic strain models (Blundy & Wood, 2003; Nielsen et al., 2017). If there is a systematic compositional dependence on the partition coefficients that is not accounted for by the parameters in the regression, the result will scatter in the distribution of calculated versus experimental values, which will also manifest in the form of a correlation of calculated versus experimental values with slopes less than 1, underestimating the values from experiments with high partition coefficients and overestimating values from experiments with low partition coefficients. However, unlike the scatter generated by analytical error, the magnitude of the scatter, and the average ability of the model to reproduce the calibration data, will not increase as the average partition coefficient decreases. This is because the uncertainty in the model will not be a function of the concentration of the trace element but rather a function of the character of the substitution mechanism, crystal lattice strain structure and melt component activity—all of which should be similar within groups of elements such as the REE for partition coefficient between any specific phase and melt.

The impact of this research lies in two areas. First, the systematic analysis of the existing database for each element in each phase will identify where the differences lie in the experimental data for each element in each phase. Second, the comparison of the regression parameters and basic predictive models for each element in each phase will inform our understanding of the influence of the different data set characteristics, including analytical error, on the accuracy and precision of such models, and how our collective choices on what systems we work on and the selection of elements we measure may influence the outcomes of different types of predictive modeling.

3. Methodology

To address the question above, we updated the LEPR/traceDs database to include experimental data published since the last major revision (Nielsen et al., 2017). Once the compilation was updated, the data characteristics for the trace element partitioning experiments involving clinopyroxene, garnet, and amphibole were calculated and assessed for a range of trace elements, including the REE and HFSE. Those data characteristics include the number of experimental determinations for each trace element in each phase (melt and mineral of interest), as well as the average and standard deviation of the major element composition of the phases present in each trace element's database. A major challenge in conducting the tests described above is the variety of analytical tools and methods used to analyze trace element experimental charges, as well as the lack of a consistent method for presentation of error estimates in the literature.

The initial phase of the interpretation was based on the correlation of the calculated natural logarithm of partition coefficients for each element of interest (ln $^{\text{mineral-melt}}D_i$) for all three phases, which are the focus of this investigation. We then calculated the correlation of (ln $^{\text{mineral-melt}}D_i$) with a range of compositional and experimental parameters. The results of that analysis were applied to understand the systematic behavior within two groups of trace elements, REE and HFSE, by investigating whether the regression parameters increase or decrease systematically within the REE as a function of ionic radius, and whether there is a difference in the regression coefficients within the HFSE and between the HFSE and REE that might be attributable to how the different charge balance requirements for +3, +4, and +5 ions manifest, and how they may differ for trace elements with +1 or +2 valence.

Finally, in addition to studying the temperature dependencies and single term linear regression (LR) of the data, we calculated multiple linear regression (MLR) parameters by including the dependencies proposed by earlier investigators as well as those observed in the linear regression analysis described below. We then compared the predictive power of each approach for each element in each of the three phases of interest using the calibration data as unknowns and comparing the patterns exhibited in the correlation of calculated ln D versus experimental determinations.

4. Results

4.1. Database Characteristics

Under ideal circumstances, the calibration data set from which we calculate constraints on trace element behavior would be similar for each element of interest in terms of the range of composition, experimental conditions, number of experimental determinations, and analytical methods applied. For example, the number of experiments in the literature, the average phase composition and the range of conditions where REE were determined in clinopyroxene and melt would be the same for all the REE (e.g., the amount of data for La and Lu would be equal). However, for each set of experiments, the investigator has different goals, and their experimental conditions and analytical protocols for run products are designed to serve these goals. This has resulted in a heterogenous experimental database where the number of experiments for any specific element is highly variable (Nielsen et al., 2017). What is not known is whether this heterogenous data set characteristic impacts our ability to develop models that can "see through" any element-to-element differences in the experimental data.

Before we attempt to understand this potential source of bias, we must first quantitatively characterize the database. It is generally presumed (Nielsen, 1990) that to calibrate predictive models, we must use a database that covers the range of T, P, and major and minor element composition to which we plan to apply the model. Due to the distinct focus of each experimental study, the database presents highly uneven coverage of the range of conditions we wish to model. This can be demonstrated by examining the experimental database characteristics for each trace element (Figures 1a–1f; Table 1). For example, the average total alkali content in liquids for which Ta has been determined in clinopyroxene and coexisting glass (Figures 1a and 1b; Table 1a) is half of the value for Er (Table 1a). Further, the average temperature for experiments with measured Ta is 100°C lower than that for Er. Even though the number of experimental determinations for Ta and Er cpx/liquid partitioning is roughly equal (74 and 85, respectively), this is not true for all commonly analyzed trace elements, with the number of cpx/liquid experiments ranging from 35 to over 300 (Table 1a). It is important to note at this point that our focus is on the number of reported experimental determinations, not the number of analyses obtained from each experiment. The convention has been to report averages based on multiple measurements from each phase present in each experimental charge. That number combines the uncertainties related to disequilibrium, counting statistics, and calibration-related error (Nielsen et al., 2017).

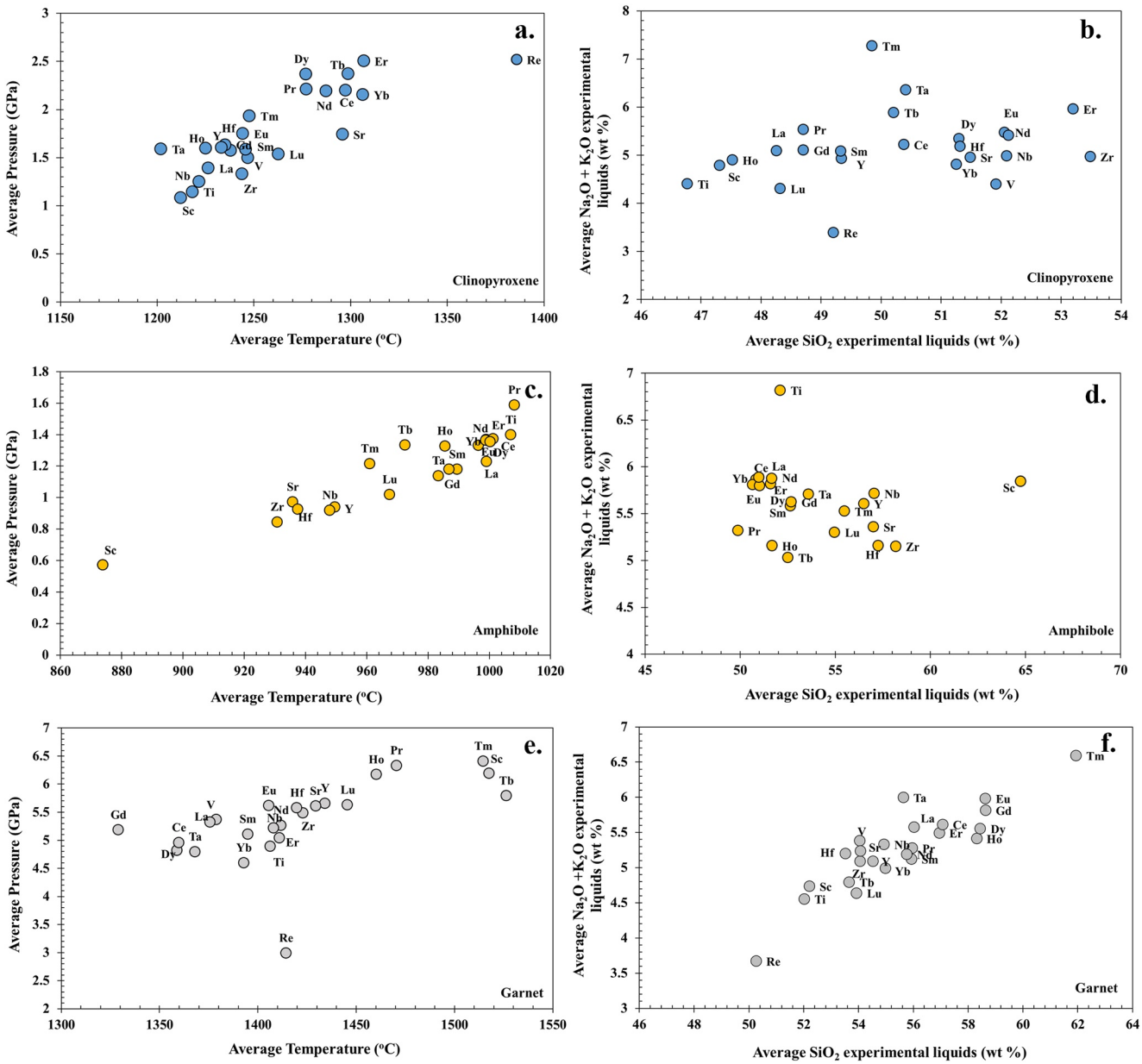

Figure 1. The average melt silica vs. total alkali content and average temperature vs. pressure range for mineral/melt trace element partitioning experiments where trace elements were measured in (a, b) clinopyroxene, (c, d) amphibole, and (e, f) garnet. Each symbol represents the average liquid composition or P/T condition specific to a particular element as determined from the LEPR/traceDs database. For example, the average liquid composition for all experiments where Gd was measured in clinopyroxene, and co-existing melt is 49 wt. % SiO_2 and 5 wt. % $Na_2O + K_2O$. These values are reported in Table 1 along with the 1 sigma (s) standard deviation on the average.

The amphibole/melt partitioning data (Figures 1c and 1d; Table 1b) exhibit an equivalent but slightly narrower range of average glass composition and experimental conditions compared to that for clinopyroxene. This difference is attributable to the relatively small field of phase stability for amphibole versus clinopyroxene. In addition, the comparative position in compositional space and experimental conditions for specific elements is different. For example, the average glass composition for amphibole-melt Sc partitioning data is near the highest alkali and SiO_2 end of the distribution, while the equivalent value for clinopyroxene is near the lowest.

The garnet partitioning data also exhibit a distinct range of glass composition and experimental conditions (Figures 1e and 1f; Table 1c). The average experimental pressure and temperature are higher than for either clinopyroxene or amphibole, as one would predict based on our understanding of garnet phase stability. Again, the distribution of

Geochemistry, Geophysics, Geosystems

10.1029/2023GC010876

Table 1
Description of the Experimental Trace Element Partitioning Database Used in This Study

Element	Atomic number	Number of experiments	Number of investigations	Temperature	Pressure	SiO_2[a]	TiO_2	Al_2O_3	Cr_2O_3	FeO	MnO	MgO	CaO	Na_2O	K_2O	P_2O_5
(a) Clinopyroxene																
Sc	21	193	24	1212 (*172*)	1.1 (*1.8*)	47.32 (*7.84*)	2.17 (*1.3*)	16.1 (*4.29*)	0.11 (*0.17*)	8.78 (*5.38*)	0.19 (*0.19*)	6.8 (*4.15*)	9.72 (*4.74*)	3.22 (*1.31*)	1.56 (*1.69*)	0.71 (*0.58*)
Ti	22	304	28	1218 (*159*)	1.1 (*1.3*)	46.77 (*6.34*)	2.42 (*1.13*)	16.53 (*3.98*)	0.08 (*0.06*)	9.23 (*4.36*)	0.18 (*0.06*)	6.55 (*3.37*)	9.93 (*4.28*)	3.29 (*1.41*)	1.11 (*0.95*)	0.68 (*0.56*)
V	23	148	26	1247 (*179*)	1.5 (*1.9*)	51.92 (*7.54*)	1.82 (*1.39*)	13.8 (*3.14*)	0.12 (*0.18*)	7.68 (*5.69*)	0.21 (*0.23*)	7.35 (*4.57*)	11.09 (*6*)	2.78 (*1.53*)	1.61 (*1.92*)	0.44 (*0.54*)
Sr	38	206	39	1296 (*177*)	1.7 (*1.8*)	51.49 (*6.1*)	2.27 (*1.45*)	14.42 (*3.24*)	0.18 (*0.26*)	9.04 (*5.62*)	0.19 (*0.23*)	5.76 (*3.42*)	9.44 (*4.18*)	3.17 (*1.77*)	1.78 (*2.2*)	0.39 (*0.37*)
Y	39	233	34	1238 (*186*)	1.6 (*1.7*)	49.34 (*7.52*)	2.32 (*1.42*)	15.61 (*3.45*)	0.17 (*0.24*)	8.79 (*4.79*)	0.18 (*0.17*)	5.73 (*3.74*)	8.93 (*4.21*)	3.3 (*1.61*)	1.63 (*1.82*)	0.57 (*0.55*)
Zr	40	285	42	1244 (*168*)	1.3 (*1.6*)	53.49 (*7.16*)	2.4 (*2.18*)	13.91 (*3.07*)	0.15 (*0.2*)	7.86 (*5.33*)	0.19 (*0.19*)	6.71 (*4.16*)	10.41 (*5.11*)	3.31 (*2*)	1.66 (*2.08*)	0.4 (*0.34*)
Nb	41	173	28	1222 (*176*)	1.2 (*1.5*)	52.1 (*6.99*)	2.82 (*2.47*)	13.52 (*3.18*)	0.19 (*0.25*)	7.95 (*5.96*)	0.2 (*0.21*)	6.68 (*4.76*)	10.2 (*5.2*)	3.2 (*1.88*)	1.78 (*2.11*)	0.42 (*0.35*)
La	**57**	**244**	**38**	**1226 (*157*)**	**1.4 (*1.6*)**	**48.26 (*7.3*)**	**2.13 (*1.36*)**	**16.45 (*3.76*)**	**0.1 (*0.17*)**	**8.61 (*4.71*)**	**0.18 (*0.17*)**	**5.93 (*3.24*)**	**9.24 (*4.4*)**	**3.34 (*1.65*)**	**1.75 (*1.99*)**	**0.67 (*0.55*)**
Ce	**58**	**127**	**28**	**1298 (*189*)**	**2.2 (*2*)**	**50.38 (*5.6*)**	**2.15 (*1.56*)**	**14.7 (*2.99*)**	**0.18 (*0.24*)**	**8.99 (*5.67*)**	**0.2 (*0.24*)**	**6.5 (*4.25*)**	**10.36 (*5.63*)**	**3.25 (*2*)**	**1.96 (*2.28*)**	**0.38 (*0.36*)**
Pr	**59**	**50**	**11**	**1277 (*230*)**	**2.2 (*2.8*)**	**48.71 (*5.79*)**	**2.03 (*1.38*)**	**13.72 (*3.81*)**	**0.06 (*0.04*)**	**10.01 (*7.99*)**	**0.27 (*0.34*)**	**5.7 (*3.54*)**	**10.83 (*5.18*)**	**2.59 (*1.56*)**	**2.93 (*2.75*)**	**0.52 (*0.42*)**
Nd	**60**	**143**	**32**	**1287 (*190*)**	**2.2 (*1.9*)**	**52.06 (*6.97*)**	**1.96 (*1.44*)**	**14.49 (*3.29*)**	**0.17 (*0.23*)**	**8.45 (*5.75*)**	**0.19 (*0.23*)**	**6 (*4.11*)**	**9.15 (*4.85*)**	**3.32 (*1.89*)**	**2.15 (*2.51*)**	**0.36 (*0.35*)**
Sm	**62**	**201**	**38**	**1246 (*171*)**	**1.6 (*1.6*)**	**49.33 (*7.03*)**	**2.08 (*1.42*)**	**15.71 (*3.51*)**	**0.12 (*0.18*)**	**8.25 (*4.81*)**	**0.2 (*0.19*)**	**6.11 (*3.71*)**	**9.29 (*4.52*)**	**3.24 (*1.71*)**	**1.84 (*2.06*)**	**0.5 (*0.44*)**
Eu	**63**	**105**	**23**	**1244 (*182*)**	**1.7 (*2*)**	**52.13 (*7.47*)**	**1.65 (*1.51*)**	**14.65 (*3.24*)**	**0.15 (*0.21*)**	**7.47 (*6.56*)**	**0.2 (*0.27*)**	**6.39 (*4.24*)**	**9.92 (*5.89*)**	**3.03 (*1.94*)**	**2.38 (*2.66*)**	**0.37 (*0.4*)**
Gd	**64**	**142**	**23**	**1235 (*181*)**	**1.6 (*2.1*)**	**48.71 (*7.7*)**	**2.15 (*1.42*)**	**15.8 (*3.52*)**	**0.17 (*0.19*)**	**8.6 (*5.03*)**	**0.2 (*0.16*)**	**5.46 (*3.17*)**	**8.94 (*4.42*)**	**3.24 (*1.63*)**	**1.86 (*1.96*)**	**0.56 (*0.47*)**
Tb	**65**	**47**	**11**	**1299 (*225*)**	**2.4 (*2.4*)**	**50.22 (*7.2*)**	**1.63 (*1*)**	**13.99 (*3.5*)**	**0.06 (*0.04*)**	**8.46 (*6.24*)**	**0.22 (*0.31*)**	**6.45 (*3.65*)**	**10.18 (*5.22*)**	**2.95 (*1.47*)**	**2.94 (*2.8*)**	**0.46 (*0.45*)**
Dy	**66**	**105**	**23**	**1277 (*199*)**	**2.4 (*2.1*)**	**51.3 (*6.69*)**	**2.12 (*1.47*)**	**14.45 (*2.98*)**	**0.18 (*0.26*)**	**8.81 (*5.91*)**	**0.2 (*0.25*)**	**5.18 (*3.2*)**	**9.01 (*4.5*)**	**3.24 (*1.74*)**	**2.1 (*2.33*)**	**0.41 (*0.37*)**
Ho	**67**	**108**	**17**	**1225 (*182*)**	**1.6 (*2*)**	**47.53 (*6.1*)**	**1.77 (*1.07*)**	**15.77 (*3.79*)**	**0.07 (*0.06*)**	**8.72 (*5.66*)**	**0.23 (*0.24*)**	**6.11 (*3.13*)**	**9.73 (*4.02*)**	**3 (*1.48*)**	**1.9 (*2.17*)**	**0.62 (*0.5*)**
Er	**68**	**85**	**23**	**1307 (*201*)**	**2.5 (*2.2*)**	**53.21 (*7.77*)**	**1.77 (*1.51*)**	**14.83 (*2.88*)**	**0.18 (*0.24*)**	**7.1 (*4.51*)**	**0.14 (*0.11*)**	**5.94 (*4.4*)**	**8.39 (*4.82*)**	**3.41 (*1.42*)**	**2.55 (*2.62*)**	**0.33 (*0.27*)**
Tm	**69**	**37**	**8**	**1248 (*262*)**	**1.9 (*3*)**	**49.85 (*5.15*)**	**1.66 (*1.27*)**	**14.61 (*3.41*)**	**0.05 (*0.04*)**	**7.8 (*6.02*)**	**0.21 (*0.18*)**	**5.59 (*2.61*)**	**11.77 (*6.49*)**	**3.59 (*3.13*)**	**3.68 (*2.58*)**	**0.43 (*0.07*)**
Yb	**70**	**180**	**35**	**1306 (*174*)**	**2.2 (*1.8*)**	**51.26 (*6.6*)**	**1.85 (*1.26*)**	**15.25 (*3.45*)**	**0.16 (*0.21*)**	**8.53 (*5.81*)**	**0.18 (*0.22*)**	**7.66 (*4.61*)**	**10.66 (*5.52*)**	**3.2 (*1.52*)**	**1.61 (*2.28*)**	**0.33 (*0.29*)**
Lu	**71**	**178**	**26**	**1263 (*160*)**	**1.5 (*1.6*)**	**48.32 (*5.34*)**	**2.02 (*1.32*)**	**15.63 (*3.33*)**	**0.08 (*0.08*)**	**9.07 (*4.88*)**	**0.2 (*0.2*)**	**6.94 (*3.62*)**	**10.01 (*3.72*)**	**2.95 (*1.37*)**	**1.35 (*1.66*)**	**0.43 (*0.35*)**
Hf	72	160	31	1233 (*191*)	1.6 (*1.8*)	51.32 (*6.59*)	1.61 (*1.19*)	14.39 (*3.01*)	0.15 (*0.2*)	7.3 (*5.85*)	0.19 (*0.22*)	6.97 (*4.71*)	10.3 (*5.39*)	3.31 (*1.88*)	1.86 (*2.22*)	0.33 (*0.36*)
Ta	73	74	22	1202 (*142*)	1.6 (*1.5*)	50.42 (*6.14*)	2.11 (*1.57*)	14.76 (*3.46*)	0.21 (*0.3*)	8.32 (*7.3*)	0.25 (*0.33*)	5.56 (*3.9*)	9.96 (*5.19*)	3.57 (*2.42*)	2.79 (*2.65*)	0.45 (*0.39*)
Re	75	35	3	1386 (*68*)	2.5 (*0.8*)	49.21 (*2.44*)	1.79 (*1.01*)	18.47 (*1.95*)	0.26	6.95 (*1.82*)	0.12 (*0.05*)	12.15 (*2.48*)	12.16 (*2.14*)	3.25 (*0.48*)	0.14 (*0.11*)	0.28 (*0.11*)
(b) Amphibole																
Sc	21	36	3	874 (*62*)	(*0.5*)0.6	64.76 (*4.58*)	0.35 (*0.24*)	15.74 (*2.65*)	0.05 (*0.03*)	2.29 (*1.49*)	0.13 (*0.04*)	0.75 (*0.59*)	3.45 (*1.23*)	4.53 (*0.96*)	1.32 (*0.49*)	0.1 (*0.08*)
Ti	22	37	4	1007 (*42*)	1.4 (*0.3*)	52.12 (*6.36*)	1.75 (*1.25*)	18.2 (*2.22*)	0.05 (*0.03*)	8.2 (*3.83*)	0.09 (*0.04*)	2.58 (*1.63*)	4.93 (*1.97*)	4.47 (*1.46*)	2.35 (*1.03*)	0.25
V	23	36	3	874 (*62*)	0.6 (*0.5*)	64.76 (*4.58*)	0.35 (*0.24*)	15.74 (*2.65*)	0.05 (*0.03*)	2.29 (*1.49*)	0.13 (*0.04*)	0.75 (*0.59*)	3.45 (*1.23*)	4.53 (*0.96*)	1.32 (*0.49*)	0.1 (*0.08*)
Sr	38	62	8	936 (*96*)	1 (*0.7*)	57.02 (*11.07*)	1.01 (*1.21*)	15.98 (*2.54*)	0.04 (*0.03*)	4.04 (*3.02*)	0.14 (*0.05*)	2.54 (*2.86*)	5.29 (*2.93*)	3.96 (*1.25*)	1.4 (*0.51*)	0.19 (*0.36*)
Y	39	83	8	950 (*88*)	0.9 (*0.6*)	56.51 (*9.94*)	1.31 (*1.34*)	16.46 (*2.37*)	0.05 (*0.03*)	5.17 (*4.08*)	0.13 (*0.04*)	2.15 (*2.54*)	4.92 (*2.54*)	4.01 (*1.32*)	1.59 (*0.99*)	0.21 (*0.34*)
Zr	40	80	9	931 (*87*)	0.8 (*0.7*)	58.19 (*10.16*)	0.88 (*1.14*)	16.37 (*2.58*)	0.04 (*0.03*)	3.62 (*2.9*)	0.14 (*0.04*)	2.19 (*2.78*)	5.32 (*2.79*)	3.95 (*1.19*)	1.2 (*0.59*)	0.21 (*0.34*)
Nb	41	83	8	948 (*86*)	0.9 (*0.6*)	57.05 (*9.35*)	1.18 (*1.27*)	16.59 (*2.46*)	0.05 (*0.03*)	5.07 (*4.14*)	0.14 (*0.04*)	1.96 (*2.18*)	4.76 (*2.41*)	4.12 (*1.27*)	1.59 (*1.01*)	0.21 (*0.34*)
La	**57**	**98**	**11**	**999 (*61*)**	**1.2 (*0.5*)**	**51.66 (*7.93*)**	**1.82 (*1.27*)**	**17.07 (*2.05*)**	**0.04 (*0.03*)**	**7.24 (*3.96*)**	**0.13 (*0.04*)**	**2.86 (*2.41*)**	**5.47 (*2.45*)**	**3.91 (*1.43*)**	**1.96 (*1.07*)**	**0.32 (*0.4*)**
Ce	**58**	**52**	**7**	**1000 (*67*)**	**1.4 (*0.5*)**	**51 (*8.59*)**	**1.91 (*1.39*)**	**17.11 (*2.34*)**	**0.05 (*0.03*)**	**7.37 (*3.81*)**	**0.13 (*0.05*)**	**3.24 (*2.72*)**	**5.61 (*2.91*)**	**3.86 (*1.63*)**	**2.02 (*0.97*)**	**0.34 (*0.52*)**

Geochemistry, Geophysics, Geosystems

10.1029/2023GC010876

Table 1
Continued

Element	Atomic number	Number of experiments	Number of investigations	Temperature	Pressure	SiO_2[a]	TiO_2	Al_2O_3	Cr_2O_3	FeO	MnO	MgO	CaO	Na_2O	K_2O	P_2O_5
Pr	**59**	**17**	**3**	**1008 (*69*)**	**1.6 (*0.7*)**	**49.89 (*13.11*)**	**2.17 (*1.62*)**	**17.34 (*3.12*)**	**0.05 (*0.03*)**	**6.07 (*3*)**	**0.12 (*0.06*)**	**4.66 (*4.11*)**	**7.22 (*4.06*)**	**3.8 (*2.25*)**	**1.52 (*0.56*)**	**0.47 (*0.73*)**
Nd	**60**	**52**	**7**	**1000 (*67*)**	**1.4 (*0.5*)**	**51 (*8.59*)**	**1.91 (*1.39*)**	**17.11 (*2.34*)**	**0.05 (*0.03*)**	**7.37 (*3.81*)**	**0.13 (*0.05*)**	**3.24 (*2.72*)**	**5.61 (*2.91*)**	**3.86 (*1.63*)**	**2.02 (*0.97*)**	**0.34 (*0.52*)**
Sm	**62**	**75**	**10**	**990 (*66*)**	**1.2 (*0.6*)**	**52.65 (*8.68*)**	**1.6 (*1.28*)**	**17.08 (*2.15*)**	**0.04 (*0.03*)**	**6.26 (*3.89*)**	**0.13 (*0.05*)**	**2.76 (*2.62*)**	**5.6 (*2.64*)**	**3.8 (*1.41*)**	**1.78 (*1.02*)**	**0.28 (*0.37*)**
Eu	**63**	**49**	**5**	**999 (*68*)**	**1.4 (*0.5*)**	**50.84 (*9.05*)**	**2 (*1.42*)**	**17.02 (*2.34*)**	**0.05 (*0.03*)**	**7.31 (*3.89*)**	**0.13 (*0.05*)**	**3.32 (*2.97*)**	**5.57 (*2.99*)**	**3.81 (*1.69*)**	**2.05 (*0.95*)**	**0.29 (*0.52*)**
Gd	**64**	**60**	**5**	**987 (*66*)**	**1.2 (*0.6*)**	**52.69 (*9.11*)**	**1.72 (*1.41*)**	**17.25 (*2.23*)**	**0.05 (*0.03*)**	**6.33 (*4.11*)**	**0.12 (*0.04*)**	**2.79 (*2.92*)**	**5.52 (*2.73*)**	**3.81 (*1.54*)**	**1.81 (*1.08*)**	**0.3 (*0.41*)**
Tb	**65**	**24**	**3**	**973 (*85*)**	**1.3 (*0.7*)**	**52.52 (*12.37*)**	**1.64 (*1.64*)**	**16.84 (*2.8*)**	**0.05 (*0.03*)**	**4.88 (*3.04*)**	**0.13 (*0.05*)**	**3.82 (*3.95*)**	**6.37 (*3.8*)**	**3.48 (*1.89*)**	**1.55 (*0.49*)**	**0.29 (*0.52*)**
Dy	**66**	**51**	**6**	**999 (*66*)**	**1.4 (*0.5*)**	**51.04 (*9.04*)**	**1.95 (*1.41*)**	**17.05 (*2.3*)**	**0.05 (*0.03*)**	**7.24 (*3.83*)**	**0.13 (*0.05*)**	**3.29 (*2.92*)**	**5.62 (*2.96*)**	**3.77 (*1.67*)**	**2.03 (*0.96*)**	**0.29 (*0.5*)**
Ho	**67**	**38**	**7**	**986 (*82*)**	**1.3 (*0.7*)**	**51.69 (*10.9*)**	**1.61 (*1.36*)**	**16.59 (*2.44*)**	**0.04 (*0.03*)**	**5.38 (*2.98*)**	**0.13 (*0.05*)**	**3.75 (*3.4*)**	**6.41 (*3.22*)**	**3.55 (*1.53*)**	**1.61 (*0.5*)**	**0.31 (*0.48*)**
Er	**68**	**51**	**6**	**1001 (*68*)**	**1.4 (*0.5*)**	**50.68 (*8.91*)**	**1.99 (*1.4*)**	**16.98 (*2.32*)**	**0.05 (*0.03*)**	**7.29 (*3.82*)**	**0.13 (*0.05*)**	**3.38 (*2.95*)**	**5.66 (*2.97*)**	**3.8 (*1.67*)**	**2 (*0.97*)**	**0.33 (*0.51*)**
Tm	**69**	**25**	**4**	**961 (*85*)**	**1.2 (*0.7*)**	**55.5 (*10.36*)**	**1.2 (*1.27*)**	**17.22 (*2.79*)**	**0.05 (*0.03*)**	**4.83 (*3.09*)**	**0.14 (*0.05*)**	**2.75 (*2.95*)**	**5.51 (*3.33*)**	**3.94 (*1.75*)**	**1.59 (*0.52*)**	**0.41 (*0.57*)**
Yb	**70**	**54**	**7**	**997 (*66*)**	**1.3 (*0.5*)**	**51.61 (*8.72*)**	**1.84 (*1.38*)**	**17.23 (*2.29*)**	**0.05 (*0.03*)**	**7.28 (*3.78*)**	**0.13 (*0.05*)**	**3.17 (*2.66*)**	**5.69 (*2.95*)**	**3.81 (*1.61*)**	**2 (*0.97*)**	**0.31 (*0.51*)**
Lu	**71**	**48**	**7**	**967 (*74*)**	**1 (*0.7*)**	**54.97 (*9.52*)**	**1.18 (*1.11*)**	**16.99 (*2.25*)**	**0.04 (*0.03*)**	**4.45 (*3.07*)**	**0.13 (*0.05*)**	**2.41 (*2.82*)**	**5.64 (*2.65*)**	**3.88 (*1.32*)**	**1.42 (*0.71*)**	**0.32 (*0.4*)**
Hf	72	78	7	938 (*87*)	0.9 (*0.7*)	57.26 (*10.18*)	0.94 (*1.08*)	16.17 (*2.34*)	0.03 (*0.03*)	4.15 (*3.23*)	0.14 (*0.04*)	2.23 (*2.66*)	5.32 (*2.63*)	3.92 (*1.15*)	1.24 (*0.53*)	0.19 (*0.33*)
Ta	73	61	6	983 (*66*)	1.1 (*0.6*)	53.6 (*8.67*)	1.55 (*1.37*)	17.35 (*2.28*)	0.05 (*0.03*)	6.13 (*4.23*)	0.13 (*0.04*)	2.48 (*2.57*)	5.35 (*2.63*)	3.94 (*1.48*)	1.76 (*1.08*)	0.31 (*0.41*)
(c) Garnet																
Sc	21	68	17	1518 (*362*)	6.2 (*5*)	52.22 (*9.41*)	1.78 (*2.64*)	12.02 (*5.1*)	0.13 (*0.17*)	8.59 (*6.96*)	0.1 (*0.08*)	10.93 (*9.79*)	7.36 (*5.22*)	3.58 (*2.23*)	1.16 (*1.05*)	0.48 (*0.57*)
Ti	22	57	17	1406 (*340*)	4.9 (*5*)	52.02 (*5.78*)	1.87 (*1.81*)	14.21 (*5.36*)	0.14 (*0.1*)	6.91 (*4.44*)	0.1 (*0.08*)	9.71 (*10.94*)	8.09 (*5.53*)	3.68 (*2.04*)	0.87 (*0.99*)	0.37 (*0.34*)
V	23	53	11	1379 (*352*)	5.4 (*5.1*)	54.06 (*6.41*)	1.91 (*1.55*)	13.46 (*3.98*)	0.15 (*0.2*)	5.64 (*3.18*)	0.1 (*0.13*)	7.08 (*9.32*)	6.15 (*3.37*)	3.93 (*1.79*)	1.45 (*1.15*)	0.34 (*0.38*)
Sr	38	71	22	1430 (*361*)	5.6 (*5.2*)	54.07 (*9.32*)	1.91 (*2.6*)	13.46 (*4.62*)	0.14 (*0.19*)	6.66 (*5.07*)	0.09 (*0.07*)	7.2 (*7*)	7.96 (*5.21*)	3.93 (*1.96*)	1.3 (*1.08*)	0.45 (*0.69*)
Y	39	109	26	1434 (*363*)	5.7 (*5.1*)	54.53 (*9.5*)	1.82 (*2.25*)	12.92 (*4.9*)	0.17 (*0.19*)	7.31 (*5.92*)	0.09 (*0.07*)	8.54 (*9.89*)	6.55 (*4.7*)	3.39 (*1.92*)	1.69 (*1.82*)	0.5 (*0.51*)
Zr	40	116	29	1423 (*358*)	5.5 (*4.9*)	54.06 (*9.44*)	1.81 (*2.17*)	13.07 (*4.78*)	0.14 (*0.18*)	7.4 (*5.72*)	0.1 (*0.07*)	8.32 (*9.54*)	6.57 (*4.57*)	3.39 (*1.86*)	1.7 (*1.76*)	0.49 (*0.5*)
Nb	41	71	22	1408 (*346*)	5.2 (*4.8*)	54.94 (*8.94*)	1.82 (*2.03*)	13.56 (*4.74*)	0.23 (*0.21*)	6.49 (*4.41*)	0.08 (*0.07*)	8.06 (*9.13*)	7.28 (*5.32*)	3.88 (*2.04*)	1.45 (*1.9*)	0.35 (*0.36*)
La	**57**	**82**	**23**	**1376 (*386*)**	**5.3 (*5.4*)**	**56.03 (*9.31*)**	**1.76 (*1.67*)**	**13.39 (*4.38*)**	**0.16 (*0.2*)**	**5.67 (*4.04*)**	**0.09 (*0.06*)**	**7.03 (*8.33*)**	**7.5 (*5.25*)**	**3.85 (*1.82*)**	**1.73 (*1.25*)**	**0.54 (*0.74*)**
Ce	**58**	**90**	**22**	**1360 (*360*)**	**5 (*4.9*)**	**57.08 (*9*)**	**1.76 (*1.58*)**	**13.55 (*3.53*)**	**0.18 (*0.2*)**	**5.75 (*3.67*)**	**0.08 (*0.06*)**	**5.72 (*6.62*)**	**6.37 (*3.61*)**	**3.72 (*1.72*)**	**1.89 (*1.71*)**	**0.42 (*0.52*)**
Pr	**59**	**51**	**12**	**1471 (*409*)**	**6.3 (*6.1*)**	**55.97 (*11.28*)**	**1.84 (*1.15*)**	**12.54 (*4.36*)**	**0.08 (*0.08*)**	**6.87 (*4.32*)**	**0.13 (*0.05*)**	**8.22 (*7.81*)**	**9.13 (*5.27*)**	**3.17 (*1.54*)**	**2.11 (*1.26*)**	**0.86 (*0.85*)**
Nd	**60**	**109**	**23**	**1412 (*373*)**	**5.3 (*4.7*)**	**55.76 (*10.28*)**	**1.72 (*2.18*)**	**12.38 (*4.78*)**	**0.18 (*0.19*)**	**7.92 (*7.35*)**	**0.09 (*0.07*)**	**7.32 (*8.52*)**	**5.78 (*3.4*)**	**3.41 (*1.82*)**	**1.78 (*1.8*)**	**0.58 (*0.51*)**
Sm	**62**	**120**	**29**	**1395 (*374*)**	**5.1 (*4.8*)**	**55.93 (*10.11*)**	**1.53 (*2.16*)**	**13.09 (*5.14*)**	**0.18 (*0.19*)**	**7.22 (*6.69*)**	**0.09 (*0.07*)**	**7.9 (*9.21*)**	**6.58 (*4.59*)**	**3.38 (*1.79*)**	**1.74 (*1.62*)**	**0.56 (*0.53*)**
Eu	**63**	**76**	**16**	**1406 (*352*)**	**5.6 (*5.3*)**	**58.63 (*9.54*)**	**1.53 (*1.48*)**	**13.34 (*3.5*)**	**0.16 (*0.2*)**	**4.86 (*3.4*)**	**0.08 (*0.06*)**	**4.92 (*6.42*)**	**5.46 (*3.29*)**	**3.84 (*1.76*)**	**2.14 (*1.76*)**	**0.53 (*0.6*)**
Gd	**64**	**81**	**16**	**1329 (*387*)**	**5.2 (*5.3*)**	**58.64 (*9.35*)**	**2.07 (*1.56*)**	**13.33 (*3.9*)**	**0.16 (*0.2*)**	**5.81 (*3.32*)**	**0.09 (*0.06*)**	**6 (*7.93*)**	**6.06 (*2.75*)**	**3.5 (*1.29*)**	**2.31 (*1.78*)**	**0.52 (*0.52*)**
Tb	**65**	**49**	**9**	**1526 (*331*)**	**5.8 (*4.2*)**	**53.66 (*12.74*)**	**1.49 (*0.75*)**	**11.71 (*4.61*)**	**0.05 (*0.03*)**	**10.58 (*7.93*)**	**0.12 (*0.03*)**	**9.54 (*7.02*)**	**9.22 (*5.37*)**	**3.11 (*1.66*)**	**1.69 (*1.37*)**	**0.98 (*0.68*)**
Dy	**66**	**87**	**18**	**1359 (*331*)**	**4.8 (*4.5*)**	**58.45 (*9.55*)**	**2.14 (*2.32*)**	**13.93 (*3.66*)**	**0.15 (*0.2*)**	**6.01 (*3.72*)**	**0.1 (*0.06*)**	**4.96 (*5.49*)**	**6.3 (*2.66*)**	**3.44 (*1.27*)**	**2.11 (*1.71*)**	**0.48 (*0.5*)**
Ho	**67**	**42**	**9**	**1460 (*372*)**	**6.2 (*5.4*)**	**58.32 (*11.51*)**	**1.71 (*0.56*)**	**12.43 (*3.28*)**	**0.06 (*0.05*)**	**6.85 (*3.68*)**	**0.12 (*0.05*)**	**6.22 (*4.97*)**	**7.97 (*1.8*)**	**3.5 (*1.41*)**	**1.91 (*1.26*)**	**0.86 (*0.85*)**
Er	**68**	**89**	**19**	**1411 (*331*)**	**5 (*4.9*)**	**56.95 (*9.91*)**	**1.89 (*1.37*)**	**13.94 (*3.91*)**	**0.17 (*0.2*)**	**6.33 (*3.63*)**	**0.1 (*0.06*)**	**6.57 (*6.93*)**	**7.5 (*4.51*)**	**3.4 (*1.3*)**	**2.09 (*1.79*)**	**0.46 (*0.49*)**
Tm	**69**	**28**	**5**	**1515 (*382*)**	**6.4 (*5.3*)**	**61.94 (*9.55*)**	**1.88 (*0.25*)**	**12.82 (*2.77*)**	**0.04 (*0.02*)**	**6.11 (*2.43*)**	**0.12 (*0.01*)**	**6.51 (*4.44*)**	**10.36 (*3.43*)**	**3.87 (*1.55*)**	**2.72 (*0.88*)**	
Yb	**70**	**144**	**27**	**1393 (*324*)**	**4.6 (*4.2*)**	**54.99 (*9.64*)**	**1.75 (*1.9*)**	**13.99 (*4.66*)**	**0.14 (*0.16*)**	**7.29 (*6.5*)**	**0.1 (*0.07*)**	**7.84 (*7.83*)**	**7.47 (*4.6*)**	**3.45 (*1.55*)**	**1.54 (*1.69*)**	**0.46 (*0.41*)**
Lu	**71**	**85**	**18**	**1446 (*415*)**	**5.6 (*5.3*)**	**53.94 (*10.78*)**	**1.47 (*1.52*)**	**11.76 (*5.2*)**	**0.13 (*0.13*)**	**8.7 (*8.05*)**	**0.09 (*0.07*)**	**9.27 (*9.4*)**	**6.9 (*4.9*)**	**3.31 (*2.01*)**	**1.33 (*1.23*)**	**0.82 (*0.61*)**

Table 1
Continued

Element	Atomic number	Number of experiments	Number of investigations	Temperature	Pressure	SiO_2[a]	TiO_2	Al_2O_3	Cr_2O_3	FeO	MnO	MgO	CaO	Na_2O	K_2O	P_2O_5
Hf	72	106	23	1420 (*388*)	5.6 (*5*)	53.53 (*10.06*)	1.52 (*2.19*)	12.27 (*5.21*)	0.14 (*0.19*)	7.97 (*7.71*)	0.08 (*0.07*)	8.65 (*9.63*)	6.13 (*4.76*)	3.44 (*1.91*)	1.76 (*1.73*)	0.66 (*0.56*)
Ta	73	63	12	1368 (*322*)	4.8 (*3.9*)	55.64 (*9.45*)	1.73 (*1.71*)	13.91 (*4.46*)	0.27 (*0.24*)	5.84 (*4.39*)	0.07 (*0.07*)	6.95 (*8.26*)	7.09 (*5.75*)	4.27 (*1.94*)	1.72 (*1.91*)	0.49 (*0.53*)
Re	75	31	3	1414 (*50*)	3 (*0.1*)	50.27 (*3.85*)	2.19 (*1.52*)	17.26 (*2.15*)		7.21 (*4.15*)	0.1 (*0.05*)	10.47 (*4.84*)	11.33 (*2.13*)	3.43 (*0.52*)	0.24 (*0.21*)	0.29 (*0.1*)

Note. This compilation includes the average and 1σ standard deviation for experimental temperature, pressure, liquid composition, number of experiments, and number of literature sources for mineral/melt partition coefficients for (a) clinopyroxene, (b) amphibole, and (c) garnet. Elements are listed in order of increasing atomic number. Experiments were included in the database only if the goal of the experiments were to achieve equilibrium and the major and trace element composition of the phases were reported. Note the range in the number of experiments and average temperature (°C), pressure (GPa), liquid compositions for each element. *Y* and the REE are highlighted in blue and Ti and the HFSE are highlighted in yellow and given in bold. Italic fonts refer to 1σ standard deviation.
[a]Oxides in wt.%.

element specific average glass compositions and experimental conditions are different for garnet compared to clinopyroxene and amphibole.

4.2. Correlation of Partition Coefficients With Composition and Experimental Conditions

The potential bias introduced into partitioning models related to the diversity of experimental conditions and composition of the coexisting phases in the calibration data set is unknown. To assess the impact of different characteristics of the database for different elements, simple linear regressions were calculated for the natural log of the partition coefficient (ln $^{\text{mineral-melt}}D_i$) versus different compositional (e.g., crystal structure) and experimental parameters (e.g., *P*, *T*) (Table 2). Each of these expressions represents the correlation of ln $^{\text{mineral-melt}}D_i$ with individual parameters. For example, considering Zr partitioning in clinopyroxene (Figure 2), one can see a general positive correlation of ln $^{\text{cpx-melt}}D_{Zr}$ versus reciprocal temperature (10000/T), tetrahedral Al (Al_{IV}), and the partition coefficient of TiO_2 (ln $^{\text{cpx-melt}}D_{TiO2}$). Each point is a single experiment for which Zr in clinopyroxene and co-existing glass were measured. The positive correlation is reflected in the value of the slope, and the correlation magnitude is reflected in R^2. The positive correlation of ln $^{\text{cpx-melt}}D_{Zr}$ with these parameters has been known for decades (Nielsen, 1990), but is notable because the correlation is self-evident in this new data set, even in the face of a dramatic increase in the number of experiments that define the correlation. The first two correlations can be attributed to the basic thermodynamics of the system and the requirement of charge balance for Zr as described above. Correlation of $^{\text{cpx-melt}}D_{Zr}$ with $^{\text{cpx-melt}}D_{Ti}$ is expected, based on their having the same valence, as well as similar substitution mechanisms (Gallahan & Nielsen, 1992).

If we examine the correlation with reciprocal temperature for individual REE and HFSE for clinopyroxene, we see that the trend for reciprocal temperature is positive, but the correlation coefficient (R^2) and the value of the slope are highly variable (Table 2). This is reflected in the range of values for ln $^{\text{cpx-melt}}D_i$ at any temperature (Figure 2; Data Set S1). In other words, the vertical distribution of ln $^{\text{cpx -melt}}D_i$ at a specific temperature is highly variable (Figure 2; Data Set S1) for elements with different presumed substitution mechanisms. The correlation of ln $^{\text{cpx-melt}}D_i$ for elements that do not require charge balance (e.g., Sr) is poor for essentially every parameter tested, including SiO_2, MgO, and Al_2O_3 content of the melt, Al_{IV}, and D_{Ti} (as noted by Mollo et al. (2020)). However, the ln $^{\text{cpx-melt}}D_i$ for elements that require charge balance in clinopyroxene exhibit significant correlation in a subset of cases, specifically, inverse temperature, Al_{IV}, and D_{Ti}.

In contrast, if we consider the case of partitioning data for amphibole (Data Set S2), there are relatively strong correlations of ln $^{\text{amp-melt}}D_i$ (Table 2) for the REE and HFSE with reciprocal temperature, Al_{IV}, and D_{Ti}. Further, ln $^{\text{amp-melt}}D_i$ for the REE and HFSE also correlates with SiO_2, MgO, and Al_2O_3 in the melt, but not for ln $^{\text{amp-melt}}D_i$ for Sr or for elements with multiple valence states. Conversely, ln $^{\text{grt-melt}}D_i$ exhibits a strong correlation (Table 3) with reciprocal temperature, and relatively weak, yet still significant, correlation with composition and D_{Ti}.

Most existing empirical models of trace element partitioning rely upon simple linear regressions for only one or a few dependent variables (e.g., Bédard, 2014; Nielsen et al., 2017). The accuracy of this simple approach depends strongly on the specific characteristics of each mineral, the data available for calibration of each element, and how strongly the conditions used for model prediction deviate from the training data. Sizable improvements in model performance are possible when considering larger multilinear models, which track partitioning dependencies for a carefully chosen set of predictor variables known to influence the thermodynamics of elemental partitioning. As an initial proof of concept, we performed multilinear regressions based on the complete set of published experimental data gathered in this study to explore the partitioning behavior of REE, HFSE, as well as a few additional geologically important elements. First, we identified the dominant contributors to elemental partitioning (by combining thermodynamics and empirical correlation analysis), and then used them to construct multiple linear regression models for trace element partitioning. The result is a set of partitioning models for clinopyroxene, garnet, and amphibole (Table 3) with predictive accuracies that are substantially improved over the simpler models (simple linear regressions).

Geochemistry, Geophysics, Geosystems

10.1029/2023GC010876

Table 2

Linear Regression Constants and Coefficient of Determination (R^2) Calculated for the Experimental Mineral/Melt Partitioning Data for (a) Clinopyroxene, (b) Amphibole, and (c) Garnet

Element	Atomic number	Number of experiments	Reciprocal temperature			SiO_2 (melt)			Al_2O_3 (melt)			MgO (melt)			Tetrahedral aluminum (Al_{IV})			Ca mole fraction (mineral)			$\ln^{\text{mineral-melt}}D_{Ti}$		
(a) Clinopyroxene			Slope	*Y*-intercept	R^2	Slope	*Y*-intercept	R^2	Slope	*Y*-intercept	R^2	Slope	*Y*-intercept	R^2	Slope	*Y*-intercept	R^2	Slope	*Y*-intercept	R^2	Slope	*Y*-intercept	R^2
Sc	21	193	0.87	−5.09	0.61	0.00	0.98	0.00	0.09	−0.60	0.20	−0.11	1.58	0.28	14.97	0.18	0.22	9.36	−0.74	0.22	**0.84**	**1.61**	**0.66**
Ti	22	304	0.35	−3.14	0.14	−0.02	0.05	0.05	0.06	−1.81	0.18	−0.07	−0.36	0.19	**16.55**	**−1.61**	**0.42**	1.14	−1.02	0.01	n/a	n/a	n/a
V	23	148	−0.07	0.79	0.00	0.07	−3.53	0.10	−0.08	1.37	0.02	−0.04	0.62	0.01	**−32.99**	**1.44**	**0.19**	−13.62	2.71	0.15	−0.17	0.26	0.01
Sr	38	206	**0.22**	**−3.69**	**0.13**	0.01	−2.72	0.01	0.01	−2.29	0.00	−0.03	−2.03	0.05	1.83	−2.29	0.01	1.81	−2.53	0.02	0.23	−2.01	0.13
Y	39	233	0.58	−4.56	0.44	0.03	−2.02	0.08	0.09	−2.07	0.18	−0.07	−0.26	0.12	13.79	−1.29	0.21	7.14	−1.83	0.16	**0.84**	**−0.02**	**0.75**
Zr	40	285	0.69	−6.60	0.27	0.02	−3.02	0.02	0.21	−4.84	0.35	−0.10	−1.32	0.14	24.66	−2.75	0.34	9.80	−3.70	0.22	**1.07**	**−1.08**	**0.70**
Nb	41	173	0.96	−10.92	0.36	0.06	−7.59	0.10	0.22	−7.38	0.26	−0.10	−3.73	0.11	21.88	−5.23	0.20	5.66	−5.35	0.05	**1.27**	**−3.45**	**0.70**
La	57	244	0.65	−7.01	0.23	0.01	−3.01	0.00	0.09	−4.17	0.16	−0.04	−2.42	0.02	13.73	−3.29	0.15	10.49	−4.42	0.20	**1.02**	**−1.84**	**0.57**
Ce	58	127	0.98	−8.66	0.56	−0.02	−1.18	0.01	0.19	−5.17	0.29	−0.03	−2.15	0.01	22.73	−3.24	0.31	11.79	−4.24	0.36	**1.17**	**−1.33**	**0.75**
Pr	59	50	1.06	−8.73	0.56	−0.01	−1.41	0.00	0.23	−4.89	0.51	−0.04	−1.56	0.01	28.43	−3.12	0.67	15.47	−4.50	0.51	**1.26**	**−0.67**	**0.92**
Nd	60	143	0.95	−7.68	0.54	0.02	−2.59	0.02	0.18	−4.16	0.32	−0.07	−1.08	0.08	18.94	−2.24	0.23	11.46	−3.36	0.31	**1.11**	**−0.56**	**0.69**
Sm	62	201	0.78	−6.12	0.49	0.01	−1.60	0.01	0.13	−2.99	0.30	−0.08	−0.49	0.13	16.83	−1.70	0.24	9.14	−2.49	0.22	**0.99**	**−0.18**	**0.66**
Eu	63	105	0.80	−6.38	0.45	0.01	−1.47	0.00	0.15	−3.26	0.26	−0.04	−0.76	0.04	18.78	−1.70	0.26	10.44	−2.78	0.27	**0.84**	**−0.39**	**0.52**
Gd	64	142	0.57	−4.75	0.36	−0.01	−0.56	0.01	0.12	−2.85	0.33	−0.01	−0.82	0.00	20.65	−1.74	0.43	8.23	−2.16	0.23	**0.75**	**−0.27**	**0.59**
Tb	65	47	1.01	−7.28	0.59	0.01	−1.43	0.01	0.22	−3.85	0.52	−0.03	−0.53	0.01	22.20	−1.62	0.45	13.33	−2.98	0.43	**1.19**	**0.43**	**0.81**
Dy	66	105	0.67	−5.12	0.48	0.01	−1.06	0.00	0.19	−3.44	0.43	−0.04	−0.54	0.02	20.80	−1.58	0.44	8.47	−2.08	0.24	**0.84**	**−0.04**	**0.72**
Ho	67	108	0.64	−4.90	0.37	0.01	−0.83	0.00	0.13	−2.64	0.43	−0.03	−0.42	0.01	20.51	−1.52	0.52	8.27	−1.99	0.23	**0.87**	**0.15**	**0.73**
Er	68	85	0.98	−6.94	0.62	0.04	−2.58	0.09	0.23	−4.00	0.47	−0.08	−0.18	0.14	15.44	−1.19	0.19	8.29	−1.88	0.24	**1.02**	**0.29**	**0.66**
Tm	69	37	0.63	−4.87	0.50	−0.01	−0.12	0.00	0.21	−3.66	0.46	−0.01	−0.53	0.00	20.72	−1.55	0.44	11.92	−2.83	0.28	**0.86**	**−0.12**	**0.78**
Yb	70	180	0.55	−4.25	0.32	0.04	−2.52	0.10	0.11	−2.36	0.26	−0.04	−0.39	0.07	11.66	−1.18	0.15	1.76	−1.00	0.01	**0.76**	**0.06**	**0.55**
Lu	71	178	0.43	−3.51	0.23	0.01	−1.09	0.01	0.12	−2.49	0.45	−0.03	−0.43	0.04	17.08	−1.41	0.42	2.86	−1.12	0.04	**0.76**	**0.00**	**0.61**
Hf	72	160	0.70	−6.01	0.38	0.02	−2.23	0.01	0.19	−4.05	0.31	−0.08	−0.71	0.14	25.49	−2.25	0.42	10.73	−3.18	0.22	**0.89**	**−0.66**	**0.70**
Ta	73	74	0.51	−0.40	0.21	0.00	−0.45	0.00	0.16	−2.88	0.41	−0.01	−0.50	0.00	18.09	−1.37	0.43	5.12	−1.44	0.09	**0.82**	**0.00**	**0.67**
(b) Amphibole			Slope	*Y*-intercept	R^2	Slope	*Y*-intercept	R^2	Slope	*Y*-intercept	R^2	Slope	*Y*-intercept	R^2	Slope	*Y*-intercept	R^2	Slope	*Y*-intercept	R^2	Slope	*Y*-intercept	R^2
Sc	21	36	0.91	−5.77	0.32	0	−0.91	0.09	**−0.22**	**5.66**	**0.64**	−0.05	2.22	0.00	−22.14	4.69	0.50	−9.29	3.22	0.01	0.27	0.97	0.57
Ti	22	37	0.23	−0.94	0.01	0.03	−0.58	0.12	0.06	−0.21	0.06	−0.18	1.31	0.31	25.53	−3.15	0.17	**−46.42**	**5.68**	**0.33**	n/a	n/a	n/a
V	23	36	−0.76	8.29	0.09	−0.02	2.62	0.00	0.06	0.71	0.02	0.01	1.63	0.00	9.84	0.53	0.04	86.28	11.26	0.31	0.09	1.24	0.03
Sr	38	62	−0.05	−0.61	0.01	0.00	−1.10	0.00	**0.08**	**−2.28**	**0.20**	0.00	−1.06	0.00	3.58	−1.52	0.05	−8.84	−0.08	0.02	−0.01	−1.01	0.01
Y	39	83	1.03	−7.89	0.68	**0.06**	**−3.07**	**0.72**	−0.05	1.32	0.02	−0.23	1.04	0.62	−19.83	3.22	0.53	5.08	−0.02	0.00	0.25	−0.38	0.58
Zr	40	80	**1.17**	**−10.47**	**0.75**	0.07	−4.59	0.69	−0.05	0.03	0.02	−0.23	−0.23	0.61	−22.28	2.11	0.49	17.13	−2.62	0.02	0.24	−1.61	0.50
Nb	41	83	0.84	−7.77	0.45	**0.06**	**−4.23**	**0.55**	−0.02	−0.56	0.00	−0.27	−0.30	0.64	−13.28	0.94	0.24	0.09	−0.94	0.00	0.20	−1.59	0.38
La	57	98	0.84	−8.32	0.31	0.05	−4.47	0.49	0.14	−4.03	0.21	**−0.19**	**−1.17**	**0.59**	−5.86	−0.84	0.04	−17.10	0.08	0.05	0.18	−2.26	0.36
Ce	58	52	0.91	−8.36	0.42	0.06	−4.10	0.59	0.10	−2.86	0.13	**−0.19**	**−0.59**	**0.68**	−10.05	0.29	0.14	−32.60	2.21	0.16	0.23	−1.85	0.50
Pr	59	17	1.31	−11.40	0.70	0.05	−3.59	0.89	**0.19**	**−4.56**	**0.82**	**−0.15**	**−0.50**	**0.81**	−17.83	1.53	0.09	−10.67	0.02	0.02	0.29	−1.69	0.39
Nd	60	52	1.02	−8.44	0.46	0.06	−3.44	0.58	**−0.20**	**0.25**	**0.66**	**−0.20**	**0.25**	**0.66**	−13.26	1.57	0.22	−34.98	3.37	0.16	0.27	−1.15	0.61
Sm	62	75	1.22	−9.59	0.54	0.06	−3.29	0.60	0.08	−1.26	0.06	**−0.21**	**0.69**	**0.60**	−16.56	2.49	0.27	−17.56	1.98	0.04	0.25	−0.68	0.60
Eu	63	49	1.11	−8.68	0.52	0.06	−2.86	0.55	0.06	−1.03	0.05	−0.18	0.64	0.58	−16.91	2.57	0.35	−39.20	4.16	0.19	**0.29**	**−0.74**	**0.66**
Gd	64	60	1.18	−9.04	0.53	0.06	−2.84	0.60	0.09	−1.13	0.07	−0.19	0.89	0.62	−16.90	2.83	0.32	−23.45	2.85	0.07	**0.25**	**−0.46**	**0.65**

Geochemistry, Geophysics, Geosystems

10.1029/2023GC010876

Table 2
Continued

Element	Atomic number	Number of experiments	Reciprocal temperature			SiO_2 (melt)			Al_2O_3 (melt)			MgO (melt)			Tetrahedral aluminum (Al_{IV})			Ca mole fraction (mineral)			$\ln^{mineral\text{-}melt}D_{Ti}$		
Tb	65	24	1.50	−11.82	0.79	0.06	−3.07	0.66	0.03	−0.22	0.01	−0.18	0.96	0.57	−27.18	3.97	0.72	−58.56	6.61	0.26	**0.34**	**−0.72**	**0.77**
Dy	66	51	1.27	−9.71	0.56	0.07	−3.15	0.65	0.08	−1.06	0.06	−0.20	0.95	0.60	−19.54	3.19	0.39	−47.55	5.28	0.24	**0.33**	**−0.62**	**0.72**
Ho	67	38	**1.51**	**−11.86**	**0.82**	0.07	−3.49	0.72	0.08	−1.17	0.05	−0.20	0.92	0.57	−29.20	4.23	0.62	−38.63	−4.35	0.11	0.30	0.68	0.70
Er	68	51	**1.45**	**−11.18**	**0.67**	0.07	−3.20	0.61	0.07	−1.06	0.05	−0.19	0.84	0.56	−20.64	3.26	0.42	−36.15	3.98	0.14	0.32	−0.68	0.67
Tm	69	25	**1.46**	**−11.59**	**0.76**	0.06	−3.24	0.46	−0.05	1.22	0.02	−0.21	0.88	0.43	−27.51	3.95	0.76	−33.75	3.90	0.10	**0.32**	**−0.73**	**0.65**
Yb	70	54	1.31	−10.29	0.62	0.07	−3.44	0.64	0.07	−1.16	0.05	−0.21	0.75	0.58	−21.17	3.20	0.46	−1.31	−10.29	0.62	**0.31**	**−0.81**	**0.66**
Lu	71	48	**1.45**	**−11.66**	**0.77**	0.07	−3.58	0.60	0.04	−0.64	0.01	−0.20	0.54	0.48	−25.48	3.53	0.58	−20.86	2.33	0.04	0.25	−0.81	0.57
Hf	72	78	**1.18**	**−10.19**	**0.73**	0.07	−4.18	0.67	−0.03	0.09	0.01	−0.23	0.11	0.54	−24.37	2.74	0.52	22.30	−2.87	0.04	0.26	1.29	0.53
Ta	73	61	1.05	−9.50	0.39	0.06	−4.38	0.51	0.10	−2.90	0.10	**−0.22**	**−0.55**	**0.59**	−10.67	0.43	0.13	−6.53	−0.41	0.01	0.20	−1.77	0.40
(c) Garnet			Slope	*Y*-intercept	R^2	Slope	*Y*-intercept	R^2	Slope	*Y*-intercept	R^2	Slope	*Y*-intercept	R^2	Slope	*Y*-intercept	R^2	Slope	*Y*-intercept	R^2	Slope	*Y*-Intercept	R^2
Sc	21	68	**0.81**	**−3.20**	**0.86**	0.04	−0.47	0.09	0.08	0.56	0.12	−0.08	2.37	0.39	−36.46	1.84	0.37	17.69	0.32	0.30	0.97	2.51	0.66
Ti	22	57	**0.77**	**−5.35**	**0.55**	0.09	−5.10	0.14	0.01	−0.79	0.00	−0.05	−0.14	0.13	−12.21	−0.50	0.05	21.71	−2.29	0.37	n/a	n/a	n/a
V	23	53	0.58	−2.69	0.41	0.11	−5.02	0.32	0.04	0.38	0.02	−0.04	1.28	0.11	−18.97	1.08	0.13	8.67	0.24	0.04	**0.89**	**1.64**	**0.53**
Sr	38	71	0.45	−7.39	0.11	−0.02	−3.68	0.01	0.08	−5.71	0.04	−0.02	−4.47	0.01	3.06	−4.67	0.00	17.98	−6.10	0.14	**0.86**	**−3.74**	**0.25**
Y	39	109	**1.07**	**−5.35**	**0.87**	0.03	−0.65	0.04	0.14	−0.55	0.19	−0.10	2.07	0.40	−43.07	1.44	0.34	22.35	−0.16	0.24	1.35	2.49	0.70
Zr	40	116	0.57	−4.46	0.50	0.00	−1.01	0.00	0.09	−2.09	0.16	−0.04	−0.62	0.10	−18.49	−0.84	0.12	13.16	1.75	0.15	**0.96**	**−0.06**	**0.71**
Nb	41	71	0.96	−10.09	0.26	−0.11	−3.54	0.00	0.13	−5.85	0.06	−0.05	−0.38	0.04	−21.20	−4.09	0.03	25.47	−5.94	0.14	**1.46**	**−2.67**	**0.43**
La	57	82	0.82	−10.09	0.22	−0.01	−4.16	0.00	0.07	−5.81	0.02	−0.02	−4.68	0.00	−1.37	−4.82	0.00	26.05	−6.87	0.11	**1.93**	**−3.00**	**0.61**
Ce	58	90	0.85	−9.47	0.23	−0.03	−2.11	0.01	0.04	−4.57	0.00	−0.04	−3.74	0.01	−26.42	−3.93	0.03	31.50	−6.46	0.22	**1.63**	**−2.34**	**0.41**
Pr	59	51	0.62	−7.38	0.31	−0.03	−2.16	0.03	0.18	−5.90	0.23	−0.04	−3.26	0.04	−15.54	−3.51	0.03	10.53	−4.26	0.06	**1.09**	**−2.07**	**0.49**
Nd	60	109	0.86	−7.87	0.55	0.02	−3.36	0.01	0.10	−3.72	0.08	−0.08	−1.90	0.17	−36.91	−2.34	0.14	16.93	−3.54	0.17	**1.31**	**−1.22**	**0.70**
Sm	62	120	0.83	−6.14	0.70	0.03	−2.55	0.04	0.12	−2.56	0.21	−0.08	−0.29	0.28	−35.09	−0.75	0.21	18.68	−2.14	0.27	**1.00**	**−0.17**	**0.77**
Eu	63	76	**1.00**	**−6.35**	**0.80**	0.00	−0.54	0.00	0.13	−2.34	0.07	−0.15	0.15	0.31	−48.68	−0.43	0.24	27.00	−2.49	0.21	1.17	0.33	0.67
Gd	64	81	**0.95**	**−6.86**	**0.70**	0.04	−2.59	0.08	0.18	−2.56	0.25	−0.10	0.42	0.30	−33.97	0.01	0.23	−1.90	0.01	0.00	1.12	0.98	0.56
Tb	65	49	**1.13**	**−6.51**	**0.82**	0.02	−1.08	0.03	0.13	−1.51	0.15	−0.10	0.97	0.21	−67.62	0.42	0.23	6.61	−0.71	0.11	0.89	0.92	0.36
Dy	66	87	**1.06**	**−5.75**	**0.83**	0.05	−1.71	0.09	0.21	−1.99	0.30	−0.17	1.83	0.42	−56.56	1.10	0.31	−3.42	1.22	0.00	1.27	2.13	0.64
Ho	67	42	**1.15**	**−6.01**	**0.89**	0.03	−1.06	0.06	0.26	−2.28	0.27	−0.22	2.33	0.45	−54.40	1.33	0.27	7.65	0.04	0.02	1.00	1.77	0.47
Er	68	89	**0.99**	**−4.64**	**0.83**	0.05	−1.33	0.14	0.15	−0.62	0.20	−0.12	2.26	0.42	−48.07	1.60	0.33	−2.88	1.60	0.00	1.01	2.39	0.39
Tm	69	28	**1.23**	**−5.85**	**0.97**	0.08	−3.54	0.18	0.35	−3.08	0.29	−0.26	3.06	0.40	−77.33	1.98	0.28	−41.00	4.02	0.34	1.26	2.24	0.51
Yb	70	144	**1.09**	**−4.75**	**0.82**	0.06	−1.22	0.14	0.09	0.79	0.08	−0.12	3.05	0.40	−45.26	2.16	0.24	24.40	0.41	0.21	1.41	3.28	0.67
Lu	71	85	**1.07**	**−4.49**	**0.83**	0.05	−0.72	0.09	0.12	0.71	0.11	−0.12	3.29	0.40	−59.12	2.51	0.34	27.98	0.20	0.27	1.55	3.43	0.72
Hf	72	106	0.36	−3.18	0.24	−0.01	−0.60	0.00	0.05	−1.58	0.06	−0.02	−0.81	0.03	−14.20	−0.89	0.07	5.13	−1.30	0.05	**0.70**	**−0.37**	**0.46**
Ta	73	63	1.17	−10.87	0.40	−0.07	0.35	0.08	0.06	−4.26	0.01	−0.05	−3.11	0.03	−30.66	−3.43	0.04	24.43	5.10	0.17	**1.47**	**−2.03**	**0.48**
Re	75	31	2.62	−17.69	0.02	0.29	−16.68	0.15	0.10	−3.88	0.01	−0.16	−0.46	0.07	134.59	−1.11	0.04	78.60	7.18	0.13	0.69	−1.26	0.00

Note. The elements are listed in increasing R^2 is a measure of the correlation or relationship between ln *D* for each element listed with a succession of possible correlated parameters. R^2 values closer to 1 can be interpreted as a higher degree of correlation (less residual scatter about the regression). For each element in each mineral, the regression constant with the highest R^2 is in bold. *Y* and the REE are highlighted in yellow. Ti and the HFSE are highlighted in blue. Temperature is in °C, and pressure is in GPa.

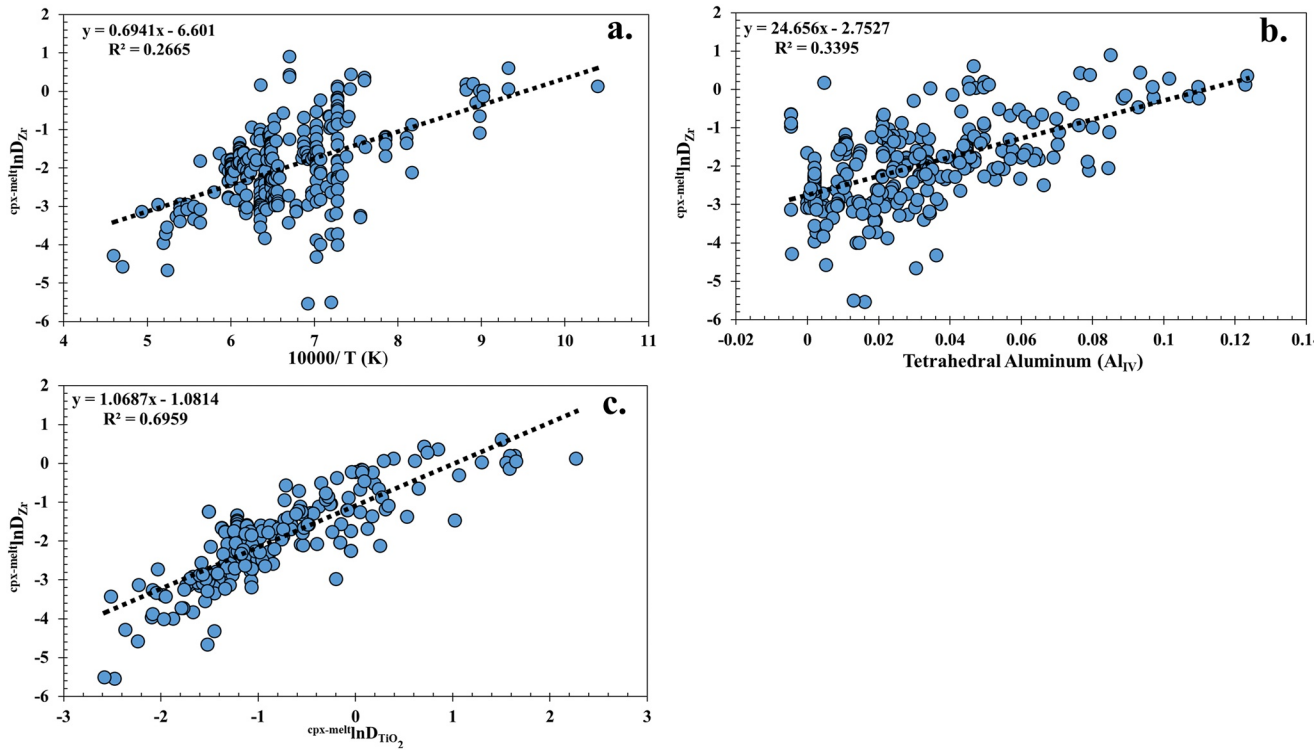

Figure 2. Correlation of the natural log of the clinopyroxene/melt partition coefficient and (a) reciprocal temperature, (b) the mole fraction of Al in tetrahedral coordination in clinopyroxene, and (c) the natural log of the clinopyroxene/melt Ti partition coefficient. Each symbol represents a single experiment. Linear regression was calculated for each correlated parameter and reported in Table 2. Such regressions were calculated independently for clinopyroxene, amphibole and garnet for each trace element shown in Table 1.

5. Discussion

5.1. Predictive Accuracy of Expressions Based on a Single Dependence

We can begin to evaluate the degree to which different models calibrated to a heterogeneous data set can predict partitioning behavior by using the expressions based on a single parameter, in this initial test, the case of temperature dependence. Using the linear expressions (Table 2) one can attempt to reproduce the experimental values used to calibrate the expressions for clinopyroxene (Figure 3), amphibole (Figure 4), and garnet (Figure 5). Each point represents a single experimental determination for that element for the selected mineral, typically presented in the literature as the average of several individual determinations from a single experimental charge. We assess the single term linear temperature regression models for each mineral by comparing experimentally observed values with the model-calculated partition coefficients, visualizing their correspondence as the degree to which data points align with the 1:1 correlation line as measured by the slope and R^2 for the distribution of calculated and experimental values.

Examining the results for the three phases we modeled (Figures 3–5), the overall pattern for the average results calculated for all elements collectively fall on a line with a slope of 1. However, if we consider the results for each element individually, the slope is less than 1 for all elements in all three minerals studied. The extent to which the slope of the calculated versus experimental correlation departs from 1 (colored trendlines in Figures 3–5) varies extensively, and can be used to explore the contribution of different sources of uncertainty.

Measurement errors introduce further noise into the experimental determinations of the partition coefficients and thus cause additional scatter that, given the variety of analytical tools and methods used, it becomes difficult to quantify if one is restricted to the reported error. Model deficiencies related to unaccounted for dependencies or interdependency of the modeled parameters reflect a model's inability to capture some of the observed variability in the data. Yet, discerning between sources of variability can be aided by examining the systematics of the correlation of the calculated and experimental values as a function of specific data characteristics.

Table 3
Multiple Linear Regression Constants Calculated for the Experimental Mineral/Melt Partitioning Data for (a) Clinopyroxene, (b) Amphibole, and (c) Garnet

Element	Z	$\ln^{\text{mineral-melt}}D_0$	Reciprocal temperature	Pressure	Melt component	Tetrahedral aluminum (Al_{IV})	Ca mole fraction (mineral)
(a) Clinopyroxene							
Sc	21	0.806 (*0.03*)	0.449 (*0.069*)	−0.017 (*0.03*)	0.412 (*0.079*)	9.724 (*1.498*)	5.147 (*0.957*)
Ti	22	−0.844 (*0.016*)	0.276 (*0.035*)	0.002 (*0.017*)	0.566 (*0.039*)	12.356 (*0.77*)	2.997 (*0.441*)
V	23	0.259 (*0.098*)	0.426 (*0.22*)	−0.002 (*0.097*)	0.109 (*0.254*)	−27.108 (*5.282*)	−12.792 (*3.27*)
Sr	38	−2.257 (*0.027*)	−0.011 (*0.054*)	0.008 (*0.025*)	0.457 (*0.064*)	3.752 (*1.307*)	3.259 (*0.931*)
Y	**39**	**−0.692 (*0.027*)**	**0.107 (*0.057*)**	**−0.091 (*0.027*)**	**0.668 (*0.07*)**	**10.189 (*1.319*)**	**3.764 (*0.835*)**
Zr	40	−1.926 (*0.032*)	0.126 (*0.064*)	−0.017 (*0.029*)	0.552 (*0.069*)	24.035 (*1.532*)	8.543 (*0.879*)
Nb	41	−4.461 (*0.056*)	0.296 (*0.115*)	−0.071 (*0.06*)	0.964 (*0.135*)	17.815 (*2.533*)	2.891 (*1.461*)
La	**57**	**−2.67 (*0.03*)**	**0.086 (*0.065*)**	**−0.184 (*0.029*)**	**0.717 (*0.066*)**	**9.628 (*1.5*)**	**6.625 (*0.968*)**
Ce	**58**	**−2.225 (*0.04*)**	**0.22 (*0.088*)**	**−0.147 (*0.035*)**	**0.521 (*0.095*)**	**10.361 (*2.06*)**	**6.774 (*1.308*)**
Pr	**59**	**−1.799 (*0.039*)**	**0.142 (*0.092*)**	**−0.118 (*0.032*)**	**0.621 (*0.108*)**	**13.659 (*2.031*)**	**5.464 (*1.42*)**
Nd	**60**	**−1.472 (*0.034*)**	**0.161 (*0.069*)**	**−0.144 (*0.03*)**	**0.714 (*0.067*)**	**13.18 (*1.686*)**	**5.978 (*1.052*)**
Sm	**62**	**−0.982 (*0.024*)**	**0.133 (*0.05*)**	**−0.137 (*0.023*)**	**0.705 (*0.052*)**	**13.936 (*1.203*)**	**4.898 (*0.713*)**
Eu	**63**	**−1.034 (*0.033*)**	**0.137 (*0.069*)**	**−0.104 (*0.029*)**	**0.636 (*0.065*)**	**15.382 (*1.733*)**	**6.323 (*1.13*)**
Gd	**64**	**−0.872 (*0.029*)**	**0.021 (*0.061*)**	**−0.156 (*0.025*)**	**0.449 (*0.068*)**	**13.869 (*1.572*)**	**3.192 (*0.885*)**
Tb	**65**	**−0.702 (*0.041*)**	**0.174 (*0.099*)**	**−0.109 (*0.034*)**	**0.617 (*0.096*)**	**14.015 (*2.171*)**	**3.339 (*1.519*)**
Dy	**66**	**−0.723 (*0.033*)**	**0.104 (*0.067*)**	**−0.105 (*0.029*)**	**0.522 (*0.076*)**	**13.433 (*1.725*)**	**3.006 (*1.158*)**
Ho	**67**	**−0.579 (*0.03*)**	**0.056 (*0.066*)**	**−0.15 (*0.025*)**	**0.599 (*0.085*)**	**11.178 (*1.553*)**	**1.704 (*0.985*)**
Er	**68**	**−0.62 (*0.038*)**	**0.269 (*0.086*)**	**−0.106 (*0.031*)**	**0.646 (*0.073*)**	**12.718 (*2.051*)**	**1.471 (*1.175*)**
Tm	**69**	**−0.633 (*0.047*)**	**0.086 (*0.093*)**	**−0.128 (*0.038*)**	**0.53 (*0.117*)**	**11.553 (*2.484*)**	**2.552 (*1.718*)**
Yb	**70**	**−0.675 (*0.028*)**	**0.097 (*0.058*)**	**−0.111 (*0.025*)**	**0.667 (*0.058*)**	**15.14 (*1.397*)**	**−0.403 (*0.918*)**
Lu	**71**	**−0.639 (*0.025*)**	**0.06 (*0.054*)**	**−0.128 (*0.022*)**	**0.568 (*0.075*)**	**13.198 (*1.223*)**	**−0.79 (*0.768*)**
Hf	72	−1.295 (*0.035*)	0.147 (*0.072*)	−0.14 (*0.032*)	0.506 (*0.09*)	19.284 (*1.653*)	4.586 (*1.219*)
Ta	73	−3.481 (*0.071*)	0.371 (*0.161*)	−0.083 (*0.074*)	1.06 (*0.169*)	21.05 (*3.19*)	−1.834 (*1.888*)
(b) Amphibole							
Sc	21	2.102 (*0.074*)	0.142 (*0.24*)	−0.129 (*0.191*)	0.448 (*0.221*)	2.978 (*4.587*)	−16.512 (*12.582*)
Ti	22	1.04 (*0.022*)	0.389 (*0.077*)	−0.308 (*0.05*)	0.944 (*0.067*)	10.928 (*1.197*)	−4.459 (*2.912*)
V	23	1.658 (*0.099*)	0.005 (*0.32*)	0.188 (*0.255*)	0.733 (*0.295*)	11.757 (*6.115*)	−40.085 (*16.773*)
Sr	38	−1.05 (*0.039*)	0.079 (*0.138*)	−0.166 (*0.103*)	0.334 (*0.115*)	13.921 (*2.687*)	−10.854 (*6.676*)
Y	**39**	**0.467 (*0.029*)**	**0.366 (*0.106*)**	**−0.201 (*0.076*)**	**0.779 (*0.085*)**	**4.37 (*1.861*)**	**−14.735 (*4.602*)**
Zr	40	−0.818 (*0.034*)	0.359 (*0.121*)	−0.332 (*0.082*)	0.732 (*0.1*)	8.157 (*2.277*)	−6.743 (*5.821*)
Nb	41	−0.935 (*0.031*)	0.282 (*0.115*)	−0.322 (*0.085*)	0.898 (*0.097*)	10.313 (*2.046*)	−19.409 (*5.108*)
La	**57**	**−1.684 (*0.027*)**	**0.336 (*0.1*)**	**−0.261 (*0.069*)**	**0.814 (*0.076*)**	**11.293 (*1.608*)**	**−12.946 (*3.95*)**
Ce	**58**	**−1.16 (*0.027*)**	**0.357 (*0.097*)**	**−0.292 (*0.073*)**	**0.805 (*0.074*)**	**10.73 (*1.641*)**	**−10.915 (*4.319*)**
Pr	**59**	**−1.156 (*0.031*)**	**0.284 (*0.113*)**	**−0.201 (*0.078*)**	**0.721 (*0.083*)**	**13.082 (*2.129*)**	**0.491 (*5.921*)**
Nd	**60**	**−0.346 (*0.031*)**	**0.377 (*0.113*)**	**−0.301 (*0.085*)**	**0.797 (*0.087*)**	**9.253 (*1.919*)**	**−12.249 (*5.051*)**
Sm	**62**	**0.151 (*0.031*)**	**0.417 (*0.118*)**	**−0.358 (*0.079*)**	**0.783 (*0.092*)**	**7.153 (*1.956*)**	**−11.326 (*5.03*)**
Eu	**63**	**0.109 (*0.036*)**	**0.391 (*0.13*)**	**−0.307 (*0.094*)**	**0.707 (*0.098*)**	**6.959 (*2.187*)**	**−12.967 (*5.833*)**
Gd	**64**	**0.395 (*0.032*)**	**0.407 (*0.121*)**	**−0.335 (*0.079*)**	**0.756 (*0.091*)**	**6.524 (*1.959*)**	**−12.144 (*5.205*)**
Tb	**65**	**0.287 (*0.049*)**	**0.508 (*0.181*)**	**−0.243 (*0.124*)**	**0.715 (*0.138*)**	**3.605 (*3.196*)**	**−3.848 (*9.618*)**
Dy	**66**	**0.357 (*0.037*)**	**0.425 (*0.136*)**	**−0.262 (*0.099*)**	**0.75 (*0.103*)**	**5.827 (*2.286*)**	**−17.068 (*6.011*)**

Table 3
Continued

Element	Z	$\ln^{\text{mineral-melt}}D_0$	Reciprocal temperature	Pressure	Melt component	Tetrahedral aluminum (Al_{IV})	Ca mole fraction (mineral)
Ho	**67**	**0.228 (*0.042*)**	**0.577 (*0.15*)**	**−0.264 (*0.105*)**	**0.687 (*0.12*)**	**3.68 (*2.807*)**	**−5.079 (*7.783*)**
Er	**68**	**0.264 (*0.041*)**	**0.494 (*0.146*)**	**−0.252 (*0.107*)**	**0.705 (*0.111*)**	**5.667 (*2.476*)**	**−12.22 (*6.535*)**
Tm	**69**	**0.289 (*0.054*)**	**0.505 (*0.194*)**	**−0.368 (*0.142*)**	**0.733 (*0.161*)**	**2.661 (*3.481*)**	**−2.485 (*10.207*)**
Yb	**70**	**0.137 (*0.039*)**	**0.489 (*0.141*)**	**−0.261 (*0.105*)**	**0.725 (*0.107*)**	**5.135 (*2.395*)**	**−12.808 (*6.288*)**
Lu	**71**	**0.052 (*0.039*)**	**0.531 (*0.145*)**	**−0.289 (*0.095*)**	**0.672 (*0.12*)**	**2.012 (*2.608*)**	**−6.554 (*7.098*)**
Hf	72	−0.472 (*0.034*)	0.354 (*0.122*)	−0.403 (*0.081*)	0.638 (*0.102*)	6.397 (*2.3*)	−5.962 (*5.745*)
Ta	73	−1.098 (*0.031*)	0.394 (*0.12*)	−0.448 (*0.08*)	0.849 (*0.094*)	11.187 (*1.946*)	−6.483 (*5.232*)
(c) Garnet							
Sc	21	1.545 (*0.04*)	0.298 (*0.059*)	−0.018 (*0.013*)	0.397 (*0.054*)	−1.043 (*1.239*)	1.647 (*1.134*)
Ti	22	−0.728 (*0.039*)	0.231 (*0.064*)	0.055 (*0.014*)	0.481 (*0.059*)	1.171 (*1.219*)	6.982 (*1.305*)
V	23	0.813 (*0.067*)	0.173 (*0.104*)	−0.002 (*0.023*)	0.422 (*0.103*)	−0.213 (*2.154*)	−1.129 (*3.315*)
Sr	38	−4.909 (*0.092*)	0.24 (*0.134*)	0.058 (*0.029*)	0.117 (*0.126*)	3.477 (*2.944*)	13.611 (*2.726*)
Y	**39**	**1.228 (*0.041*)**	**0.536 (*0.059*)**	**−0.03 (*0.013*)**	**0.425 (*0.056*)**	**−0.197 (*1.418*)**	**6.742 (*1.249*)**
Zr	40	−0.927 (*0.055*)	0.35 (*0.078*)	−0.013 (*0.018*)	0.166 (*0.075*)	1.795 (*1.922*)	6.262 (*1.689*)
Nb	41	−4.35 (*0.135*)	0.269 (*0.203*)	0.014 (*0.045*)	0.386 (*0.179*)	2.888 (*4.319*)	17.45 (*4.223*)
La	**57**	**−5.072 (*0.15*)**	**0.574 (*0.21*)**	**0.054 (*0.047*)**	**0.396 (*0.213*)**	**6.965 (*4.925*)**	**16.049 (*4.154*)**
Ce	**58**	**−4.146 (*0.151*)**	**0.513 (*0.208*)**	**−0.006 (*0.049*)**	**0.247 (*0.209*)**	**3.652 (*5.085*)**	**13.945 (*5.315*)**
Pr	**59**	**−3.611 (*0.105*)**	**0.579 (*0.139*)**	**−0.005 (*0.036*)**	**0.103 (*0.19*)**	**8.665 (*6.669*)**	**12.534 (*3.178*)**
Nd	**60**	**−2.531 (*0.07*)**	**0.559 (*0.098*)**	**−0.01 (*0.023*)**	**0.177 (*0.098*)**	**1.922 (*2.438*)**	**8.076 (*2.409*)**
Sm	**62**	**−0.925 (*0.055*)**	**0.606 (*0.078*)**	**−0.031 (*0.018*)**	**0.1 (*0.079*)**	**2.428 (*1.978*)**	**7.154 (*1.57*)**
Eu	**63**	**−0.77 (*0.067*)**	**0.575 (*0.087*)**	**−0.026 (*0.021*)**	**0.264 (*0.088*)**	**1.579 (*2.123*)**	**9.878 (*2.224*)**
Gd	**64**	**−0.181 (*0.06*)**	**0.665 (*0.08*)**	**−0.024 (*0.021*)**	**0.435 (*0.105*)**	**4.619 (*3.817*)**	**7.008 (*2.342*)**
Tb	**65**	**0.127 (*0.085*)**	**0.553 (*0.119*)**	**−0.072 (*0.034*)**	**0.27 (*0.147*)**	**0.523 (*5.508*)**	**3.088 (*2.327*)**
Dy	**66**	**0.928 (*0.054*)**	**0.652 (*0.072*)**	**−0.061 (*0.021*)**	**0.42 (*0.097*)**	**1.309 (*3.701*)**	**6.306 (*2.202*)**
Ho	**67**	**0.982 (*0.077*)**	**0.669 (*0.105*)**	**−0.038 (*0.028*)**	**0.536 (*0.153*)**	**1.34 (*4.774*)**	**4.173 (*2.991*)**
Er	**68**	**1.464 (*0.048*)**	**0.552 (*0.067*)**	**−0.054 (*0.018*)**	**0.438 (*0.084*)**	**0.308 (*3.342*)**	**2.941 (*1.54*)**
Tm	**69**	**1.393 (*0.085*)**	**0.617 (*0.116*)**	**−0.05 (*0.033*)**	**0.584 (*0.164*)**	**−0.508 (*5.127*)**	**3.168 (*3.437*)**
Yb	**70**	**2.054 (*0.039*)**	**0.531 (*0.058*)**	**−0.046 (*0.014*)**	**0.585 (*0.058*)**	**−0.685 (*1.475*)**	**3.923 (*1.188*)**
Lu	**71**	**2.117 (*0.057*)**	**0.504 (*0.081*)**	**−0.032 (*0.018*)**	**0.592 (*0.083*)**	**−0.89 (*1.901*)**	**3.786 (*1.54*)**
Hf	72	−1.033 (*0.054*)	0.181 (*0.076*)	−0.021 (*0.018*)	0.047 (*0.075*)	1.85 (*1.875*)	4.619 (*1.623*)
Ta	73	−3.676 (*0.121*)	0.561 (*0.182*)	0.055 (*0.048*)	0.221 (*0.161*)	2.814 (*3.835*)	16.911 (*3.796*)

Note. The trace elements are listed in order of atomic number (Z). Y and the REE are highlighted in yellow and given in bold. Ti and the HFSE are highlighted in blue. Italic fonts refer to 1σ standard deviation.

If predictive models use experimental calibration databases that have a wide range of melt composition, and they do not accommodate compositional dependencies for partition coefficients, the result will be horizontal scatter—a greater range in experimental values compared to values calculated by applying the regressions to the calibration data set, and thus a slope that is less than 1:1 as a function of analytical/experimental error and uncompensated dependencies. Note that these sources of uncertainty will have different effects on the correlation of calculated values with experimental ones. Inclusion of two phases into the analytical volume will have a greater effect on the experimental uncertainty (scatter) at low partition coefficient values (Nielsen et al., 2017). However, the differences in the compositional range of the experiments (calibration data set) will have a more systematic effect, which is independent of the partition coefficient, affecting both compatible and incompatible elements equally.

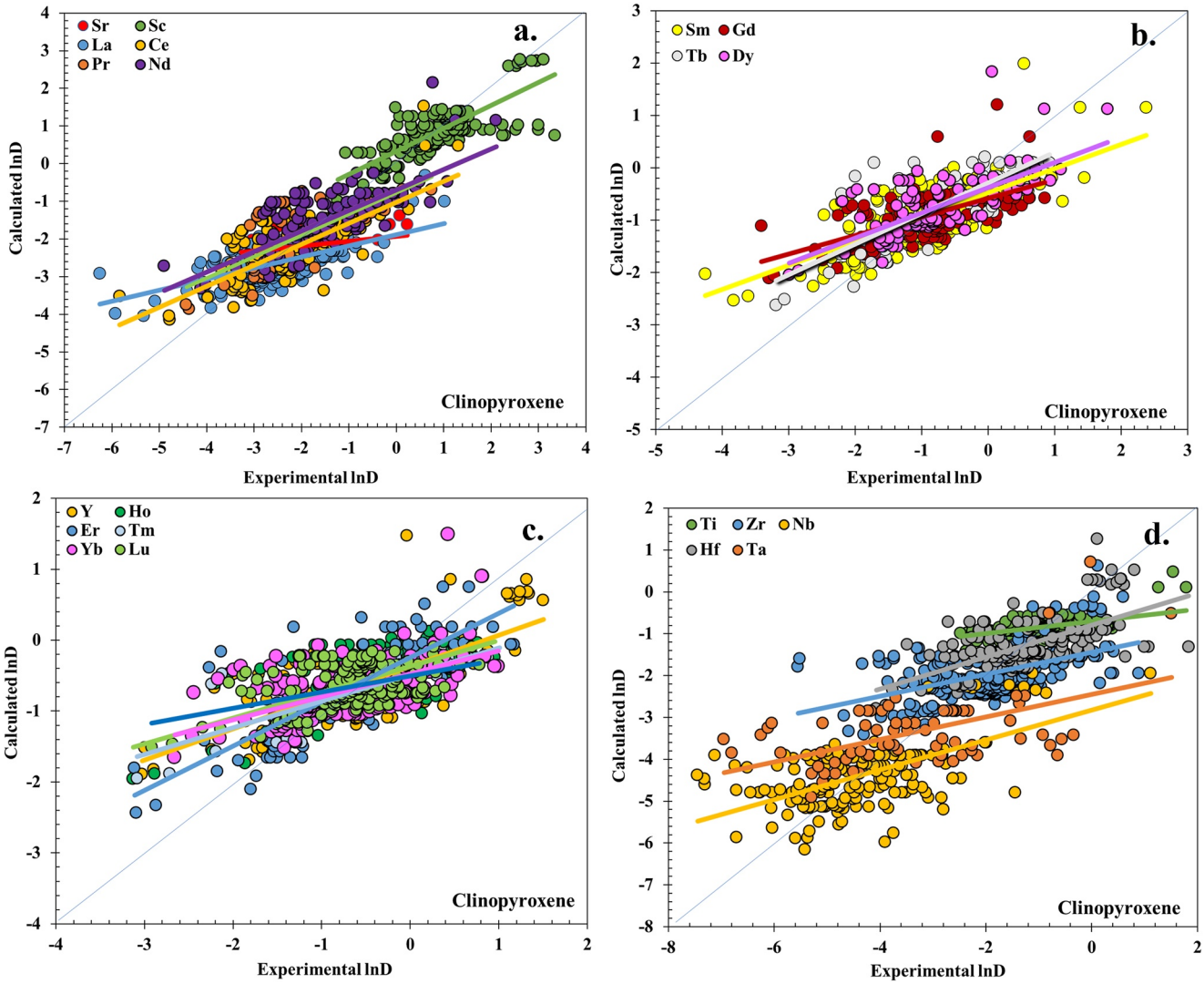

Figure 3. Correlation of partition coefficients calculated for clinopyroxene using the single term linear regressions for temperature dependence (Table 2) with experimentally determined values (Data Set S1). (a) Sc, Sr, and Light Rare Earth Elements (REE), (b) medium REE, (c) Y and heavy REE, and (d) High Field Strength Elements (HFSE). Each symbol represents a single experimental determination for that element. The experiments collectively follow a 1:1 correlation, but the results for individual elements are characterized by a slope less than 1 (colored trendlines). Note that all trendlines have a slope that is equal to or less than 1.

We can assess the underlying sources of uncertainty in the calculated or experimental partition coefficients by comparing the slopes of the calculated versus experimental correlation within and between groups of elements. If we begin with calculated versus experimental values for the three phases of interest using the linear regression on reciprocal temperature, one can see that for most elements, garnet (Figure 5) has less scatter (smaller range of calculated D vs. experimental D for each element) than either clinopyroxene (Figure 3) or amphibole (Figure 4). Further, the magnitude of the horizontal scatter as approximated by the calculated versus experimental slope appears uniform for all the REE and HFSE in the clinopyroxene database. In contrast, the horizontal scatter shrinks at higher ln $^{\text{mineral-melt}}D_i$ values for both amphibole and garnet, as indicated by the rotation of the trendlines as a function of experimental ln $^{\text{mineral-melt}}D_i$. Our results imply that analytical uncertainty is a higher proportion of the predictive uncertainty for expressions describing partitioning in garnet and amphibole than for clinopyroxene and that the inadequacy of the assumption of ideality (assumption of activity to be the same as concentration) is most influential for clinopyroxene. These results are consistent with the relative complexity of the processes related to the substitution of REE and HSFE in clinopyroxene compared to garnet, as well as the greater range of P, T, and composition in the clinopyroxene data (Table 1).

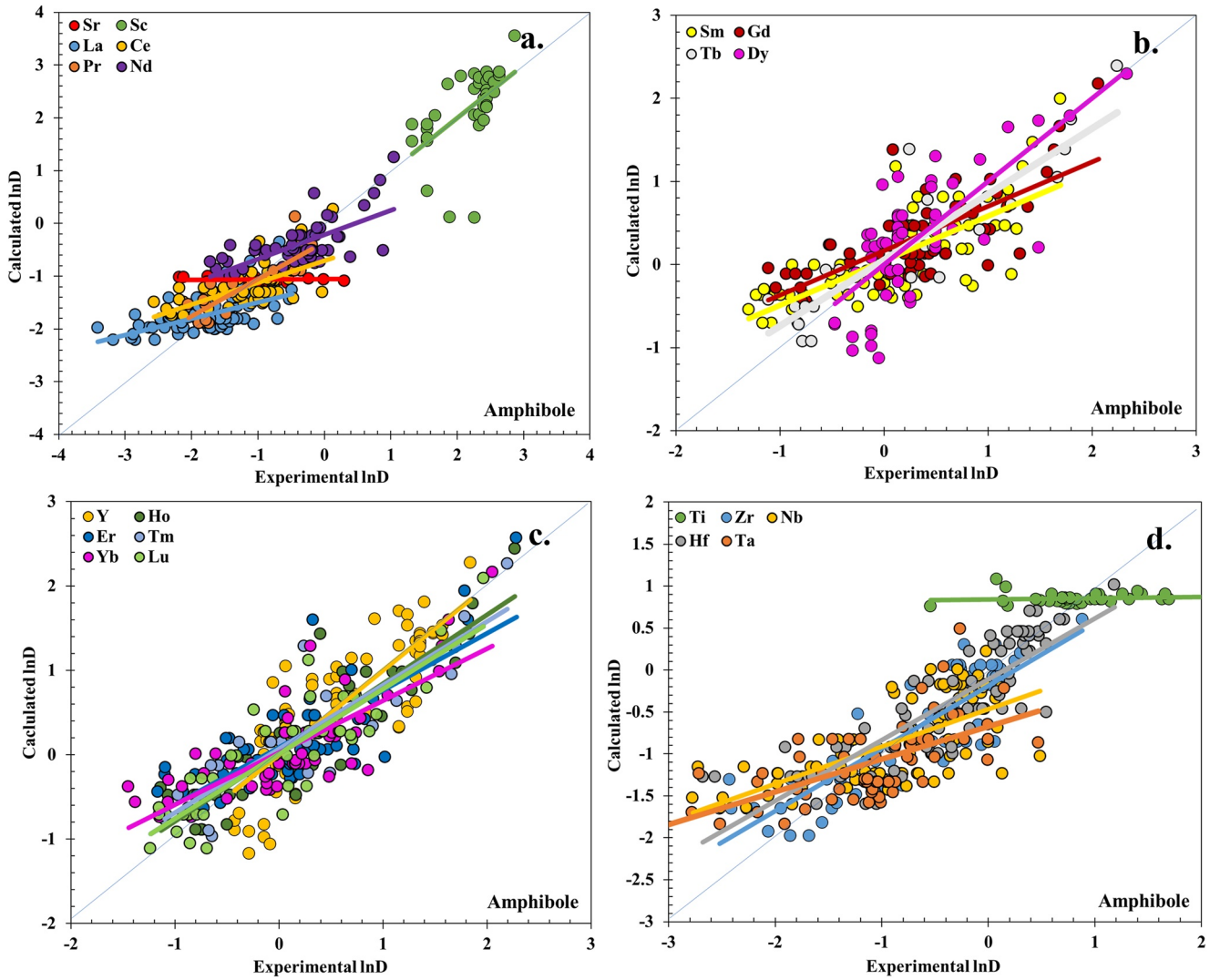

Figure 4. Correlation of partition coefficients calculated for amphibole using the single term linear regressions for temperature dependence (Table 2) with experimentally determined values (Data Set S2). (a) Sc, Sr and Light Rare Earth Elements (REE), (b) medium REE, (c) Y and heavy REE, and (d) High Field Strength Elements (HFSE). Each symbol represents a single experimental determination for that element. The experiments collectively follow a 1:1 correlation, but the results for individual elements are characterized by a slope less than 1 (colored trendlines). Note that all trendlines have a slope that is equal to or less than 1.

5.2. Systematics of Temperature Dependence Within the Rare Earth Elements

The partitioning of REE between most rock forming minerals and melt displays a progressive pattern correlated to ionic radius (Onuma et al., 1968). We can then assume that any model for REE partitioning should produce results that exhibit a "smooth" pattern so long as the conditions are within the range where the REE valence state of +3. In addition, we can infer that the temperature dependence should also exhibit a regular pattern and manifest that pattern in terms of the slope of ln $^{\text{mineral-melt}}D_i$ versus reciprocal temperature. If we analyze those values (slope column under reciprocal temperature in Table 2) for $^{\text{mineral-melt}}D_{\text{REE}}$ as a function of atomic number for clinopyroxene (Figure 6a), amphibole (Figure 6b), and garnet (Figure 6c), there is a negative correlation of the temperature dependence and atomic number for clinopyroxene while a positive correlation for amphibole and garnet. It is important to note that the regression constant that describes temperature dependence increases or decreases by 20%–40% across the REE (Figure 6). This would result in a flatter pattern of ln $^{\text{mineral-melt}}D_{\text{REE}}$ versus atomic number for clinopyroxene at lower temperature, and steeper patterns for amphibole and garnet. Such changes in REE patterns have been observed before and been attributed to changes in the influence of charge balancing Al (e.g., Wood & Blundy, 2001). Therefore, the observed differences in steepness in REE patterns may be due to a combination of factors and may be influenced by the fact that temperature and Al activity/concentration are not independent. Although there is

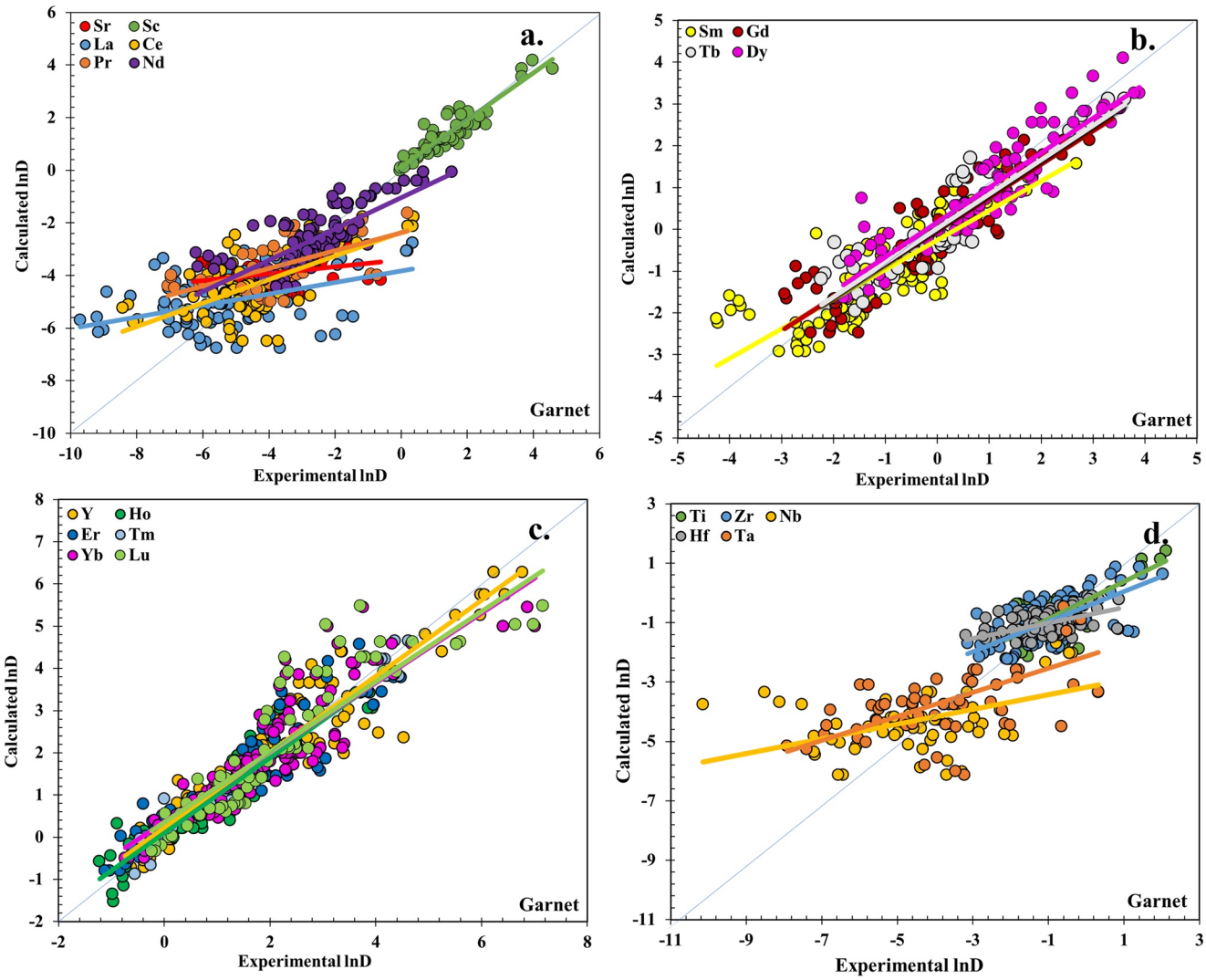

Figure 5. Correlation of partition coefficients calculated for garnet using the single term linear regressions for temperature dependence (Table 2) with experimentally determined values (Data Set S3). (a) Sc, Sr and Light Rare Earth Elements (REE), (b) medium REE, (c) Y and heavy REE, and (d) High Field Strength Elements (HFSE). Each symbol represents a single experimental determination for that element. The experiments collectively follow a 1:1 correlation, but the results for individual elements are characterized by a slope less than 1 (colored trendlines). Note that all trendlines have a slope i.e., equal to or less than 1.

significant correlation of the behavior of the REE with atomic number, not all element's correlation with reciprocal temperature is linearly aligned but fall above or below a best-fit line (Figure 6). If we apply such single term linear regression constants to predict partitioning behavior (Figure 7), the result is an irregular pattern across the REE.

The possibility that there is a progressive change in differential temperature dependence in addition to progressive changes in the partition coefficient has been recognized before, either attributed to statistical "noise" from the results for one element to another or as a systematic progression (Dohmen & Blundy, 2014; Nielsen, 1988) that relates to differences in the calibration database (Bédard, 2006, 2014; Nielsen et al., 2017).

The element-to-element variation can be accommodated if one has a standard with which to link the temperature dependence (or any other observed dependence). In their investigation of the systematics of trace element partitioning in plagioclase, Dohmen and Blundy (2014) tied the element-element variation to the behavior of an element with presumed similar behavior and a large database (number of experimental determinations)—in that case, all +1 elements were tied to Na, all +2 cations were tied to Ca, and all +3 cations were tied to La. Another approach is to "force" the regressions for modeled trace element into a regular pattern by assuming that the impact of any dependency will be the same for all elements that fall into the same behavioral group (e.g., REE, HFSE, LILE). This approach successfully produces a smooth pattern of behavior for the REE but does not accommodate

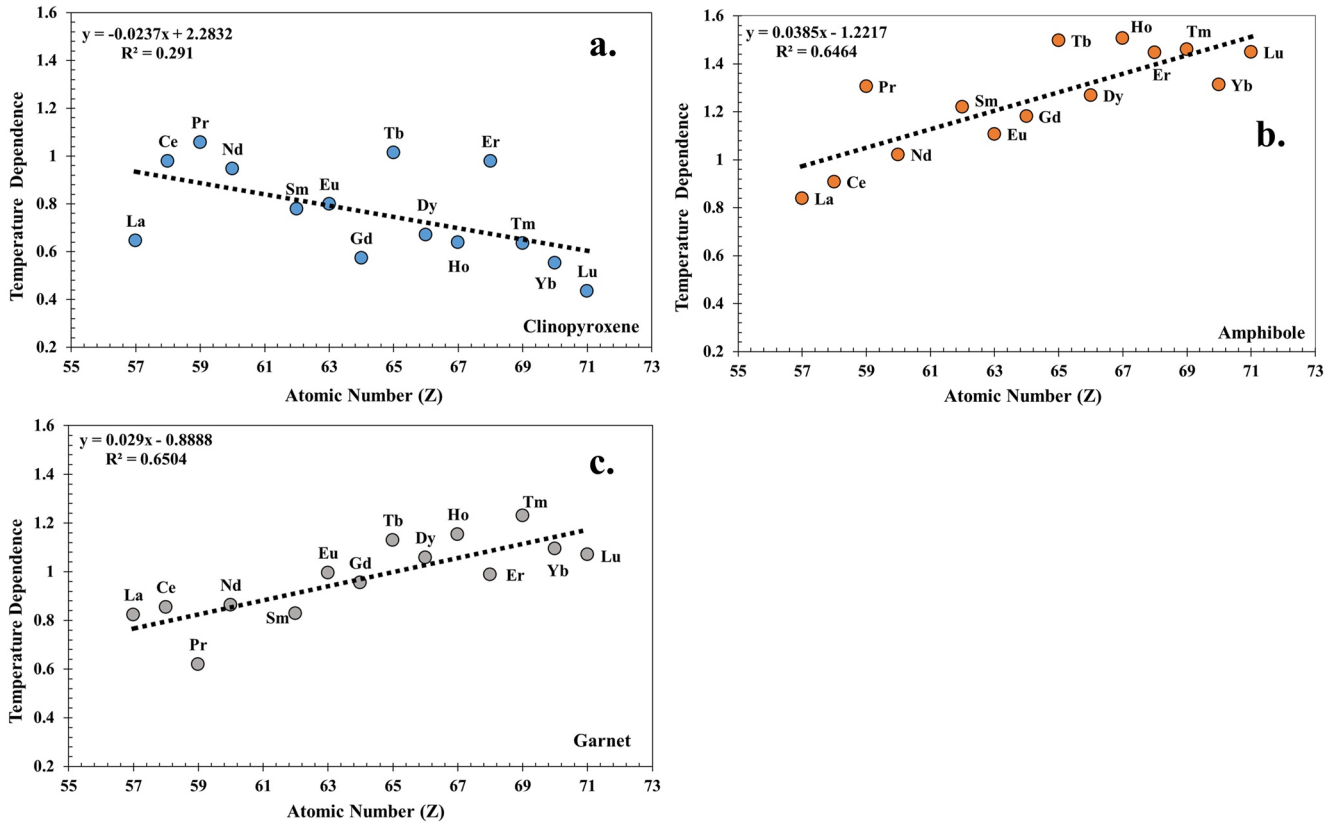

Figure 6. Correlation of the calculated temperature dependence with Z for (a) clinopyroxene, (b) amphibole, and (c) garnet. The temperature dependence is defined as the correlation of ln *D* versus reciprocal temperature (Table 2). The presumption of a progressive change as a function of atomic number is based on the systematic change in ionic radius for the REE. The trend is negative for clinopyroxene but positive for amphibole and garnet. The linear regression represents an estimate of the change in the dependence of atomic number with reciprocal temperature from (Table 2).

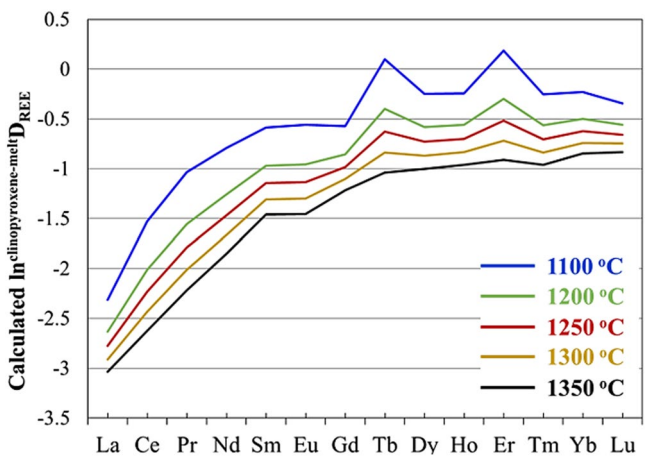

Figure 7. Calculated clinopyroxene-melt partition coefficients using expressions describing temperature dependence alone. Note that the pattern becomes increasingly irregular, with decreasing temperature. The elements related to the largest offsets are Tb and Er.

the possibility that there was a systematic change in the temperature dependence as a function of atomic number, as we see for clinopyroxene, amphibole, and garnet (Figure 6). In other words, we are assuming that the known differences in the database characteristics (e.g., number of experiments, pressure and temperature range, liquid composition) for all elements with the same valence do not matter. We can evaluate this assumption and the magnitude to which variation in dependence within a group is systematic by examining the degree to which the correlation of ln $^{\text{mineral-melt}}D_{\text{REE}}$ to reciprocal temperature with atomic number (Figure 8) departs from the best fit line, and how that departure from systematic behavior correlates with other aspects of the database. The results are similar for all three minerals studied here (Figures 8a–8c), and can be characterized as a rough (low R^2) negative correlation of the departure from the trend shown for the slope of the ln $^{\text{mineral-melt}}D_i$/ reciprocal temperature correlation versus number of experiments, together with an estimate of the departure of the progressive trend within the REE. In effect, the calculated slope that represents the temperature dependence is negatively correlated with the number of experiments in the calibration data set. This means that elements for which there are more experimental determinations (one of the differences in database characteristics) exhibit less of a temperature dependence than one would predict on the basis of the overall results for the other REE. It is important to note that a negative correlation is observed for clinopyroxene, amphibole, and garnet, in spite of the differences

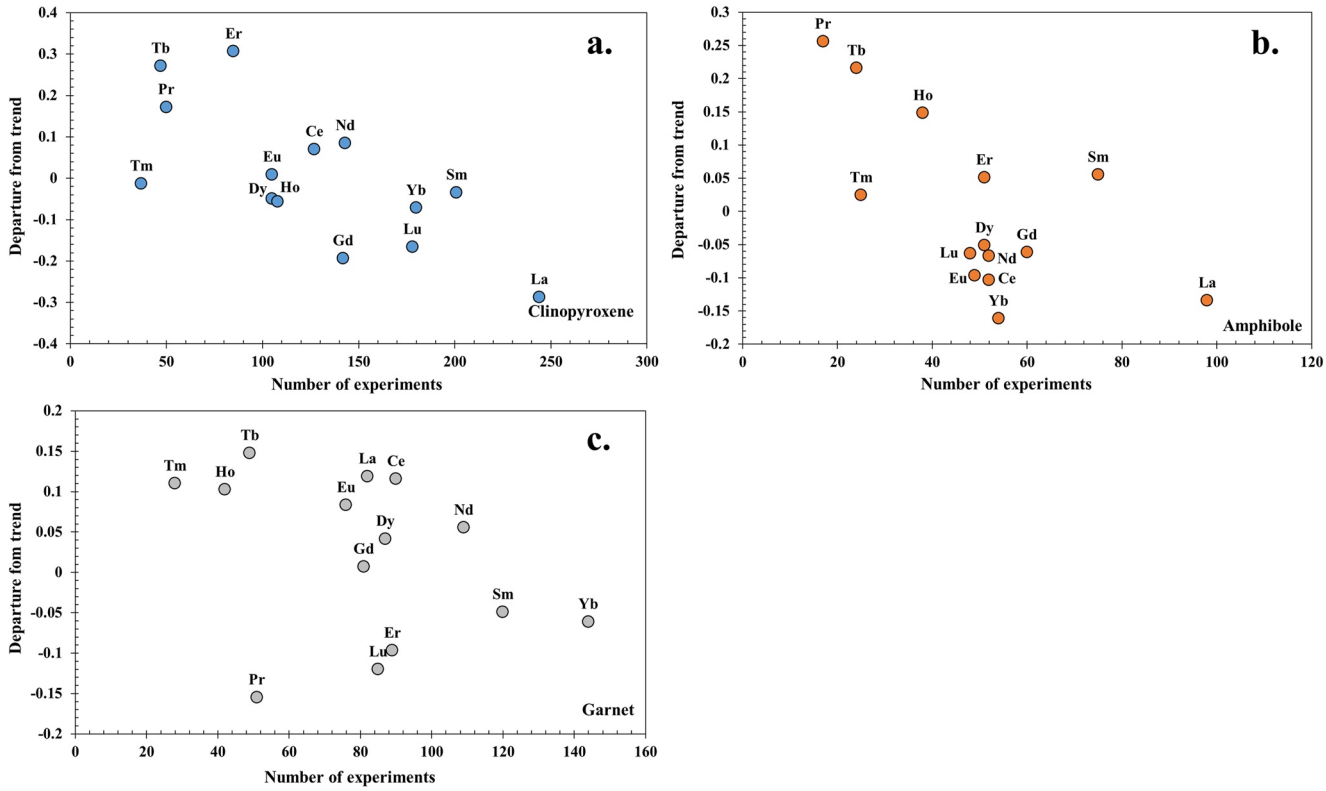

Figure 8. Correlation of the departure from the observed temperature dependence with atomic number (Figure 6) with the number of experiments where the REE (a) clinopyroxene, (b) amphibole, and (c) garnet/melt partition coefficients are reported. For example, from Figure 6a, one can see that the data for Tb partitioning data have a temperature dependence that is 0.3 above the line that describes the trend in that figure. There are 50 clinopyroxene/melt partition coefficient experiments in the literature. In contrast, there are ~250 published La partition coefficients for clinopyroxene/melt, and the calculated temperature dependence is 0.3 below the line in Figure 6a. Note that the trend is negative in all three mineral/melt systems.

observed in the overall number of experiments, and the differences documented in the single term linear regression correlations (Table 2).

The underlying reason for this correlation of regression bias with the number of experiments is unclear. It is present for data from minerals whose partitioning data are otherwise distinct in terms of average phase composition, number of experiments, and the distribution of the number of experiments within the group. One explanation may be that experimental approaches are developed primarily based on the need to explore compositions and conditions that were not previously examined. In that case, new data will tend to expand the compositional diversity and range of conditions of the data and may result in greater scatter (in predictive models) if there are unaccounted for dependencies or if the observed dependencies are not independent.

5.3. Predictive Accuracy of Expressions Based on Multiple Linear Regressions

5.3.1. Multiple Linear Regressions

Since our ultimate goal is to develop a methodology for predicting trace element behavior, it is imperative that we use an approach that will allow us to "see through" both the effects of non-ideal mixing of trace element components and the possible impact of the heterogeneous calibration data set used to calibrate predictive models. Building on the calculations based on temperature dependence alone (single term linear regression), we expanded the analysis to multi-linear regressions to simultaneously determine the combined effect of several geochemical parameters on trace element partitioning. To build a practical predictive model that remains theoretically grounded, even for conditions far from the calibration data, we begin by developing a model that is sensitive to T, P, and phase composition. This selection of predictor variables for the multi-linear regression is demanded by their large thermodynamic impact on trace element partitioning. Anything capable of strongly altering the energetics of trace element

exchange between liquids and coexisting crystals is a strong candidate for inclusion in a multi-linear regression model. The specific terms we selected provide simple yet robust metrics that capture the dominant factors influencing elemental substitutions through alterations to the local geometries of crystal lattice sites and the corresponding pseudo-lattice sites in the atomic structure of the liquid. To obtain a functional and robust regression model, we must define a set of experimental measurements that adequately capture these primary thermodynamic effects.

For the multi-linear regression model, we selected a set of experimentally constrained metrics that jointly capture the dominant factors influencing the energetics of lattice site substitution. In summary, liquid polymerization affects liquid component activities. Ca-content of the mineral influences the strain related to the changes in the crystal lattice caused by the substitution of the large Ca ion into the octahedral sites in clinopyroxene, amphibole, and garnet (Forsythe et al., 1994; Fujinawa & Green, 1997; Hill et al., 2000; Nielsen, 1988; Wood & Blundy, 2001 and many others). The mole fraction of Al in the tetrahedral site (Al_{IV}) is related to paired substitution of elements with valences of +1, +3, +4, and +5 that require charge balance to occupy octahedral sites normally occupied by Ca, Mg, and Fe (Mollo et al., 2020; Nielsen, 1988). This is achieved by first recognizing that the energetics of elemental partitioning are influenced both by physical variables, like temperature and pressure (which strains lattice sites), as well as chemical factors that include mineral and liquid composition, liquid polymerization, and volatiles. All of these parameters are interdependent in ways that influence the outcome of any regression analysis. Once parameters are selected, the next step is to standardize data to optimize computational effectiveness during the fitting process, improve statistical interpretation of the fitted model parameters, and enable the introduction of additional constraints to provide model robustness especially in data-limited or data-heterogeneous systems. Standardized data represent a simple linear transformation of the original data set, where the mean value is subtracted off and deviations from that mean are scaled by the standard deviation of the data. Thus, in a standardized data set, every variable is centered on zero and varies typically between −1 and +1 (at the 1s level accounting for 68% of the data). Accordingly, we generated a standardized data set by transforming the experimental parameters and measured partition coefficients described above.

We constructed a standardized set of experimental parameters selected based on the observed correlation with partitioning behavior (Table 2). We carried out multi-linear regressions on the standardized data using the "statsmodels" package, an open-source package for statistical modeling available in the Python programming language. These standard ordinary least squares regression fits are carried out in a simple set of python-based Jupyter Notebooks, which simultaneously carry out and document the analysis. The primary output from these Python-based notebooks is a set of results tables that summarize the fitted models, and also include regression diagnostics that quantify the goodness of fit for each model. This same analysis is repeated for every trace element in the database and for each of the three minerals studied here (clinopyroxene, amphibole, and garnet).

Applying basic multi-linear regression certainly improves performance over single-term linear models but still allows large variations in the model coefficients in response to insufficient data coverage for many elements. Due to their direct links with the thermodynamic process of elemental site substitution, we expect that the model coefficients should all take on reasonable values (with standardized magnitudes that do not deviate strongly from zero). But experimental data coverage is highly variable within the database, both in terms of raw numbers of measurements as well as the completeness of sampling the key factors influencing partitioning (e.g., temperature, pressure, and compositions). At the same time, preliminary correlation analysis revealed that the partitioning behavior of Ti was usefully predictive of the behavior of nearly every element for all three minerals studied. In fact, the single-term correlation strength was generally stronger for D_{Ti} than for any other factor for both clinopyroxene and amphibole and was still at least reasonably predictive for garnet. This observation points to the underlying physical and chemical similarities between Ti-partitioning and generalized trace element partitioning (though the strength of this connection depends on many factors not fully explored, most notably any differences in the dominant site-substitution mechanism). Given the surprising effectiveness of Ti for predicting the behavior of every element explored, we thus introduced an additional Ti-based regularization constraint on the multi-linear regressions, which helped to constrain the allowable partitioning behavior for even the elements where data coverage is not sufficient to ensure physically reasonable model parameters. Because of standardized variables, every coefficient is placed on the same unitless scale. This allows easy direct comparison between the coefficients for each partitioning factor (e.g., inverse temperature, pressure, Al_{IV} content), enabling us to compare the relative strength of each on the overall partitioning. To interpret these standardized coefficient values, we can view the coefficients as a simple mapping between how the typical level of variability for variable X impacts the variability seen in the log-partitioning factor. For instance, a coefficient of 0.5 means that a typical change in variable X of 1s translates into a 0.5 s change in

the ln $^{\text{mineral-melt}}D_i$ value. Due to the standardization of all variables, statistical coefficients must be of the order ±1 or smaller. Coefficients express dependence relative to a 1s change in the predict-ed ln $^{\text{mineral-melt}}D_i$ values. The data must have a variability of ±1 standard deviation by the construction of the standardized variables, so large magnitude coefficients are statistically difficult to realize. Large coefficients are highly unlikely because they require perfect compensation of multiple competing factors, so that large changes induced by variable X1 are mostly canceled by opposing effects from variable X2 (along with X3, X4, and so on…). Standardization allows us to impose constraints on the variables to produce models that are stable as a function of the changes in calibration parameters (e.g., they depart from reality slowly). Given the benefits of the standardization process, along with the observed correlations with Ti-partitioning, we can safely assume Ti-regularizing prior constraints for every slope coefficient, constraining each to lie in the range of ±0.2 (at the 1s level, e.g., with 68% confidence) relative to the fitted coefficient values for Ti. Given that the correlations with D_{Ti} were strong for nearly every element in all three minerals ($0.4 \leq R^2 \leq 0.9$), this approach imposes the limit that every coefficient deviates from the Ti coefficient values by less than ±0.4 with 95% confidence (2s).

The results of these Ti-constrained (regularized) regressions (Figures 9–11; Table 3) for clinopyroxene, amphibole, and garnet, respectively, exhibit improved prediction accuracy for the experimental values (slope that approaches 1, for a linear fit to the calculated and experimental partitioning values i.e., characterized by R^2 approaching 1). Despite dramatic improvements, examination of the regression coefficient means and errors demonstrates that the parameters still retain non-negligible variability from element to element within the REE, pointing to areas for future improvement. Overall, the accuracy of these regularized multi-linear models is strongly improved compared with the results for the linear regression based on reciprocal temperature alone (as documented by the rotation of the slope toward the 1:1 line as well as improved R^2 values).

5.3.2. Comparison of Predictive Error Between Single Term (Reciprocal Temperature) Linear and Multiple Linear Regressions

In the comparison described below, we will attempt to quantify differences in the predictive error of partitioning models and use the comparative results to assess the role of database characteristics. We use the calibration data set as unknowns and applied the regression parameters to that data (Tables 2 and 3) to test the internal consistency of the data by calculating partition coefficients and assessing their relationship/correlation to the experimental values. This comparison may be made between models by comparing the square of the calculated-experimental values—normalized to the number of experimental determinations for each number (root mean square deviation—RMSD) and use that as a measure of the model's predictive power (Figures 12a–12c, Data Set S4).

For the three minerals studied, the multiple linear regression results exhibit greater predictive power (lower RMSD) compared to the linear regression based solely on reciprocal temperature. As noted above, this is consistent with the observed differences in the slopes of the trendlines for the calculated versus experimental values (Figures 3, 4, 5, 9, 10, and 11). In general, the trendlines for calculated versus experimental values are closer to 1 for the results from the multiple linear regression. To reduce the level of complexity in the graphical representation of the results (Figure 12), we will consider only Sr outside the REE, and the HFSE.

If we first consider the results for clinopyroxene (Figure 12a), the predictive power for the individual element partition coefficients calculated using the multiple linear regression are all lower than for the linear regression-based results. In addition, the trend of predictive error with average ln D exhibits a negative correlation, as one would predict if there were increased analytical error at low ln D. As noted above, if analytical error is a primary factor in the observed differences in correlation coefficient for each element, then the analytical error on the experimental values would decrease as ln D increased toward a value of ~0 (D of 1), and as concentration in the experimentally produced crystal approached that in the co-existing melt. However, this interpretation is complicated by the fact that many experiments are doped with the element of interest to different levels.

If we analyze the same data for amphibole (Figure 12b), we see a different pattern in RMSD compared with clinopyroxene. First, the calculated results for the two models are not correlated with the average ln D for each element (Figure 12b), indicating no improved correlation between calculated and observed values for higher ln D (more compatible elements). Second, the RMSD for the linear regression-calculated values is higher at low ln D than the RMSD for the multiple linear results (MLR more predictive for more incompatible elements). However, RMSD values for average ln D above 0 are consistently (but not exclusively) higher for the multiple linear regression-based estimates (MLR less predictive for more compatible elements).

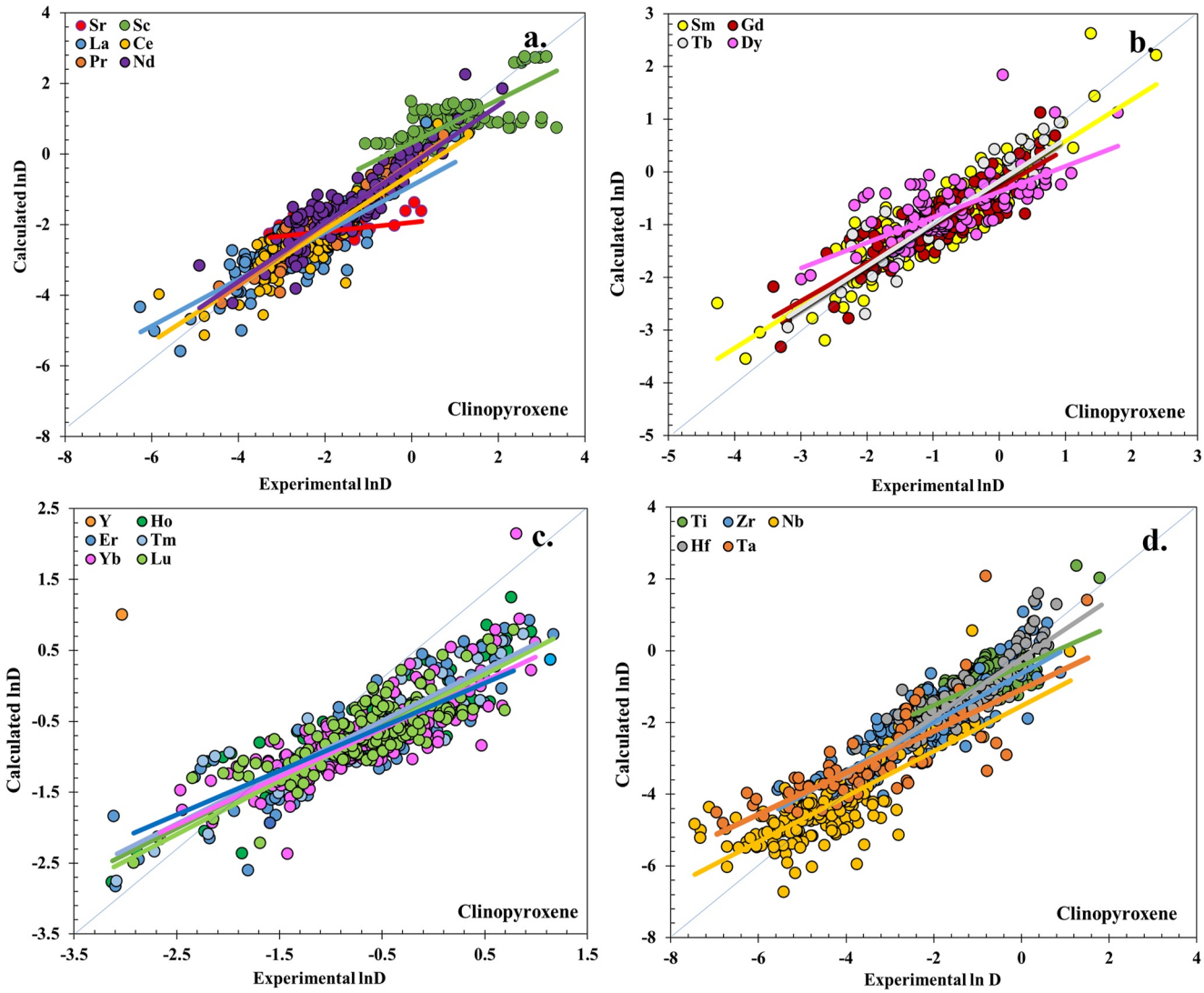

Figure 9. Calculated versus experimental $^{\text{mineral-melt}}D_i$ using multiple linear regression (MLR) parameters (Table 3) for clinopyroxene (Data Set S1). (a) Sc, Sr and Light Rare Earth Elements (REE), (b) medium REE, (c) Y and heavy REE, and (d) High Field Strength Elements (HFSE). Each symbol represents a single experimental determination for that element. The experiments collectively follow a 1:1 correlation, but the results for individual elements are characterized by a slope less than 1 (colored trendlines). Note that all trendlines have a slope that is equal to or less than 1.

The correlation of calculated versus experimental garnet partitioning experimental data results are similar in that they (Figure 12c) exhibit lower RMSD (more predictive) for multiple regression results at low average ln D than for linear regression results (blue above orange at low ln D) but reverse for compatible elements characterized by an average ln $D \sim 0$ (orange above blue).

Taken collectively, these results indicate that the inclusion of extra terms in multiple linear regression will improve the predictive power for clinopyroxene/melt partitioning data, less so for amphibole and garnet. The increased predictive power seen with the inclusion of additional terms is also consistent with the wider range of composition, P and T where clinopyroxene is stable in natural systems (Figure 1). In the case of garnet/melt partitioning, the lower level of improvement in predictive power associated with the inclusion of additional terms suggests that the dependencies associated with composition are less important than the influence of propagated error associated with measurement of the additional terms, as can be seen in the rotation of the trendlines for calculated versus experimental results (e.g., Figure 11a). Unfortunately, a quantitative analysis of the propagated error for the entire database is difficult because of the multiple analytical tools used, as well as the wide range of doping levels—and the differences in each of those factors for different elements in any specific mineral.

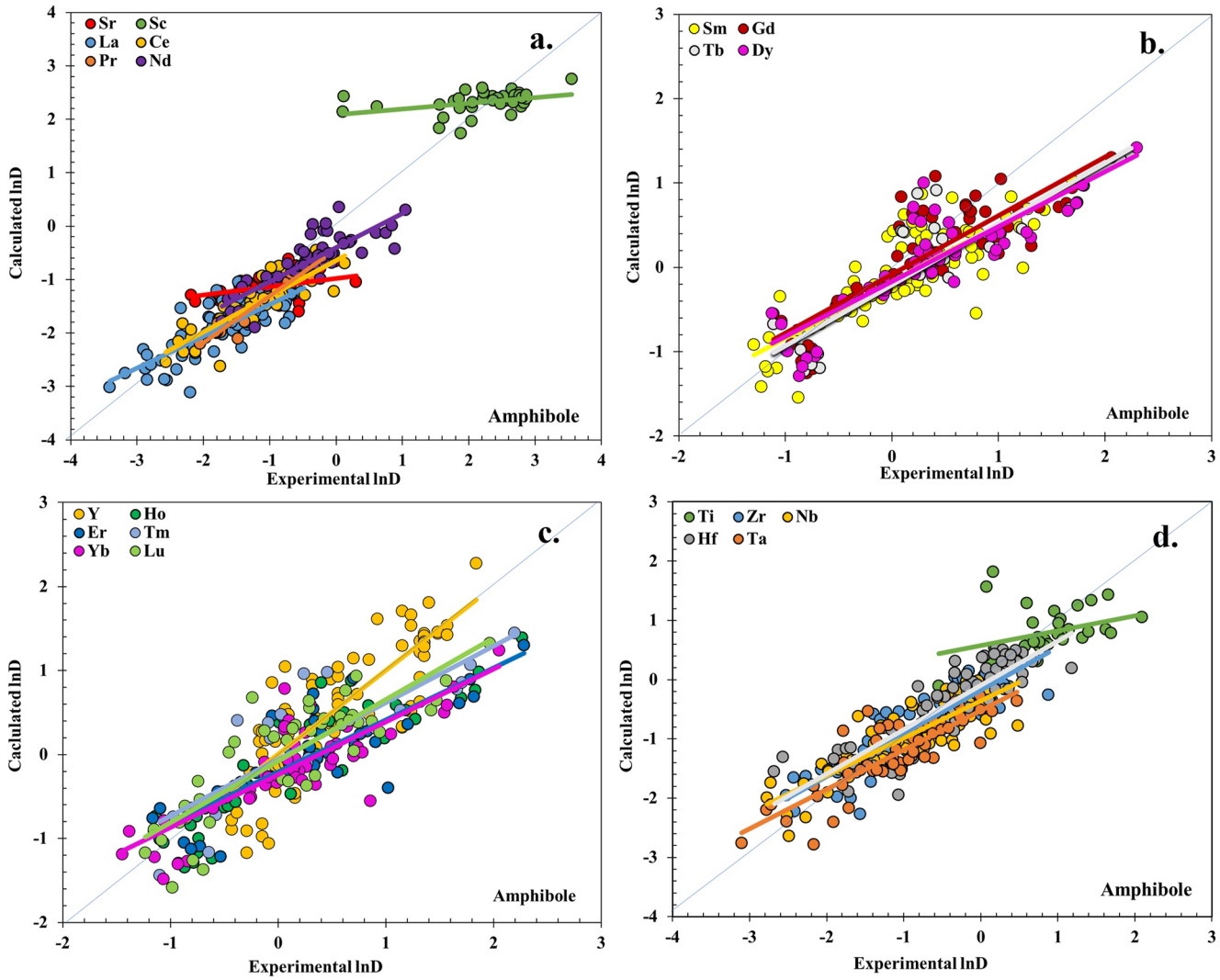

Figure 10. Calculated versus experimental $^{\text{mineral-melt}}D_i$ using multiple linear regression (MLR) parameters (Table 3) for amphibole (Data Set S2). (a) Sc, Sr and Light Rare Earth Elements (REE), (b) medium REE, (c) Y and heavy REE, and (d) High Field Strength Elements (HFSE). Each symbol represents a single experimental determination for that element. The experiments collectively follow a 1:1 correlation, but the results for individual elements are characterized by a slope less than 1 (colored trendlines). Note that all trendlines have a slope that is equal to or less than 1.

6. Conclusions

Using an expanded calibration database comprised of published experimentally determined partition coefficients, we confirmed that REE and HFSE partitioning in clinopyroxene, amphibole, and garnet is correlated to temperature, pressure, melt composition, Ca content, Al_{IV}, Si_{VI} (garnet), and D_{Ti}. These dependencies were identified several decades ago on smaller, more restricted databases, but had not been reaffirmed with new experimental data. This new analysis has identified additional details of the dependencies, including how the magnitude of the dependence varies from mineral to mineral. The correlation of $^{\text{mineral/melt}}\ln D_i$ for REE and HFSE in clinopyroxene and amphibole with Al_{IV} and D_{Ti} are similar to one another, in spite of the difference in valence. The strongest dependence for garnet/melt REE and HFSE partitioning is with reciprocal temperature.

Predictive models may be developed based on any individual parameter dependence or, using multiple linear regression analysis, by including all parameters in the regression for which there is an observed correlation with partitioning behavior. If one uses any one of the individual dependencies, the result is that the impact of the others (combined dependencies) is not accounted for. However, the calculated results of those models are not linearly correlated with the calibration data set (calculated and experimental values for partitioning do not lie on

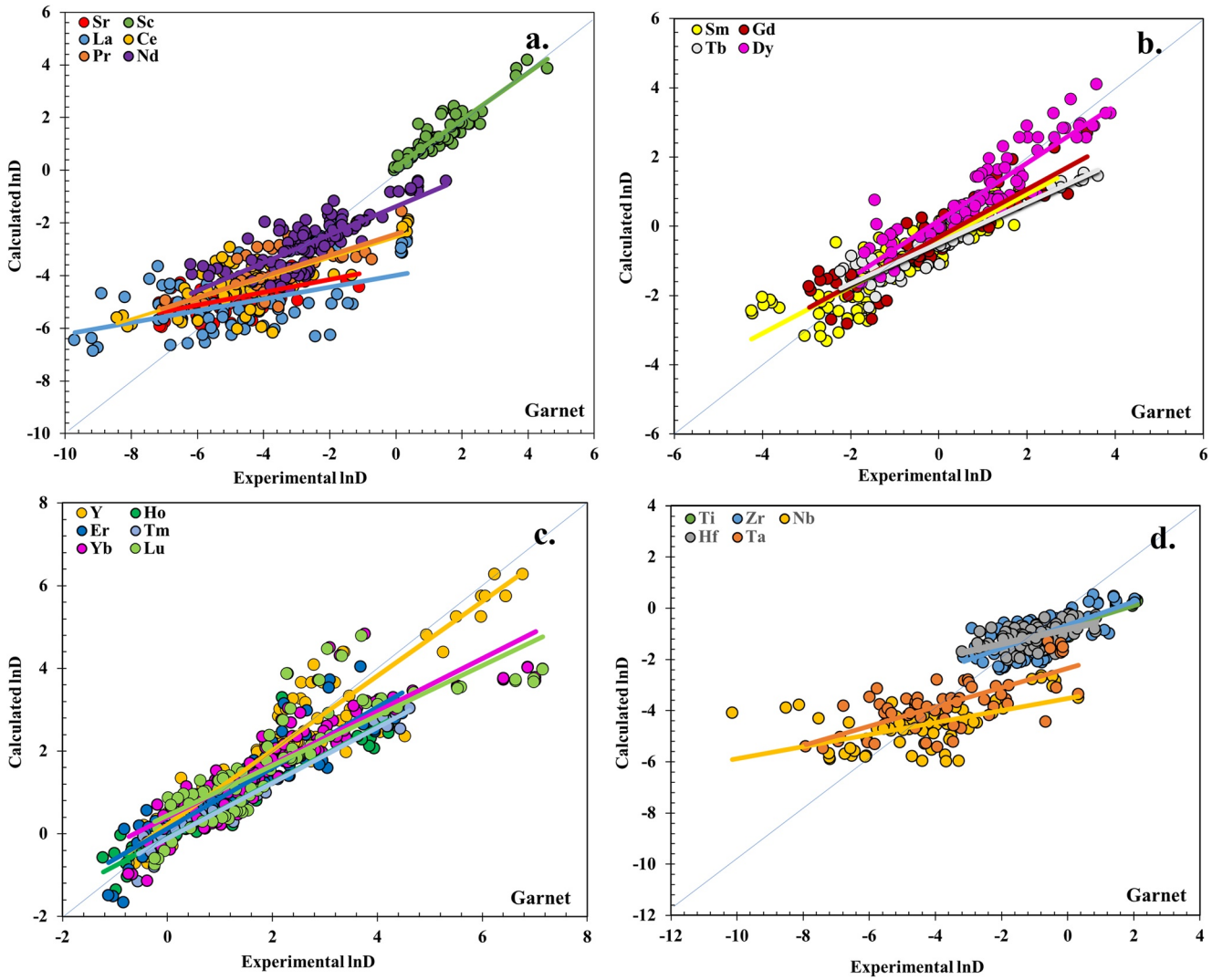

Figure 11. Calculated versus experimental $^{\text{mineral-melt}}D_i$ using multiple linear regression (MLR) parameters (Table 3) for garnet (Data Set S3). (a) Sc, Sr and Light Rare Earth Elements (REE), (b) medium REE, (c) Y and heavy REE, and (d) High Field Strength Elements (HFSE). Each symbol represents a single experimental determination for that element. The experiments collectively follow a 1:1 correlation, but the results for individual elements are characterized by a slope less than 1 (colored trendlines). Note that all trendlines have a slope that is equal to or less than 1.

a 1:1 line). The range of predicted (calculated) values is therefore narrower than that of the experimental values on which the model is based and appears "flatter," characterized by a trendline slope less than 1. The difference between the distribution of the calculated values versus the experimental values is dependent on the impact of all the other unaccounted parameters, including analytical error.

Additional scatter may be related to the difference in the configuration of the calibration data set. In the case of the temperature dependence of REE partitioning (as approximated by the slope of ln $^{\text{mineral-melt}}D_{\text{REE}}$ vs. 10000/T), clinopyroxene, amphibole, and garnet are correlated with atomic number and ionic radius, with that dependence on atomic number being negative for clinopyroxene and positive for amphibole and garnet. The correlation is irregular, with some values for temperature dependence above the correlated line, and others below. The irregularity of the correlation of temperature dependence and atomic number will result in irregular patterns for calculated REE partition coefficients across the range of REE. The source of that irregularity can be seen in the correlation of the magnitude of departures from the temperature dependence versus atomic number. Such departures are negatively correlated with the number of experimental determinations for each element. The precise provenance of this negative correlation is unknown but may be related to how the experimental investigations for specific elements are designed (including dopant levels), and which elements pose

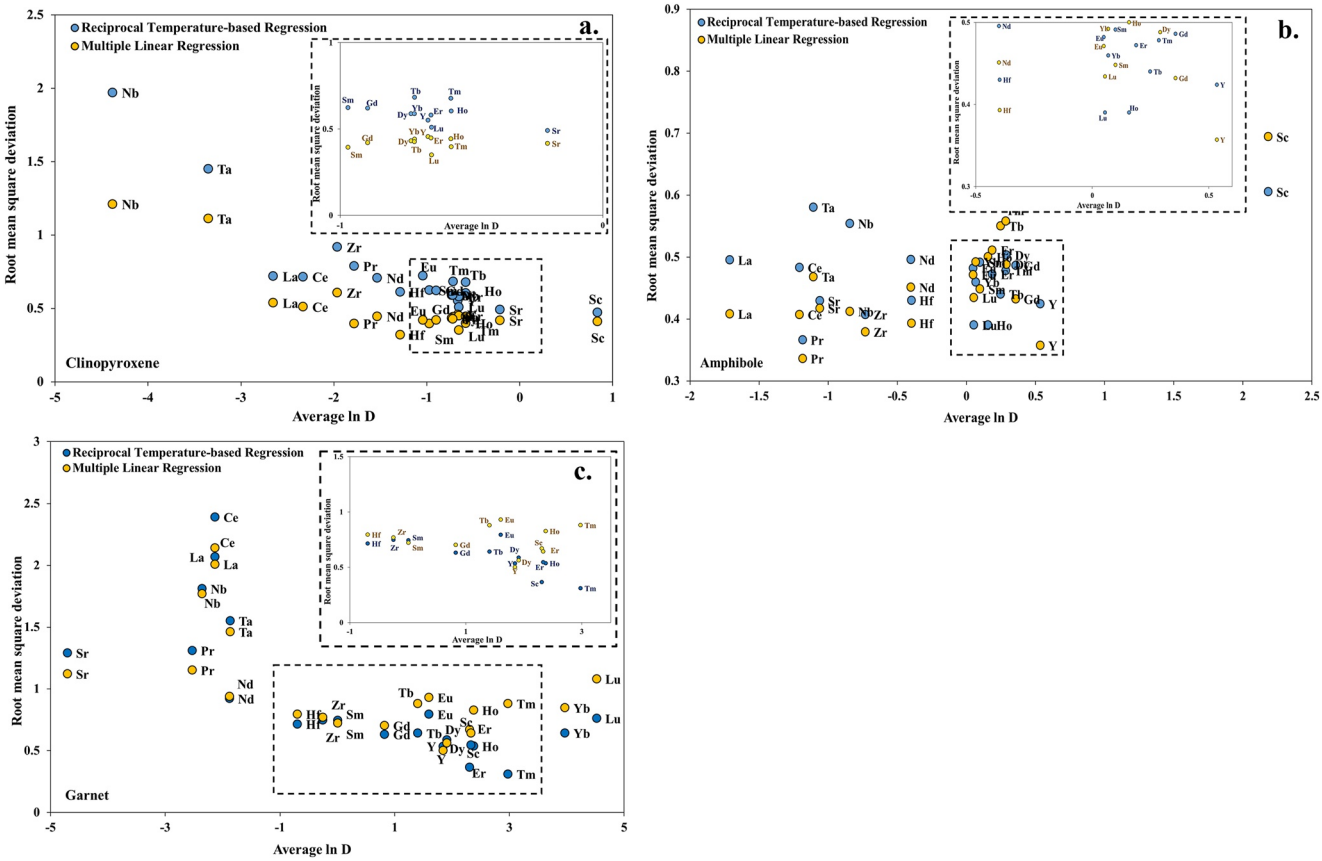

Figure 12. Predictive power (difference between calculated and experimental values) in terms of root mean square deviation (root of sum of the square of the difference between the calculated and experimental values) vs. experimentally determined average ln *D* for (a) clinopyroxene, (b) amphibole, and (c) garnet. Blue symbols represent calculated values using a linear correlation of ln *D* with reciprocal temperature (Table 2). Orange symbols represent calculated values using multiple linear regression correlating ln *D* with a number of dependent parameters (Table 3). The inset figures with dashed squares are close-up views of the specified region.

more difficult analytical problems due to a combination of factors including low concentration, low sensitivity, or signal overlap. The multiple source of uncertainty makes it difficult to quantify the magnitude of the irregularity (e.g., is the irregularity statistically meaningful). Even if the irregularity of the modeled results is within the error of the regression, it does not inform our understanding of the trend of the dependency as a function of atomic number. That dependency should be regular (based on our understanding of the behavior of groups of elements such as the REE). However, the rough correlation of RMSD and temperature dependency with the number of experiments for all three phases suggests that there are underlying properties of the existing data that may be related to experimental design—on the part of literally hundreds of experimentalists over a period of 50 years.

The predictive power (reduced predictive error) of expressions describing partitioning behavior may be improved by the application of multiple regression analysis. However, our results for multiple regression exhibit significant element-element irregularity in the regression parameters, and significant differences in the magnitude of those parameters among the three minerals. The results for multiple regression generally exhibit higher levels of correlation than single term temperature-dependent regressions, but do not reproduce the predicted consistent behavior within the REE. Rather, the modeled REE patterns exhibit increasingly irregularity as one simulates conditions at the margins of the calibration data set. Similar patterns are likely present within other element groups such as the HFSE and LILE but are less obvious due to the more complex differences in ionic radius and charge within those groups. Nevertheless, it is possible that such irregularities would impact the modeling of, for example, LILE/HFSE or REE/HFSE ratios (e.g., Y/Zr, Ba/Nb). This may also be caused by the differences in the substitution mechanisms for different phases for elements with variable valences, particularly for +1, +2 cations compared to +3, +4, +5 cations.

Estimates of the predictive power of models based on either single term linear regressions or multiple linear regression exhibit different patterns for reduced residual scatter relative to 1:1 calculated versus experimental trend as exhibited in R^2 of the regression or root mean square deviation (RMSD) for the predicted values. Further, for clinopyroxene and to some degree for garnet, the RMSD of calculated values versus the experimental values trend lower as the average partition coefficients trend higher. This would be the expected result if the inclusion of additional parameters effectively improves the precision of the model—with a majority of the remaining scatter due to analytical error. Such error is correlated to concentration and indirectly to the partition coefficient. However, the results for amphibole do not show a correlation of RMSD with ln D. In addition, there remains a significant element to element variation in the regression parameters within groups of elements presumed to behave coherently. This can be attributed to differences in the number and characteristics of experimental determinations for each element in each mineral. Increase in the accuracy of predictive models will require increased sophistication in our approach to regression analysis, involving regularization of the controlling parameters. More importantly, we must account for the fact that the controlling parameters for clinopyroxene, amphibole, and garnet have different impact on predictive models due to the differences in substitution mechanisms, the range of composition representative of the stability field of each phase, and the resultant differences in the calibration data sets.

Data Availability Statement

The dataset is available through the traceDs database site (Nielsen & Ustunisik, 2022a, 2022b, 2022c).

Acknowledgments
Support for this work, including support for E.C. thesis was provided by the NSF/OCE&MGG-1948838, NSF/EarthCube-2026016, and EAR/GI-2148990 grants to G.U. and R.L.N. A.S.W. thanks the NSF/EAR-1948806 and EAR-2026904 for financial support that made this research possible. We thank Mark S. Ghiorso for useful conversations about this work. Authors benefitted from the detailed and constructive comments by Silvio Mollo and Penny Wieser. We also thank the editor Marie Edmonds for the time and effort put forth.

References

Beard, C. D., van Hinsberg, V. J., Stix, J., & Wilke, M. (2019). Clinopyroxene/melt trace element partitioning in sodic alkaline magmas. *Journal of Petrology*, *60*(9), 1797–1823. https://doi.org/10.1093/petrology/egz052

Beattie, P., Drake, M., Jones, J., Leeman, W., Longhi, J., McKay, G., et al. (1993). Terminology for trace-element partitioning. *Geochimica et Cosmochimica Acta*, *57*(7), 1605–1606. https://doi.org/10.1016/0016-7037(93)90015-o

Bédard, J. H. (2006). Trace element partitioning in plagioclase feldspar. *Geochimica et Cosmochimica Acta*, *70*(14), 3717–3742. https://doi.org/10.1016/j.gca.2006.05.003

Bédard, J. H. (2007). Trace element partitioning coefficients between silicate melts and orthopyroxene: Parameterizations of D variations. *Chemical Geology*, *244*(1–2), 263–303. https://doi.org/10.1016/j.chemgeo.2007.06.019

Bédard, J. H. (2014). Parameterizations of calcic clinopyroxene—Melt trace element partition coefficients. *Geochemistry, Geophysics, Geosystems*, *15*(2), 303–336. https://doi.org/10.1002/2013GC005112

Blundy, J., & Wood, B. (2003). Partitioning of trace elements between crystals and melts. *Earth and Planetary Science Letters*, *210*(3–4), 383–397. https://doi.org/10.1016/s0012-821x(03)00129-8

Dohmen, R., & Blundy, J. (2014). A predictive thermodynamic model for element partitioning between plagioclase and melt as a function of pressure, temperature, and composition. *American Journal of Science*, *314*(9), 1319–1372. https://doi.org/10.2475/09.2014.04

Forsythe, L. M., Nielsen, R. L., & Fisk, M. R. (1994). High-field-strength element partitioning between pyroxene and basaltic to dacitic magmas. *Chemical Geology*, *117*(1–4), 107–125. https://doi.org/10.1016/0009-2541(94)90124-4

Fujinawa, A., & Green, T. H. (1997). Experimental study of partitioning of Hf and Zr between amphibole, clinopyroxene, garnet, and silicate melts. *Journal of Mineralogy Petrology and Economic Geology*, *92*(2), 69–89. https://doi.org/10.2465/ganko.92.69

Gallahan, W. E., & Nielsen, R. L. (1992). The partitioning of Sc, Y, and the rare Earth elements between high-Ca pyroxene and natural mafic to intermediate lavas at 1 atmosphere. *Geochimica et Cosmochimica Acta*, *56*(6), 2387–2404. https://doi.org/10.1016/0016-7037(92)90196-P

Ghiorso, M. S., & Sack, R. O. (1995). Chemical mass transfer in magmatic processes IV. A revised and internally consistent thermodynamic model for the interpolation and extrapolation of liquid-solid equilibria in magmatic systems at elevated temperatures and pressures. *Contributions to Mineralogy and Petrology*, *119*(2), 197–212. https://doi.org/10.1007/bf00307281

Goldschmidt, V. M. (1937). The principles of distribution of chemical elements in minerals and rocks. The seventh Hugo Müller Lecture, delivered before the Chemical Society on March 17th, 1937. *Journal of the Chemical Society*, *0*(0), 655–673. https://doi.org/10.1039/jr9370000655

Green, T. H. (1994). Experimental studies of trace-element partitioning applicable to igneous petrogenesis—Sedona 16 years later. *Chemical Geology*, *117*(1–4), 1–36. https://doi.org/10.1016/0009-2541(94)90119-8

Hazen, R. M., Downs, R. T., Conrad, P. G., Finger, L. W., & Gasparik, T. (1994). Comparative compressibilities of majorite-types garnets. *Physics and Chemistry of Minerals*, *21*(5), 344–349. https://doi.org/10.1007/BF00202099

Hill, E., Wood, B. J., & Blundy, J. D. (2000). The effect of Ca-Tschermaks component on trace element partitioning between clinopyroxene and silicate melt. *Lithos*, *53*(3–4), 203–215. https://doi.org/10.1016/S0024-4937(00)00025-6

Hilyard, M., Nielsen, R. L., Beard, J. S., Patinō-Douce, A., & Blencoe, J. (2000). Experimental determination of the partitioning behavior of rare Earth and high field strength elements between pargasitic amphibole and natural silicate melts. *Geochimica et Cosmochimica Acta*, *64*(6), 1103–1120. https://doi.org/10.1016/s0016-7037(99)00379-8

Irving, A. J. (1978). A review of experimental studies of crystal/liquid trace element partitioning. *Geochimica et Cosmochimica Acta*, *42*(6), 743–770. https://doi.org/10.1016/0016-7037(78)90091-1

Leake, B. E., Woolley, A. R., Arps, C. E. S., Birch, W. D., Gilbert, M. C., Grice, J. D., et al. (1997). Nomenclature of amphiboles: Report of the subcommittee on amphiboles of the international mineralogical association, commission on new minerals and mineral names. *American Mineralogist*, *82*(9–10), 1019–1037. https://doi.org/10.1180/minmag.1997.061.405.13

Mollo, S., Blundy, J., Scarlato, P., De Cristofaro, S. P., Tecchiato, V., Di Stefano, F., et al. (2018). An integrated P-T-H_2O-lattice strain model to quantify the role of clinopyroxene fractionation on REE+Y and HFSE patterns of mafic alkaline magmas: Application to eruptions at Mt. Etna. *Earth-Science Reviews*, *185*, 32–56. https://doi.org/10.1016/j.earscirev.2018.05.014

Mollo, S., Blundy, J., Scarlato, P., Vetere, F., Holtz, F., Bachmann, O., & Gaeta, M. (2020). A review of the lattice strain and electrostatic effects on trace element partitioning between clinopyroxene and melt: Applications to magmatic systems saturated with Tschermak-rich clinopyroxenes. *Earth-Science Reviews*, 103351. https://doi.org/10.1016/j.earscirev.2020.103351

Nielsen, R. L. (1985). A method for the elimination of the compositional dependence of trace element distribution coefficients. *Geochimica et Cosmochimica Acta*, *49*(8), 1775–1779. https://doi.org/10.1016/0016-7037(85)90148-6

Nielsen, R. L. (1988). A model for the simulation of combined major and trace element liquid lines of descent. *Geochimica et Cosmochimica Acta*, *52*(1), 27–38. https://doi.org/10.1016/0016-7037(88)90053-1

Nielsen, R. L. (1990). Simulation of igneous differentiation processes. *Reviews in Mineralogy and Geochemistry*, *24*(1), 65–105.

Nielsen, R. L., & Beard, J. S. (2000). Magnetite–melt HFSE partitioning. *Chemical Geology*, *164*(1–2), 21–34. https://doi.org/10.1016/s0009-2541(99)00139-4

Nielsen, R. L., Ghiorso, M. S., & Trischman, T. (2015). What we have learned about the existing trace element partitioning data during the population phase of TraceDs. In *AGU fall meeting abstracts* (pp. V33C–V3119).

Nielsen, R. L., & Ustunisik, G. K. (2022a). Clinopyroxene/melt partition coefficient experiments v. 2, Version 1.0 [Dataset]. Interdisciplinary Earth Data Alliance (IEDA). https://doi.org/10.26022/IEDA/112325

Nielsen, R. L., Ustunisik, G., Lange, A. E., Tepley, F. J., III, & Kent, A. J. (2020). Trace element and isotopic characteristics of plagioclase megacrysts in plagioclase ultraphyric basalts (PUB). *Geochemistry, Geophysics, Geosystems*, *21*(2), e2019GC008638. https://doi.org/10.1029/2019gc008638

Nielsen, R. L., Ustunisik, G., Weinsteiger, A. B., Tepley, F. J., III, Johnston, A. D., & Kent, A. J. (2017). Trace element partitioning between plagioclase and melt: An investigation of the impact of experimental and analytical procedures. *Geochemistry, Geophysics, Geosystems*, *18*(9), 3359–3384. https://doi.org/10.1002/2017gc007080

Nielsen, R. L., & Ustunisik, G. K. (2022b). Garnet/melt partition coefficient experiments v. 2, Version 1.0 [Dataset]. Interdisciplinary Earth Data Alliance (IEDA). https://doi.org/10.26022/IEDA/112323

Nielsen, R. L., & Ustunisik, G. K. (2022c). Amphibole/melt partition coefficient experiments v. 2, Version 1.0 [Dataset]. Interdisciplinary Earth Data Alliance (IEDA). https://doi.org/10.26022/IEDA/112324

Onuma, N., Higuchi, H., Wakita, H., & Nagasawa, H. (1968). Trace element partition between two pyroxenes and the host lava. *Earth and Planetary Science Letters*, *5*, 47–51. https://doi.org/10.1016/s0012-821x(68)80010-x

Profeta, L., Lehnert, K., Ji, P., Ustunisik, G., Nielsen, R., Vieglais, D., et al. (2023). Open and FAIR sample based data sharing through the IEDA2 facility (No. EGU23-10300). In *Copernicus meetings*.

Sun, C., Graff, M., & Liang, Y. (2017). Trace element partitioning between plagioclase and silicate melt: The importance of temperature and plagioclase composition, with implications for terrestrial and lunar magmatism. *Geochimica et Cosmochimica Acta*, *206*, 273–295. https://doi.org/10.1016/j.gca.2017.03.003

Sun, C., & Liang, Y. (2012). Distribution of REE between clinopyroxene and basaltic melt along a mantle adiabat: Effects of major element composition, water, and temperature. *Contributions to Mineralogy and Petrology*, *163*(5), 807–823. https://doi.org/10.1007/s00410-011-0700-x

Sun, C., & Liang, Y. (2013). Distribution of REE and HFSE between low-Ca pyroxene and lunar picritic glass melts around multiple saturation points. *Geochimica et Cosmochimica Acta*, *119*, 340–358. https://doi.org/10.1016/j.gca.2013.05.036

Weiser, P. E., Kent, A. J. R., Till, C. B., Donovan, J., Neave, D. A., Blatter, D. L., & Krawczynki, M. J. (2023). Barometers behaving Badly I: Assessing the influence of analytical and experimental uncertainty on clinopyroxene thermobarometry calculations at crustal conditions. *Journal of Petrology*, *64*, 1–27. https://doi.org/10.1093/petrology/egac126

Wood, B. J., & Blundy, J. D. (1997). A predictive model for rare Earth element partitioning between clinopyroxene and anhydrous silicate melt. *Contribution to Mineralogy and Petrology*, *129*(2–3), 166–181. https://doi.org/10.1007/s004100050330

Wood, B. J., & Blundy, J. D. (2001). The effect of cation charge on crystal-melt partitioning of trace elements. *Earth and Planetary Science Letters*, *188*(1–2), 59–71. https://doi.org/10.1016/s0012-821x(01)00294-1

Wood, B. J., & Fraser, D. G. (1976). *Elementary thermodynamics for geologists*. Oxford University Press.

Wood, B. J., & Fraser, D. G. (1977). *Elementary thermodynamics for geologists*. Oxford University Press.

Yao, L., Sun, C., & Liang, Y. (2012). A parameterized model for REE distribution between low-Ca pyroxene and basaltic melts with applications to REE partitioning in low-Ca pyroxene along a mantle adiabat and during pyroxenite-derived melt and peridotite interaction. *Contributions to Mineralogy and Petrology*, *164*(2), 261–180. https://doi.org/10.1007/s00410-012-0737-5

References From the Supporting Information

Adam, J., & Green, T. H. (1994). The effects of pressure and temperature on the partitioning of Ti, Sr and REE between amphibole, clinopyroxene, and basanitic melts. *Chemical Geology*, *117*(1–4), 219–233. https://doi.org/10.1016/0009-2541(94)90129-5

Baker, M. B., & Wyllie, P. J. (1992). High-pressure apatite solubility in carbonate-rich liquids: Implications for mantle metasomatism. *Geochimica et Cosmochimica Acta*, *56*(9), 3409–3422. https://doi.org/10.1016/0016-7037(92)90388-y

Barth, M. G., Foley, S. F., & Horn, I. (2002). Partial melting in Archean subduction zones: Constraints from experimentally determined trace element partition coefficients between eclogitic minerals and tonalitic melts under upper mantle conditions. *Precambrian Research*, *113*(3–4), 323–340. https://doi.org/10.1016/S0301-9268(01)00216-9

Beattie, P. (1993a). The generation of uranium series disequilibria by partial melting of spinel peridotite: Constraints from partitioning studies. *Earth and Planetary Science Letters*, *117*(3–4), 379–391. https://doi.org/10.1016/0012-821X(93)90091-M

Beattie, P. (1993b). On the occurrence of apparent non-Henry's Law behavior in experimental partitioning studies. *Geochimica et Cosmochimica Acta*, *57*(1), 47–55. https://doi.org/10.1016/0016-7037(93)90467-b

Bennett, S. L., Blundy, J., & Elliott, T. (2004). The effect of sodium and titanium on crystal-melt partitioning of trace elements. *Geochimica et Cosmochimica Acta*, *68*(10), 2335–2347. https://doi.org/10.1016/j.gca.2003.11.006

Blundy, J., & Dalton, J. (2000). Experimental comparison of trace element partitioning between clinopyroxene and melt in carbonate and silicate systems, and implications for mantle metasomatism. *Contributions to Mineralogy and Petrology*, *139*(3), 356–371. https://doi.org/10.1007/s004100000139

Blundy, J., Robinson, J., & Wood, B. (1998). Heavy REE are compatible in clinopyroxene on the spinel lherzolite solidus. *Earth and Planetary Science Letters*, *160*(3–4), 493–504. https://doi.org/10.1016/s0012-821x(98)00106-x

Blundy, J., & Wood, B. (1994). Prediction of crystal–melt partition coefficients from elastic moduli. *Nature*, *372*(6505), 452–454. https://doi.org/10.1038/372452a0

Bottinga, Y., & Weill, D. F. (1972). The viscosity of magmatic silicate liquids; a model calculation. *American Journal of Science*, *272*(5), 438–475. https://doi.org/10.2475/ajs.272.5.438

Brice, J. C. (1975). Some thermodynamic aspects of the growth of strained crystals. *Journal of Crystal Growth*, *28*(2), 249–253. https://doi.org/10.1016/0022-0248(75)90241-9

Canil, D., & Fedortchouk, Y. (2000). Clinopyroxene-liquid partitioning for vanadium and the oxygen fugacity during formation of cratonic and oceanic mantle lithosphere. *Journal of Geophysical Research*, *105*(B11), 26003–26016. https://doi.org/10.1029/2000jb900221

Chamorro, E. M., Brooker, R. A., Wartho, J. A., Wood, B. J., Kelley, S. P., & Blundy, J. D. (2002). Ar and K partitioning between clinopyroxene and silicate melt to 8 GPa. *Geochimica et Cosmochimica Acta*, *66*(3), 507–519. https://doi.org/10.1016/s0016-7037(01)00784-0

Dalou, C., Koga, K. T., Shimizu, N., Boulon, J., & Devidal, J. (2011). Experimental determination of F and Cl partitioning between lherzolite and basaltic melt. *Contributions to Mineralogy and Petrology*, *163*(4), 591–609. https://doi.org/10.1007/s00410-011-0688-2

Dalou, C., Koga, K. T., Shimizu, N., Boulon, J., & Devidal, J. (2012). Experimental determination of F and Cl partitioning between lherzolite and basaltic melt. *Contributions to Mineralogy and Petrology*, *163*(4), 591–609. https://doi.org/10.1007/s00410-011-0688-2

Dasgupta, R., Hirschmann, M. M., McDonough, W. F., Spiegelman, M., & Withers, A. C. (2009). Trace element partitioning between garnet lherzolite and carbonatite at 6.6 and 8.6 GPa with applications to the geochemistry of the mantle and of mantle derived melts. *Chemical Geology*, *262*(1–2), 57–77. https://doi.org/10.1016/j.chemgeo.2009.02.004

Davis, A. D., & Hirschmann, M. M. (2013). The effects of K_2O on the compositions of near-solidus melts of garnet peridotite at 3 GPa and the origin of basalts from enriched mantle. *Contributions to Mineralogy and Petrology*, *166*(4), 1029–1046. https://doi.org/10.1007/s00410-013-0907-0

Davis, F. A., Humayun, M., Hirschmann, M. M., & Cooper, R. S. (2013). Experimentally determined mineral/melt partitioning of first-row transition elements (FRTE) during partial melting of peridotite at 3 GPa. *Geochimica et Cosmochimica Acta*, *104*, 232–260. https://doi.org/10.1016/j.gca.2012.11.009

Deer, W. A., Howie, R. A., & Zussman, J. (1992). *An introduction to the rock-forming minerals:* Essex. Longman Scientific and Technology.

Defant, M. J., & Nielsen, R. L. (1990). Interpretation of open system petrogenetic processes: Phase equilibria constraints on magma evolution. *Geochimica et Cosmochimica Acta*, *54*(1), 87–102. https://doi.org/10.1016/0016-7037(90)90197-s

Dunn, T. (1987). Partitioning of Hf, Lu, Ti, and Mn between olivine, clinopyroxene and basaltic liquid. *Contributions to Mineralogy and Petrology*, *96*(4), 476–484. https://doi.org/10.1007/bf01166692

Dunn, T., & McCallum, I. S. (1982). The partitioning of Zr and Nb between diopside and melts in the system diopside-albite-anorthite. *Geochimica et Cosmochimica Acta*, *46*(4), 623–629. https://doi.org/10.1016/0016-7037(82)90163-6

Fabbrizio, A., Schmidt, M. W., & Petrelli, M. (2021). Effect of fO2 on Eu partitioning between clinopyroxene, orthopyroxene and basaltic melt: Development of a Eu3+/Eu2+ oxybarometer. *Chemical Geology*, *559*, 119967. https://doi.org/10.1016/j.chemgeo.2020.119967

Fabbrizio, A., Stalder, R., Hametner, K., Gunther, D., & Marquardt, K. (2013). Experimental partitioning of halogens and other trace elements between olivine, pyroxenes, amphibole and aqueous fluid at 2 GPa and 900-1,300°C. *Contributions to Mineralogy and Petrology*, *166*, 639–653. https://doi.org/10.1007/s00410-013-0902-5

Fellows, S. A., & Canil, D. (2012). Experimental study of the partitioning of Cu during partial melting of Earth's mantle. *Earth and Planetary Science Letters*, *337–338*, 133–143. https://doi.org/10.1016/j.epsl.2012.05.039

Fonseca, R. O. C., Mallmann, G., Sprung, P., Sommer, J. E., Heuser, A., Speelmanns, I. M., & Blanchard, H. (2014). Redox controls on tungsten and uranium crystal/silicate melt partitioning and implications for the U/W and Th/W ratio of the lunar mantle. *Earth and Planetary Science Letters*, *404*, 42017–42113. https://doi.org/10.1016/j.epsl.2014.07.015

Frei, D., Liebscher, A., Wittenberg, A., & Shaw, C. S. J. (2003). Crystal chemical controls on rare Earth element partitioning between epidote-group minerals and melts: An experimental and theoretical study. *Contributions to Mineralogy and Petrology*, *146*(2), 192–204. https://doi.org/10.1007/s00410-003-0493-7

Gaetani, G. A. (2004). The influence of melt structure on trace element partitioning near the peridotite solidus. *Contributions to Mineralogy and Petrology*, *147*(5), 511–527. https://doi.org/10.1007/s00410-004-0575-1

Gaetani, G. A., & Grove, T. L. (1995). Partitioning of rare Earth elements between clinopyroxene and silicate melt: Crystal-chemical controls. *Geochimica et Cosmochimica Acta*, *59*(10), 1951–1962. https://doi.org/10.1016/0016-7037(95)00119-0

Gaetani, G. A., Kent, A. J. R., Grove, T. L., Hutcheon, I. D., & Stolper, E. M. (2003). Mineral/melt partitioning of trace elements during hydrous peridotite partial melting. *Contributions to Mineralogy and Petrology*, *145*(4), 391–405. https://doi.org/10.1007/s00410-003-0447-0

Girnis, A. V., Bulatov, V. K., Brey, G. P., Gerdes, A., & Hofer, H. E. (2013). Trace element partitioning between mantle minerals and silico-carbonate melts at 6-12 GPa and applications to mantle metasomatism and kimberlite genesis. *Lithos*, *160–161*, 183–200. https://doi.org/10.1016/j.lithos.2012.11.027

Girnis, A. V., Bulatov, V. K., Lahaye, Y., & Brey, G. P. (2006). Partitioning of trace elements between carbonate-silicate melts and mantle minerals: Experiment and petrological consequences. *Petrology*, *14*(5), 492–514. https://doi.org/10.1134/S0869591106050055

Grassi, D., Schmidt, M. W., & Gunther, D. (2012). Element partitioning during carbonated pelite melting at 8, 13, and 22 GPa and the sediment signature in the EM mantle components. *Earth and Planetary Science Letters*, *327–328*, 84–96. https://doi.org/10.1016/j.epsl.2012.01.023

Green, T. H., Blundy, J. D., Adam, J., & Yaxley, G. M. (2000). SIMS determination of trace element partition coefficients between garnet, clinopyroxene and hydrous basaltic liquids at 2-7.5 Gpa and 1080-1200°C. *Lithos*, *53*(3–4), 165–187. https://doi.org/10.1016/S0024-4937(00)00023-2

Green, T. H., & Pearson, N. J. (1987). An experimental study of Nb and Ta partitioning between Ti-rich minerals and silicate liquids at high pressure and temperature. *Geochimica et Cosmochimica Acta*, *51*(1), 55–62. https://doi.org/10.1016/0016-7037(87)90006-8

Green, T. H., Sie, S. H., Ryan, C. G., & Cousens, D. R. (1989). Proton microprobe-determined partitioning of Nb, Ta, Sr and Y between garnet, clinopyroxene and basaltic magma at high pressure and temperature. *Chemical Geology*, *74*(3–4), 201–216. https://doi.org/10.1016/0009-2541(89)90032-6

Hack, P. J., Nielsen, R. L., & Johnston, A. D. (1994). Experimentally determined rare-Earth element and Y partitioning behavior between clinopyroxene and basaltic liquids at pressures up to 20 kbar. *Chemical Geology*, *117*(1–4), 89–105. https://doi.org/10.1016/0009-2541(94)90123-6

Hammouda, T., Moine, B. N., Devidal, J. L., & Vincent, C. (2009). Trace element partitioning during partial melting of carbonated eclogites. *Physics of the Earth and Planetary Interiors*, *174*(1–4), 60–69. https://doi.org/10.1016/j.pepi.2008.06.009

Hart, S. R., & Dunn, T. (1993). Experimental Cpx/melt partitioning of 24 trace elements. *Contributions to Mineralogy and Petrology*, *113*(1), 42022–42028. https://doi.org/10.1007/BF00320827

Hauri, E. H., Wagner, T. P., & Grove, T. L. (1994). Experimental and natural partitioning of Th, U, Pb, and other trace elements between garnet, clinopyroxene, and basaltic melts. *Chemical Geology*, *117*(1–4), 149–166. https://doi.org/10.1016/0009-2541(94)90126-0

Huang, F., Lundstrom, C. C., & McDonough, W. F. (2006). Effect of melt structure on trace-element partitioning between clinopyroxene and silicic, alkaline, aluminous melts. *American Mineralogist*, *91*(8–9), 1385–1400. https://doi.org/10.2138/am.2006.1909

Johnson, K. T. (1998). Experimental determination of partition coefficients for rare Earth and high-field-strength elements between clinopyroxene, garnet, and basaltic melt at high pressures. *Contributions to Mineralogy and Petrology*, *133*(1–2), 60–68. https://doi.org/10.1007/s004100050437

Klemme, S., Blundy, J. D., & Wood, B. J. (2002). Experimental constraints on major and trace element partitioning during partial melting of eclogite. *Geochimica et Cosmochimica Acta*, *66*(17), 3109–3123. https://doi.org/10.1016/S0016-7037(02)00859-1

Klemme, S., Van der Laan, M., Foley, S. F., & Gunther, M. (1995). Experimentally determined trace and minor element partitioning between clinopyroxene and carbonatite melt under upper mantle conditions. *Earth and Planetary Science Letters*, *133*(3–4), 439–448. https://doi.org/10.1016/0012-821X(95)00098-W

Klimm, K., Blundy, J. D., & Green, T. H. (2008). Trace element partitioning and accessory phase saturation during H_2O-saturated melting of basalt with implications for subduction zone chemical fluxes. *Journal of Petrology*, *49*(3), 523–553. https://doi.org/10.1093/petrology/egn001

Laubier, M., Grove, T. L., & Langmuir, C. H. (2014). Trace element mineral/melt partitioning for basaltic and basaltic andesitic melts: An experimental and laser ICP-MS study with application to the oxidation state of mantle source regions. *Earth and Planetary Science Letters*, *392*, 265–278. https://doi.org/10.1016/j.epsl.2014.01.053

Liu, X., Xiong, X., Audetat, A., & Li, Y. (2015). Partitioning of Cu between mafic minerals, Fe-Ti oxides and intermediate to felsic melts. *Geochimica et Cosmochimica Acta*, *151*, 86–102. https://doi.org/10.1016/j.gca.2014.12.010

Liu, X., Xiong, X., Audetat, A., Li, Y., Song, M., Li, L., et al. (2014). Partitioning of copper between olivine, orthopyroxene, clinopyroxene, spinel, garnet and silicate melts at upper mantle conditions. *Geochimica et Cosmochimica Acta*, *125*, 1–22. https://doi.org/10.1016/j.gca.2013.09.039

Lofgren, G., Huss, G., & Wasserburg, G. (2006). An experimental study of trace-element partitioning between Ti-Al-clinopyroxene and melt: Equilibrium and kinetic effects including sector zoning. *American Mineralogist*, *91*(10), 1596–1606. https://doi.org/10.2138/am.2006.2108

Lundstrom, C. C., Shaw, H. F., Ryerson, F. J., Phinney, D. L., Gill, J. B., & Williams, Q. (1994). Compositional controls on the partitioning of U, Th, Ba, Pb, Sr and Zr between clinopyroxene and haplobasaltic melts: Implications for uranium series disequilibria in basalts. *Earth and Planetary Science Letters*, *128*(3–4), 407–423. https://doi.org/10.1016/0012-821X(94)90159-7

Lundstrom, C. C., Shaw, H. F., Ryerson, F. J., Williams, Q., & Gill, J. (1998). Crystal chemical control of clinopyroxene-melt partitioning in the Di-Ab-an system: Implications for elemental fractionations in the depleted mantle. *Geochimica et Cosmochimica Acta*, *62*(16), 2849–2862. https://doi.org/10.1016/s0016-7037(98)00197-5

Mallmann, G., & O'Neill, H. S. C. (2007). The effect of oxygen fugacity on the partitioning of Re between crystals and silicate melt during mantle melting. *Geochimica et Cosmochimica Acta*, *71*(11), 2837–2857. https://doi.org/10.1016/j.gca.2007.03.028

Martin, L. H. J., Schmidt, M. W., Mattsson, H. B., Ulmer, P., Hametner, K., & Gunther, D. (2012). Element partitioning between immiscible carbonatite, Äìkamafugite melts with application to the Italian ultrapotassic suite. *Chemical Geology*, *320–321*, 96–112. https://doi.org/10.1016/j.chemgeo.2012.05.019

Matzen, A. K., Baker, M. B., Beckett, J. R., & Stolper, E. M. (2013). The temperature and pressure dependence of nickel partitioning between olivine and silicate melt. *Journal of Petrology*, *54*(12), 2521–2545. https://doi.org/10.1093/petrology/egt055

McDade, P., Blundy, J. D., & Wood, B. J. (2003). Trace element partitioning between mantle wedge peridotite and hydrous MgO-rich melt. *American Mineralogist*, *88*(11–12), 1825–1831. https://doi.org/10.2138/am-2003-11-1225

McKay, G., Wagstaff, J., & Yang, S.-R. (1986). Clinopyroxene REE distribution coefficients for shergottites: The REE content of the Shergotty melt. *Geochimica et Cosmochimica Acta*, *50*(6), 927–837. https://doi.org/10.1016/0016-7037(86)90374-1

Mercer, C. N., & Johnston, A. D. (2008). Experimental studies of the P-T-H_2O near-liquidus phase relations of basaltic andesite from North Sister Volcano, High Oregon Cascades: Constraints on lower-crustal mineral assemblages. *Contributions to Mineralogy and Petrology*, *155*(5), 571–592. https://doi.org/10.1007/s00410-007-0259-8

Michely, L. T., Leitzke, F. P., Speelmanns, I. M., & Fonseca, R. O. C. (2017). Competing effects of crystal chemistry and silicate melt composition on trace element behavior in magmatic systems: Insights from crystal/silicate melt partitioning of the REE, HFSE, Sn, In, Ga, Ba, Pt and Rh. *Contributions to Mineralogy and Petrology*, *172*(6), 39. https://doi.org/10.1007/s00410-017-1353-1

Mollo, S., Blundy, J. D., Iezzi, G., Scarlato, P., & Langone, A. (2013). The partitioning of trace elements between clinopyroxene and trachybasaltic melt during rapid cooling and crystal growth. *Contributions to Mineralogy and Petrology*, *166*(6), 1633–1654. https://doi.org/10.1007/s00410-013-0946-6

Nandedkar, R. H., Hürlimann, N., Ulmer, P., & Müntener, O. (2016). Amphibole–melt trace element partitioning of fractionating calc-alkaline magmas in the lower crust: An experimental study. *Contributions to Mineralogy and Petrology*, *171*(8), 1–25. https://doi.org/10.1007/s00410-016-1278-0

Nicholls, I. A., & Harris, K. L. (1980). Experimental rare Earth element partition coefficients for garnet, clinopyroxene and amphibole coexisting with andesitic and basaltic liquids. *Geochimica et Cosmochimica Acta*, *44*(2), 287–308. https://doi.org/10.1016/0016-7037(80)90138-6

Nielsen, R. L., Sours-Page, R. E., & Harpp, K. S. (2000). Role of a Cl-bearing flux in the origin of depleted ocean floor magmas. *Geochemistry, Geophysics, Geosystems*, *1*(5), 1007. https://doi.org/10.1029/1999gc000017

Novella, D., Frost, D. J., Hauri, E. H., Bureau, H., Raepsaet, C., & Roberge, M. (2014). The distribution of H_2O between silicate melt and nominally anhydrous peridotite and the onset of hydrous melting in the deep upper mantle. *Earth and Planetary Science Letters*, *400*, 1–13. https://doi.org/10.1016/j.epsl.2014.05.006

Ottolini, L., Laporte, D., Raffone, N., Devidal, J., & Fevre, B. L. (2008). New experimental determination of Li and B partition coefficients during upper mantle partial melting. *Contributions to Mineralogy and Petrology*, *157*(3), 313–325. https://doi.org/10.1007/s00410-008-0336-7

Pertermann, M., & Hirschmann, M. M. (2002). Trace-element partitioning between vacancy-rich eclogitic clinopyroxene and silicate melt. *American Mineralogist*, *87*(10), 1364–1376. https://doi.org/10.2138/am-2002-1012

Pertermann, M., Hirschmann, M. M., Hametner, K., Gunther, D., & Schmidt, M. W. (2004). Experimental determination of trace element partitioning between garnet and silica-rich liquid during anhydrous partial melting of MORB-like eclogite. *Geochemistry, Geophysics, Geosystems*, *5*(5), Q05A01. https://doi.org/10.1029/2003GC000638

Rapp, R. P., Norman, M. D., Laporte, D., Yaxley, G. M., Martin, H., & Foley, S. F. (2010). Continent formation in the Archean and chemical evolution of the cratonic lithosphere: Melt–rock reaction experiments at 3–4 GPa and petrogenesis of Archean Mg-diorites (sanukitoids). *Journal of Petrology*, *51*(6), 1237–1266. https://doi.org/10.1093/petrology/egq017

Ray, G. L., Shimizu, N., & Hart, S. R. (1983). An ion microprobe study of the partitioning of trace elements between clinopyroxene and liquid in the system diopside-albite-anorthite. *Geochimica et Cosmochimica Acta*, *47*(12), 2131–2140. https://doi.org/10.1016/0016-7037(83)90038-8

Righter, K., Campbell, A. J., Humayun, M., & Hervig, R. L. (2004). Partitioning of Ru, Rh, Pd, Re, Ir, and Au between Cr-bearing spinel, olivine, pyroxene and silicate melts. *Geochimica et Cosmochimica Acta*, *68*(4), 867–880. https://doi.org/10.1016/j.gca.2003.07.005

Righter, K., & Drake, M. J. (2000). Metal/silicate equilibrium in the early Earth, New constraints from the volatile moderately siderophile elements Ga, Cu, P, and Sn. *Geochimica et Cosmochimica Acta*, *64*(20), 3581–3597. https://doi.org/10.1016/S0016-7037(00)00466-X

Righter, K., Drake, M. J., & Yaxley, G. (1997). Prediction of siderophile element metal-silicate partition coefficients to 20 Gpa and 2800°C: The effects of pressure, temperature, oxygen fugacity, and silicate and metallic melt composition. *Physics of the Earth and Planetary Interiors*, *100*(1–4), 115–134. https://doi.org/10.1016/S0031-9201(96)03235-9

Rollinson Hugh, R. (1993). *Using geochemical data: Evaluation, presentation. Interpretation*. Pearson Education Limited.

Rosenthal, A., Hauri, E. H., & Hirschmann, M. M. (2015). Experimental determination of C, F, and H partitioning between mantle minerals and carbonated basalt, CO_2/Ba and CO_2/Nb systematics of partial melting, and the CO_2 contents of basaltic source regions. *Earth and Planetary Science Letters*, *412*, 77–87. https://doi.org/10.1016/j.epsl.2014.11.044

Salters, V. J. M., Longhi, J. E., & Bizimis, M. (2002). Near mantle solidus trace element partitioning at pressures up to 3.4 GPa. *Geochemistry, Geophysics, Geosystems*, *3*(7), 1–23. https://doi.org/10.1029/2001GC000148

Schmidt, K. H., Bottazzi, P., Vannucci, R., & Mengel, K. (1999). Trace element partitioning between phlogopite, clinopyroxene and leucite lamproite melt. *Earth and Planetary Science Letters*, *168*(3–4), 287–299. https://doi.org/10.1016/S0012-821X(99)00056-4

Shimizu, H. (1980). Experimental study on rare-Earth element partitioning in minerals formed at 20 and 30kb for basaltic systems. *Geochemical Journal*, *14*(4), 185–202. https://doi.org/10.2343/geochemj.14.185

Shimizu, H., Samgen, K., & Musada, A. (1982). Experimental study on rare-Earth element partitioning in olivine and clinopyroxene formed at 10 and 20 kb for basaltic systems. *Geochemical Journal*, *16*(3), 107–117. https://doi.org/10.2343/geochemj.16.107

Shimizu, N. (1974). An experimental study of the partitioning of K, Rb, Cs, Sr and Ba between clinopyroxene and liquid at high pressure. *Geochimica et Cosmochimica Acta*, *38*(12), 1789–1798. https://doi.org/10.1016/0016-7037(74)90162-8

Skulski, T., Minarik, W., & Watson, B. (1994). High-pressure experimental trace-element partitioning between clinopyroxene and basaltic melts. *Chemical Geology*, *117*(1–4), 127–147. https://doi.org/10.1016/0009-2541(94)90125-2

Spandler, C., Yaxley, G., Green, D. H., & Rosenthal, A. (2008). Phase relations and melting of anhydrous K-bearing eclogite from 1200 to 1600°C and 3 to 5 GPa. *Journal of Petrology*, *49*(4), 771–795. https://doi.org/10.1093/petrology/egm039

Spandler, C., Yaxley, G., Green, D. H., & Scott, D. (2010). Experimental phase and melting relations of metapelite in the upper mantle: Implications for the petrogenesis of intraplate magmas. *Contributions to Mineralogy and Petrology*, *160*(4), 569–589. https://doi.org/10.1007/s00410-010-0494-2

Stalder, R., Foley, S. F., Brey, G. P., & Horn, I. (1998). Mineral-aqueous fluid partitioning of trace elements at 900-1,200°C and 3.0-5.7 GPa: New experimental data for garnet, clinopyroxene, and rutile, and implications for mantle metasomatism. *Geochimica et Cosmochimica Acta*, *62*(10), 1781–1801. https://doi.org/10.1016/S0016-7037(98)00101-X

Sun, C., & Liang, Y. (2014). An assessment of subsolidus re-equilibration on REE distribution among mantle minerals olivine, orthopyroxene, clinopyroxene, and garnet in peridotites. *Chemical Geology*, *372*, 80–91. https://doi.org/10.1016/j.chemgeo.2014.02.014

Suzuki, T., Hirata, T., Yokoyama, T. D., Imai, T., & Takahashi, E. (2012). Pressure effect on element partitioning between minerals and silicate melt: Melting experiments on basalt up to 20 GPa. *Physics of the Earth and Planetary Interiors*, *208–209*, 59–73. https://doi.org/10.1016/j.pepi.2012.07.008

Tiepolo, M., Vannucci, R., Oberti, R., Foley, S., Bottazzi, P., & Zanetti, A. (2000). Nb and Ta incorporation and fractionation in titanian pargasite and kaersutite: Crystal-chemical constraints and implications for natural systems. *Earth and Planetary Sciences*, *176*(2), 185–201. https://doi.org/10.1016/S0012-821X(00)00004-2

Toplis, M. J., & Corgne, A. (2002). An experimental study of element partitioning between magnetite, clinopyroxene and iron-bearing silicate liquids with particular emphasis on vanadium. *Contributions to Mineralogy and Petrology*, *144*(1), 22–37. https://doi.org/10.1007/s00410-002-0382-5

Tuff, J., & Gibson, S. A. (2007). Trace-element partitioning between garnet, clinopyroxene and Fe-rich picritic melts at 3 to 7 GPa. *Contributions to Mineralogy and Petrology*, *153*(4), 369–387. https://doi.org/10.1007/s00410-006-0152-x

Wang, J., Xiong, X., Takahashi, E., Zhang, L., Li, L., & Liu, X. (2019). Oxidation state of arc mantle revealed by partitioning of V, Sc, and Ti between mantle minerals and basaltic melts. *Journal of Geophysical Research: Solid Earth*, *124*(5), 4617–4638. https://doi.org/10.1029/2018jb016731

Watson, E. B., Othman, D. B., Luck, J. M., & Hofmann, A. W. (1987). Partitioning of U, Pb, Cs, Yb, Hf, Re and Os between chromian diopsidic pyroxene and haplobasaltic liquid. *Chemical Geology*, *62*(3–4), 191–208. https://doi.org/10.1016/0009-2541(87)90085-4

Watson, E. B., & Ryerson, F. J. (1986). Partitioning of zirconium between clinopyroxene and magmatic liquids of intermediate composition. *Geochimica et Cosmochimica Acta*, *50*(11), 2523–2526. https://doi.org/10.1016/0016-7037(86)90035-9

Wood, B. J., & Trigila, R. (2001). Experimental determination of aluminous clinopyroxene-melt partition coefficients for potassic liquids, with application to the evolution of the Roman province potassic magmas. *Chemical Geology*, *172*(3–4), 213–223. https://doi.org/10.1016/S0009-2541(00)00259-X

Xiong, X. L., Adam, J., & Green, T. H. (2005). Rutile stability and rutile/melt HFSE partitioning during partial melting of hydrous basalt: Implications for TTG genesis. *Chemical Geology*, *218*(3–4), 339–359. https://doi.org/10.1016/j.chemgeo.2005.01.014

Yakob, J. L., Feineman, M. D., Deane, J. A., Jr., Eggler, D. H., & Penniston-Dorland, S. C. (2012). Lithium partitioning between olivine and diopside at upper mantle conditions: An experimental study. *Earth and Planetary Science Letters*, *329–339*, 11–21. https://doi.org/10.1016/j.epsl.2012.01.035

Zhang, B., Hu, X., Li, P., Tang, Q., & Zhou, W. (2019). Trace element partitioning between amphibole and hydrous silicate glasses at 0.6–2.6 GPa. *Acta Geochimica*, *38*(3), 414–429. https://doi.org/10.1007/s11631-019-00322-4